

國立交通大學

電信工程研究所

博士論文

新穎交錯耦合濾波器之開發設計與寬頻高階馬
迅平衡非平衡轉換器合成設計

Development and Design of Novel Cross-Coupled
Filters and Exact Synthesis of New High-Order
Wideband Marchand Balun

研究生：呂哲慶 (Jhe-Ching Lu)

指導教授：張志揚 (Chi-Yang Chang)

中華民國 九十八年 九月

新穎交錯耦合濾波器之開發設計與寬頻高階馬迅平衡非
平衡轉換器合成設計

Development and Design of Novel Cross-Coupled Filters
and Exact Synthesis of New High-Order Wideband
Marchand Balun

研究生：呂哲慶

Student: Jhe-Ching Lu

指導教授：張志揚

Advisor: Dr. Chi-Yang Chang



A Dissertation
Submitted to Institute of Communication Engineering
College of Electrical and Computer Engineering
National Chiao Tung University
in Partial Fulfillment of the Requirements
for the Degree of Doctor of Philosophy
in
Communication Engineering
September 2009
Hsinchu, Taiwan

新穎交錯耦合濾波器之開發設計與寬頻高階馬迅平衡非平 衡轉換器合成設計

研究生:呂哲慶

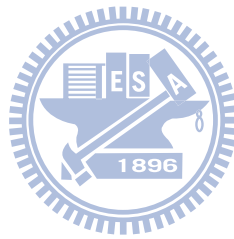
指導教授:張志揚

國立交通大學電信工程研究所

摘要

本論文主要的研究方向分成兩大部分，分別為微波濾波器設計與馬迅平衡非平衡轉換器設計。第一部分是研究運用四分之一波長步階阻抗共振腔設計高性能濾波器、如何快速設計交錯耦合濾波器、以及發展新穎耦合濾波器。文中介紹使用四分之一波長步階阻抗共振腔來實現具有源級與負載相耦合的四角互耦的濾波器響應，可以任意控制第二對傳輸零點的位置。一般而言絕大部分的設計都是使用耦合係數與外部品質因子來設計濾波器，一旦共振腔型式固定，所萃取的耦合係數只能使用在當時濾波器的中心頻率與當時的實體佈局方式，而且一旦傳輸零點位置改變，共振腔擺放的位置也要改變，重新建立耦合係數與外部品質因子，而且其初始設計離最佳化的廣義柴比雪夫響應相差太多，必須調整濾波器的次數太多，造成難以快速設計。本論文提出以傳統平行耦合線濾波器來達到具有交錯耦合的功能，好處是能夠有最佳的初始設計以及優越的傳輸零點位置的擺放。此外，文中也提出新穎耦合濾波器圖形，此濾波器提供了對稱型的實體佈局實現非對稱的濾波器響應，也克服了傳輸零點非常靠近帶通頻率所造成在平面實體佈局技術的困難度。

論文的第二部份敘述使用傳輸線元件的分佈式電路所組成的網路的合成方法。此合成方法可以預測所有頻率點響應，所使用到的理查變數(Richards variable)、傳輸線網路、理查理論(Richards theorem)、黑田恆等式以及傳輸線近似合成函數都有討論。此外，文中也會提出高階寬頻馬迅平衡非平衡阻抗轉換器的電路，以及如何準確合成具有柴比雪夫響應的馬迅平衡非平衡阻抗轉換器。此種新提出的高階馬迅電路適合寬頻響應。

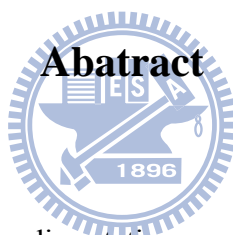


Development and Design of Novel Cross-Coupled Filters and Exact Synthesis of New High-Order Wideband Marchand Balun

Student: Jhe-Ching Lu

Advisor: Dr. Chi-Yang Chang

**Institute of Communication Engineering
National Chiao Tung University**



The research topics in this dissertation are divided into two parts; one is microwave filter design, the other is Marchand Balun design. The first topic is to utilize quarter-wave stepped impedance resonator to design high performance filter, study how to quickly design cross-coupled filters, and develop novel coupling schemes. In this dissertation, quarter-wave stepped impedance resonators are utilized to realize quadruplet and canonical-form coupling schemes. The proposed filter is easy to apply and control the source-load cross coupling. General speaking, most of the filter designs are to use coupling coefficients and external quality factor to design cross-coupled filters. Once the physical layout of the resonator is decided, the extracted coupling coefficients can be only used at the center frequency. Furthermore, if one coupling coefficient in the coupling matrix changes sign for shifting the transmission zero from one side of the passband to the other, the physical layout must

be reconfigured. The initial design of cross-coupled filters based on segmentation method is not good enough, so tuning of filter performances must spend much time. This dissertation presents new cross-coupled filters based on a conventional parallel-coupled filter. The proposed filters have the advantages of the ability to locate a transmission zero on the lower or upper stopband and a good initial design. Additionally, the novel coupling schemes are presented to exhibit bisymmetric coupling matrix. The novel coupling schemes provide the implementations of symmetric layouts to realize asymmetric filter responses. Using the novel coupling schemes implementation of generalized Chebyshev filters with transmission zeros very close to the passband can be easily realized in planar technology.

The second topic is to describe the synthesis method of the networks which are composed of the distributed transmission line circuits. The synthesis method is exact at all frequencies. Richards variable, transmission line networks, Richards theorem, kuroda identities and transmission line approximating functions are discussed in detailed. In addition, high-order wideband Marchand baluns are presented in this dissertation and the exact synthesis of the proposed Marchand baluns with Chebyshev responses are introduced. The proposed high-order Marchand baluns are suitable to design wideband responses.

誌 謝

首先，我最要感謝的是從小養育我長大的奶奶，還常常記得小時候的我體弱多病，常常得半夜找醫生，都是奶奶與姑姑們陪伴照顧著，沒有奶奶，我今日要求取博士學位，幾乎是不可能的，也感謝我能成長在喜樹這個好風水的鄉村，感謝喜樹的一切。

我要特別感謝張志揚教授的指導。張教授的開朗與耐心以及對專業知識的熟稔，對於研究工作的進展有莫大的助益，也特別感謝老師給予學生研究的自由度。另外我也要感謝口試委員陳俊雄、郭仁財、呂良鴻、鍾世忠、林根煌、張盛富以及林祐生教授，在這七位口試委員的協助建議下，使本論文更顯完善。也要感謝在我博一時在研究上有些不懂的地方，而能準確重點地點破我的疑問的廖竟谷博士，很高興能夠與廖博士討論一些濾波器上的問題。

接下來要感謝的另一批人是我那些台南從小到大的朋友。回到台南，常常跟你們混在一起，還蠻好玩的蠻開心的，讓我可以消除壓力，對後來的研究也有幫助。也感謝電子所黃博士、廖博士在我經濟困難之時幫助我。總之要感謝的貴人相當多，謝謝你們。

呂哲慶 於交大
民國九十八年九月

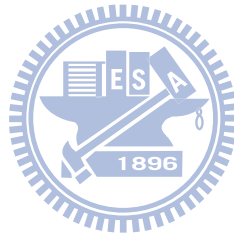
Contents

Abstract (Chinese)	I
Abstract (English).....	III
Acknowledgements.....	V
Contents.....	VI
List of Tables	VIII
List of Figures	IX
Chapter 1 Introduction	1
1.1 Microwave filters.....	1
1.1.1 Review of Coupled Resonator Filters and Cross-Coupled Filters.....	2
1.1.2 Motivation.....	5
1.1.3 Literature Survey of Coupling Schemes and Realizations of Cross-Coupled Resonator Filters.....	6
1.1.4 Original Contribution of this Dissertation.....	7
1.2 Balun.....	8
1.2.1 Literature Survey.....	9
1.2.2 Objective and Contribution in the Second Topic of this Dissertation.....	13
1.3 Organization of this Dissertation.....	14
Chapter 2 Theory of Microwave Resonator Filters and Distributed Circuit Design	17
2.1 Basic Theory for Cross-Coupled Resonator Filters.....	17
2.1.1 Synthesis theory of Advanced Coupling Matrix in the Normalized Domain.....	17
2.1.2 Useful Impedance and Admittance Inverters and Coupled-Line Circuits.....	30
2.1.3 Segmentation Method for Coupled Resonator Filters.....	36
2.1.4 Stepped Impedance Resonators.....	41
2.1.5 Relations between the Coupling Matrix and Design Parameters of Coupled-Resonator Filters.....	43
2.2 Distributed Circuits with Transmission Line Elements.....	44
2.2.1 Richards Variable and Transmission Line Networks.....	45
2.2.2 Richards Theorem and Kuroda Identities.....	47
2.2.3 Transmission Line Approximating Functions and Synthesis Procedure.....	51

Chapter 3 Quarter-Wave Stepped-Impedance Resonator Filters with Quadruplet and Canonical Form Responses.....	55
3.1 Introduction.....	55
3.2 Coupling Schemes and Stepped Impedance Resonators.....	57
3.3 Filter Design Examples and Results.....	61
Chapter 4 Microstrip Parallel-Coupled Filters with Cross Coupling.....	65
4.1 Introduction.....	65
4.2 Phase Relationships and Generation of Finite Transmission Zeros.....	69
4.3 Cross-Coupling Schemes.....	73
4.4 Filter Design Examples.....	79
4.5 Results and Discussion.....	85
Chapter 5 Bisymmetric Coupling Schemes with Generalized Chebyshev Responses.....	91
5.1 Introduction.....	91
5.2 The New Modified Coupling Schemes.....	95
5.3 The Synthesized Coupling Matrices and the Parallel-Coupled Line Section.....	99
5.4 Design Examples and Experiment Results.....	105
Chapter 6 Exact Synthesis of New High-Order Wideband Marchand Balun...114	114
6.1 Introduction.....	114
6.2 Derivation of a Fifth-Order Marchand Balun.....	116
6.3 Synthesis and Design of Two Balun Examples.....	121
6.4 Physical Implementation and Experimental Results.....	125
6.5 A Sixth-Order S-Plane Prototype Balun.....	129
Chapter 7 Conclusion and Future work.....	130
7.1 Conclusion.....	130
7.2 Future Work.....	131
References.....	132

List of Table

Table 2.1. Interesting well-known coupling topologies.....	23
Table 2.2. $ABCD$ matrices for distributed LC ladder and a unit element.....	52
Table 4.1. The relative phase shifts of the main coupling path, the proper phases of the cross coupling paths to generate transmission zeros, corresponding responses, and delay line electrical length.....	73
Table 4.2. The physical dimensions of the two proposed filters.....	84
Table 4.3. The dimensions of the first designed mixed cascaded quadruplet and trisection filter with finite transmission zeros closed to the passband.....	89
Table 6.1 The relationships between distributed circuits in the f -plane and high-pass circuits in the S -plane, and the corresponding $ABCD$ parameters.....	118



List of Figures

Fig. 1.1.	Realization of an ideal balun by an ideal transformer.....	9
Fig. 1.2.	Marchand balun. (a) Type 1. (b) Type 2. (c) Type 3.....	10
Fig. 1.3.	Equivalent circuit of Marchand balun.....	11
Fig. 1.4.	Roberts balun (clipped from Fig. 3 in [103]).....	11
Fig. 1.5.	Broadside-coupled balun (clipped from Fig. 2 in [111]).....	12
Fig. 1.6.	A coupled-line Marchand balun.....	13
Fig. 2.1.	Lowpass filter prototypes with ladder networks. (a) Begin with a shunt capacitor. (b) Begin with a series inductor.....	18
Fig. 2.2.	Alternative lowpass prototype networks using inverter. (a) K -inverters. (b) J -inverters.....	18
Fig. 2.3.	(a) Equivalent circuit of n -coupled resonators in low pass domain. (b) Its network representation.....	19
Fig. 2.4.	The coupling route of the example filter.....	22
Fig. 2.5.	A two-port network.....	26
Fig. 2.6.	Canonical transversal topology.....	26
Fig. 2.7.	A diagram shows that a 3-order transversal topology transforms into a wanted coupling topology.....	29
Fig. 2.8.	Bandpass filters. (a) Use impedance inverters. (b) Use admittance inverters.....	31
Fig. 2.9.	Generalized bandpass filters. (a) K -inverters. (b) J -inverters.....	31
Fig. 2.10.	Inverters. (a) Lumped-element K inverters. (b) Lumped- and distributed -elements K inverters. (b) Lumped-element J inverters. (b) Lumped- and distributed-elements J inverters.....	33
Fig. 2.11.	Pole-producing admittance inverters [57].....	34
Fig. 2.12.	Parallel- and antiparallel-coupled line circuits and its equivalent circuits... ..	35
Fig. 2.13.	(a) Electrical coupling. (b) Magnetic coupling. (c) Mixed coupling.....	37
Fig. 2.14.	Equivalent circuit of the I/O resonator with single loading.....	39
Fig. 2.15.	Typical coupling structures of coupled resonators. (a) Electric coupling. (b) Magnetic coupling. (c) and (d) Mixed coupling.....	40
Fig. 2.16.	A diagram of simulated responses of (a) electric coupling and (b) magnetic coupling.....	40
Fig. 2.17.	Two typical feeding structures of coupled-resonator filters. (a) Tapped-line line coupling. (b) Coupled-line coupling.....	41
Fig. 2.18.	A diagram of simulated responses of the circuits in Fig. 2.17(b).....	41

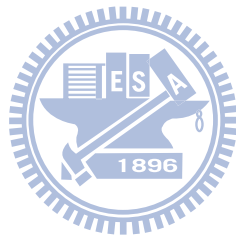
Fig. 2.19.	Quarter-wavelength stepped impedance resonator type.....	42
Fig. 2.20.	A 2-order cross-coupled bandpass filter circuit.....	44
Fig. 2.21.	Mapping between real frequency variable ω and distributed frequency variable Ω	46
Fig. 2.22.	Element transformation corresponding to the Richards transformation..	46
Fig. 2.23.	Richards transmission applied to an interconnecting transmission line..	47
Fig. 2.24.	A circuit used to illustrate the Richards theorem.....	48
Fig. 2.25.	The four Kuroda identities where $n^2 = 1 + Z_2/Z_1$	50
Fig. 2.26.	(a) A high-pass prototype circuit. (b) A low-pass prototype circuit.....	52
Fig. 3.1.	The circuit layouts of the proposed microstrip quarter-wave SIR filters. (a) The fourth-order quadruplet filter. (b) The fourth-order quadruplet filter with source-load coupling.....	57
Fig. 3.2.	Coupling schemes for the bandpass filters proposed in this dissertation. (a) Quadruplet. (b) Canonical form.....	58
Fig. 3.3.	The basic structure of the quarter-wave SIR.....	59
Fig. 3.4.	Basic coupling structures of the proposed filters. (a) The electric coupling. (b) The magnetic coupling. (c) The mixed coupling. (d) The coupled-line coupling for input/output coupling.....	60
Fig. 3.5.	The constructed filters. (a) The quadruplet filter. (b) The quadruplet filter with source/load coupling.....	62
Fig. 3.6.	Measured and simulated performances of the quadruplet filter of Fig. 4.5(a). (a) In a narrow-band. (b) In a wide band.....	63
Fig. 3.7.	Measured and simulated performances of the quadruplet filter with source /load coupling in Fig. 5(b). (a) In a narrow-band. (b) In a wide band....	64
Fig. 4.1.	The cross-coupled parallel coupled filter. (a) The schematic layout. (b) Coupling and routing scheme corresponding to (a).....	69
Fig. 4.2.	The equivalent lumped-element circuit of a fourth-order parallel coupled filter.....	70
Fig. 4.3.	The cascaded trisection filter. (a) The coupling scheme. (b) The corresponding equivalent lumped-element circuit of a fourth-order parallel coupled filter with cross couplings. Either the inverter J_{AD} or J_{AE} corresponds to M_{S2} and either the inverter J_{JF} or J_{JG} corresponds to M_{3L}	74
Fig. 4.4.	The mixed cascaded quadruplet and trisection filter. (a) The coupling scheme. (b) The corresponding equivalent lumped-element circuit of a fourth-order parallel coupled filter with cross coupling. Either the inverter	

	J_{AF} or J_{AG} corresponds to M_{S3} and either the inverter J_{JF} or J_{JG} corresponds to M_{3L}	74
Fig. 4.5.	The low-pass responses of the three CT filters with all in-band return loss 20dB. Case 1, normalized transmission zeros at $\Omega=3$ and $\Omega=-2$. Case 2, normalized transmission zeros at $\Omega=3$ and $\Omega=2$. Case 3, normalized transmission zeros at $\Omega=-3$ and $\Omega=-2$	77
Fig. 4.6.	The ideal responses of the two CQT filters. (a) The bandpass response corresponding to (3.4) with a typical Chebyshev response as a reference. (b) The bandpass response corresponding to (3.5).....	80
Fig. 4.7.	The circuit layouts of the proposed filters. (a) The first designed mixed cascaded quadruplet and trisection filter. The length and line width of coupling/shielding line are 4.318 mm and 0.177 mm, respectively. (b) The second designed mixed cascaded quadruplet and trisection filter...	81
Fig. 4.8.	The layouts of the implemented filters. (a) The first designed filter. (b) The second designed filter.....	83
Fig. 4.9.	The measured and simulated performances of the two implemented filters. (a) The first designed filter. (b) The second designed filter.....	86
Fig. 4.10.	The sensitivity analysis of the first mixed cascade quadruplet and trisection filter for under etching of 0.0508 mm (2mil) and over etching of 0.0508 mm respectively.....	86
Fig. 4.11.	The simulated performances of the first mixed cascaded quadruplet and trisection filter with finite transmission zeros at $\Omega=\pm 1.4, 4$	88
Fig. 4.12.	The simulated performances of the first mixed cascaded quadruplet and trisection filter with finite transmission zeros at $\Omega=+1.5, \pm 3$	90
Fig. 5.1.	Cross coupling schemes generating transmission zeros at precise frequencies. Conventional coupling schemes: (a) two-pole trisection. (b) three-pole cascade trisections (CQ). (c) three-pole quadruplet. Proposed coupling schemes: (d) two-pole interactive cross-coupling trisection scheme. (e) three-pole interactive cross-coupling quadruplet scheme. (f) four-pole interactive cross-coupling quadruplet scheme. (g) modified four-pole canonical form scheme with two pairs of transmission zeros. (h) modified three-pole cascade trisections (CT) scheme.....	94
Fig. 5.2.	(a) Parallel-coupled line section and (b) its equivalent circuit using a J -inverter.....	104
Fig. 5.3.	Ideal performances calculated from the synthesized coupling matrices in (5.13) solid line, and (5.15) dotted line.....	106
Fig. 5.4.	The layouts and the simulated and measured performances of the filters in	

	Fig. 5.1(d). (a) Layout for the design with a transmission zero at $\Omega=3$ (unit: mils). (b) Layout for the design with a transmission zero at $\Omega=-5$ (unit: mils). (c) Simulated and measured results corresponding to Fig. 5.4(a). (d) Simulated and measured results corresponding to Fig. 5.4(b).....	107
Fig. 5.5.	The proposed three-order CT filter. (a) Ideal real frequency responses. (b) Layout (unit: mils). (c) Simulated and measured results.....	108
Fig. 5.6.	The proposed third-order quadruplet filter. (a) Two ideal frequency responses: one is to consider the matrix in (5.19) solid line and the other is to exclude all the cross-coupling elements in (5.19) dotted line. (b) Layout (unit: mils). (c) Simulated and measured performances. (d) Layout for realizing the coupling scheme in Fig. 5.1(c).....	111
Fig. 5.7.	The modified fourth-order quadruplet filter. (a) Ideal responses. (b) Layout (unit: mils). (c) Simulated and measured performances.....	112
Fig. 5.8.	The modified fourth-order quadruplet filter with source-load cross coupling. (a) Layout (unit: mils). (b) Simulated and measured performances.....	113
Fig. 6.1.	The distributed circuit of the proposed fifth-order Marchand balun.....	116
Fig. 6.2.	The proposed fifth-order Marchand balun. (a) The two-port distributed circuit simplified in Fig. 6.1. (b) Its S -plane high-pass circuit.....	117
Fig. 6.3.	The first transformation. (a) The kuroda identity transformation from [131]. (b) After kuroda identity transformation in Fig. 6.2(b).....	119
Fig. 6.4.	The second transformation. (a) New exact circuit transformation. (b) Apply exact circuit transformation in Fig. 6.4(a) to Fig. 6.3(b).....	120
Fig. 6.5.	The final fifth-order S -plane high-pass prototype of Marchand balun...	120
Fig. 6.6.	The ideal responses of the first and second designed baluns with bandwidth of 131% and 152%, respectively.....	125
Fig. 6.7.	Physical layout of the first designed fifth-order balun with $S_C=j0.6$ (unit: mm).....	126
Fig. 6.8.	Measured and simulated performances of the first designed fifth-order balun. (a) $ S_{11} $, $ S_{21} $ and $ S_{31} $. (b) Amplitude balance and phase difference.....	126
Fig. 6.9.	Physical layout of the second designed fifth-order balun with $S_C=j0.4$ (unit: mm).....	127
Fig. 6.10.	Measured and simulated performances of the second designed fifth-order balun. (a) $ S_{11} $, $ S_{21} $ and $ S_{31} $. (b) Amplitude balance and phase difference	

.....128

Fig. 6.11. The sixth-order *S*-plane high-pass prototype of Marchand balun.....129



Chapter 1 Introduction

This dissertation includes two topics. The first topic is devoted to novel microwave cross-coupled filter design. The second topic is to design new higher-order Marchand balun based on exact synthesis technique.

1.1 Microwave Filters

Microwave filters are one of the important components in modern microwave communication systems. The frequency of *microwave* ranges from 300 MHz to 300 GHz corresponding to wavelengths (in free space) from 1 m to 1mm. The concept of electromagnetic waves should be used to describe the features of microwave components including microwave filters. Microwave filters are used to pass the wanted signals at frequencies within the passband and suppress the unwanted signals in the stopband. Filters for microwave applications must meet ever tighter specifications on electrical performances, and on size, weight, and reliability. The demands are growing more stringent on losses, steepness of cutoff, bandwidth, and linearity of phase shift (flat group delay). New features such as electronic tunability are being sought. Integrations of microwave filters with couplers, amplifiers, and frequency multipliers are becoming more important on system performance. To handle the rapid advance of applications of the modern communication systems, network analysis, accurate synthesis, design and diagnosis of filter networks have become one of the key technologies to fulfill the new challenges of reliability, insensitivity, low manufacturing cost, and minimum tuning effect on filter performance [1]-[2]. The historical review describing the development of the microwave filters is given in [3]-[5]. Different filter types and important references are given. Recently, among various kinds of microwave filters, microwave coupled-resonator filters are very popular. Generally, coupled-resonator filters with

cross coupling between nonadjacent resonators can exhibit steeper transfer function or flatter group delay, and they are called cross-coupled filters. The theory of cross-coupled filters [6], [7] provides a systematic design procedure that allows a filter with sharper selectivity and/or equalized group delay for various requirements in microwave systems. Most important characteristics of cross-coupled filters can be obtained by the corresponding coupling matrices.

1.1.1 Review of Coupled Resonator Filters and Cross-Coupled Filters

Initially, the research work on the design and synthesis of microwave filters can be traced back to the 1930's [3]. At that time, network theory was probably the most advanced topic in engineering. The famous cascade synthesis theory as far back as 1939 [8] was published by S. Darlington. In his work, modern filter designs such as filters with finite frequency transmission zeros are included. The theory of direct-coupled cavity filters based on low-pass lumped-element prototype was presented by Fano and Lawson [3]. The main problem of Fano and Lawson theory was the lack of specific formulas for the low-pass prototype. The paper proposed by Cohn in [9] gives a comprehensive theory and extends the range of applicability to much broader bandwidths, i.e., about 20 percent in terms of guide wavelength. Later, in the 1960's, a remarkable improvement in the applicable bandwidth to beyond 20 percent was made by Leo Young [10]. He succeeded in realizing the direct-coupled filters beyond 20 percent by using a distributed rather than a lumped-element prototype filter. In 1966, Levy [11] established a quite direct design in cavity filters and, thus enabling the desired parameters of the filter, i.e., number of cavities, ripple level, and band edges to be a simple formula which is used to derive the correct distributed prototype.

The first description of cross-coupled filters may be appeared to be by J. R. Pierce in the late 40's [12]. However, the developments of cross-coupled filters took

place after 1965 or so. The cross coupling between nonadjacent resonators are introduced to generate transmission zeros. The cross coupling are mainly generated by the multipath. Applying suitable multi-path effect can bring transmission zeros from infinite to finite frequencies in the transfer function. Thus, attenuation poles at finite frequencies, or group delay flattening, or even both simultaneously can be achieved by observing the phases of the signals between different paths. A lot of related research works on the filter with cross coupling have been reported [12]-[33]. Furthermore, filter synthesis utilizing optimization techniques [34], [35] are used to obtain the required filtering functions.

Synthesis technique and implementation methods for the cross-coupled filters, which are shown in [12]-[35], have been developed for couples of decades. The most significant developments took place in the 1970's in laboratories concerned with satellite communications, particularly at COMSAT by Atia and Williams [19]-[20], [23]. Their work on elliptic function and linear-phase waveguide filters using dual-mode cavities with cross coupling was particular significant. The dual-mode cavity filters introduced by Atia and Williams have resulted in the virtual standardization of these designs for satellite transponders.

Recently, one of the most important progresses in generalized filter synthesis is done by Richard Cameron. Richard Cameron published two papers [36], [37] which focused on generalizing the synthesis technique for the cross-coupled resonator filter with the generalized Chebyshev filtering function. With his work, N prescribed finite-position transmission zeros in an N th-degree network are described. The synthesis method includes multiple input/output couplings, i.e., couplings may be made directly from the source and/or to load to internal resonators. The synthesized $N+2$ fully canonical coupling matrix for transversal array can completely describe all the possible generalized Chebyshev responses. With a series of similarity

transformations, the fully canonical coupling matrix can be reconfigured into a wanted coupling topology which is more convenient for the realization. The basic theory will be shown in Chapter 2.

Another attractive topic developed for several decades is the computer-aided diagnosis and tuning of cross-coupled filters. This is due to the continuous demand on reducing the manufacturing cost and development time for various filters with different specifications. It should be pointed out that filters with generalized Chebyshev responses are more difficult to fine tuned than that with Chebyshev or Butterworth responses. Thus, without a systematic adjustment method, it would spend much time on the tuning of filter performances, particularly for highly selective filters. Several research works focused on this problem [38]-[51]. The first effort for the adjustment and alignment of microwave filters can be traced back to Dishal [38] in the early 50's when he utilized the filter return loss as the criterion for tuning. Atia and Williams [39] proposed a method for measurement of inter-resonator couplings based on measuring the phase responses of the reflection coefficient of a short-circuited network which consists of identical synchronously-tuned resonators. Thal [40] utilized the equivalent circuit in conjunction with phase measurement for filter diagnosis. In [41], a tuning method with short circuited networks for singly terminated filters is presented. In [42]-[44], different optimization strategies and schemes for parameter extraction are explored. Analytic methods in [45]-[47] are derived to extract the coupling matrix from the locations of system zeros and poles. In [48]-[50], the powerful Cauchy method is applied to get the rational polynomial approximation of reflection and transmission coefficients from the EM simulated results. In [51], eigenvalue approach is used to optimize the coupling matrix. The method in [52] utilized the Cauchy method in [48]-[50] to obtain the corresponding coupling matrix, and then optimize the rotation matrix to get the wanted coupling

topology. Besides, sensitivity of coupled resonator filters is analyzed in [53]. Thus, research concerning about cross-coupled filters have been studied for a long time, and up to present some researches are presenting.

1.1.2 Motivation

The requirements of highly selectivity, flat group delay, compact sizes, and wider rejection bandwidth are the significant studies of microwave filters. In addition, high reliability, low sensitivity, low manufacturing cost, and minimized fine-tuning steps on filter performance are also important.

Filters exhibiting high selectivity, broader upper stopband, and compact sizes are popular topics. Many published papers have achieved the requirements. However, the design method to control the finite transmission zeros is complex or difficult in most of the published papers. Furthermore, the layouts are usually too complicated for the published filters. To overcome the difficulties, a filter utilizing a 4-order canonical-form coupling scheme with $\lambda/4$ stepped impedance resonators may be a good choice.

In conventional cross-coupled filter designs, especially for microstrip filters, adjustment the distance and the orientation of each pair of neighboring resonators to get proper signs and magnitudes of the corresponding coupling coefficients is very tedious and time-consuming. The design curves of coupling coefficient and external Q for filters are generated from an electromagnetic (EM) field solver. Such filter designs can be found in Hong's book [6]. When using this method as the initial dimensions of filters, filter designer has to spend much time to tune filter performances. To solve the drawbacks, new procedures to quick design of cross-coupled filters are demanded.

Another interesting topic is coupling schemes. The traditional 3-order trisection filter has one transmission zero on upper or lower stopband and the 4-order quadruplet filter has a pair of transmission zeros on both stopband. The order of the

advanced trisection and quadruplet can be two and three, respectively. However, there are problems of conventional or advanced trisection and quadruplet. As the transmission zero is close to the passband, serious asynchronously-tuned resonators for trisection cause serious effect on filter passband responses. Besides, when finite transmission zeros are very close to the passband, both trisection and quadruplet filters suffer from unrealizable gaps to implement the strong cross couplings. Thus, the solution of the problems may require new coupling schemes which can achieve trisection and quadruplet responses with transmission zeros close to the passband.

With the discussion described above, the first topic in this dissertation mainly focuses on different circuit design of filter with compact sizes, high selectivity and broad upper stopband, the development of new approach to cross-coupled filters, and novel coupling schemes with transmission zeros very close to passband.

1.1.3 Literature Survey of Coupling Schemes and Realizations of Cross-Coupled Resonator Filters

The existing well-known coupling schemes and the realizations of these coupling schemes are surveyed as follows.

In the past, numbers of research works concentrate on the coupling topologies of canonical form, cascade trisection (CT), and cascade quadruplet (CQ) [6], [24], [54]-[61]. Recently, the progressive development is to include source and load to nonadjacent resonator cross coupling [7], [52], [63]-[67]. The implementations of the three different coupling schemes were presented in [68]-[85]. In [70], the cross-coupling concept was firstly applied to the microstrip filters. Because of the increasing power of computations of computers, Hong and Lancaster introduced the method that by using electromagnetic (EM) simulators to get the S -parameters of the desired structure the cross-coupled resonator filters realized in microstrip line can be designed [70]-[72]. The coplanar waveguide structure is also presented to design

cross-coupled filters [83], [84]. Furthermore, broadside coupled coplanar stripline bandpass filters are designed to have finite transmission zeros successfully [85]. All the papers in [68]-[85] can use this method to design canonical form, cascade trisection, and cascade quadruplet filters with finite transmission zeros.

Recently, coupling schemes which exhibit so called zero-shifting properties were introduced and applied to waveguide resonator filters [66], [86], [87]. The main characteristic of the zero-shifting properties is the ability to shift a transmission zeros from one side of the passband to the other by adjusting the resonator frequencies of resonators instead of changing the sign of cross coupling. The doublet, extended doublet and box section with zero-shifting characteristic have been successfully implemented in microstrip form [88]-[90]. However, the coupling schemes are inherently sensitive due to the two main coupling paths.

As described above, it is worth studying new cross-coupled schemes and filter structures to solve these disadvantages.

1.1.4 Original Contribution of this Dissertation

The main contributions to cross-coupled filters in the first topic of this dissertation are addressed in three aspects.

First, a fourth-order canonical-form microstrip filter utilizing quarter-wave stepped-impedance resonators is presented. The requirements of compact sizes, sharp selectivity, and wide upper stopband for filters are achieved. The proposed circuit layout is easy to apply the source-load coupling and adjust the coupling strength.

Second, filters based on a conventional parallel-coupled structure [91]-[94] which exhibit generalized Chebyshev responses are proposed. The cross-coupled mechanisms of the proposed filters are originally investigated and presented. The observations of the two-port admittance matrix in the network can obtain the relative insertion phase from source or load to each open end of resonators. Thus, the cross

coupling can be applied using a delay line with proper electrical length. Due to the use of a conventional parallel-coupled structure, good initial dimensions can be obtained by the analytic method. Using the proposed structure, the conventional time-consuming adjusting procedure to obtain initial physical dimensions of filters, which is described in [6], is no longer required. Two fourth-order mixed cascade quadruplet and trisection filters are implemented to show properties of insensitive layout, flexible responses, good performance, and quick design procedures. With this approach, designer can eliminate tedious segmentation method for the filter design.

Finally, in this dissertation new coupling schemes where the corresponding coupling matrices show the bisymmetric property are proposed. Most of new coupling schemes have the properties of synchronous-tuned resonators, bisymmetric coupling matrices, and relatively weak cross-coupled strengths for finite transmission zeros very close to the passband. Filters with symmetrical layout are possible to implement the proposed bisymmetric coupling matrix that fine tuning of the filter would be much easier. Low-order planar filters with the proposed coupling schemes can achieve high selectivity.

1.2 Balun

In an unbalanced port, one of its two terminals is connected to the ground, an example being the output of a conventional signal generator. A balanced port, on the other hand, is one where both terminals are floating with respect to ground. Baluns are devices for interconnecting a balanced port to an unbalanced one. The ideal balun is a lossless, perfectly matched, two-port network whose properties are independent of frequency and power level, and may also provide impedance transformations as well. The ideal balun can be realized by the ideal transformer shown in Fig. 1.1, and deviations from the ideal depend solely on how closely one can realize the ideal transformer in practice.

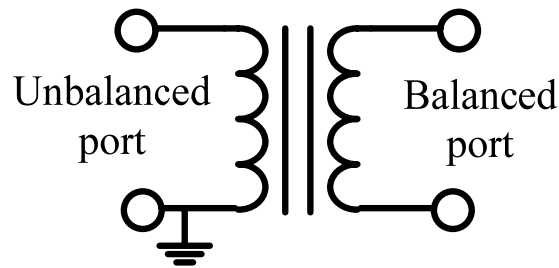


Fig. 1.1. Realization of an ideal balun by an ideal transformer.

1.2.1 Literature Survey

Baluns (balanced-to-unbalanced) are important group of components which are used in circuits where a transition between unbalanced and balanced modes of excitation is required. The applications of baluns are frequently used in realizing balanced mixers, amplifiers, frequency multipliers, phase shifters, modulators, and dipole feeds, and numerous other applications. Over the past half-century, several different kinds of baluns [102]-[126] have been developed, and some research works on active baluns [127]-[129] are also attractive. In the course textbook [94], the contents of baluns and its applications may be good resources.

Among the various kinds of baluns, Marchand balun [102] is relatively popular because of its excellent amplitude and phase balance. Marchand's famous paper [102] was published in December 1944. Marchand described three types of balun of increasing complexity and performance, which are shown in Fig. 1.2. The most sophisticated of the three types of baluns is shown in Fig. 1.2(c). The direct inspection of third type of balun can obtain the equivalent circuit shown in Fig. 1.3. To analyze and synthesize this balun the electrical lengths of the open and short-circuit stubs as well as the lengths of transmission lines must be the same, in which case the lengths of transmission lines are referred to as Unit Elements (U.E.) in filter technology. The description of Unit Elements will be discussed in Chapter 2.

In December 1957, Roberts [103] published a paper describing the coaxial balun

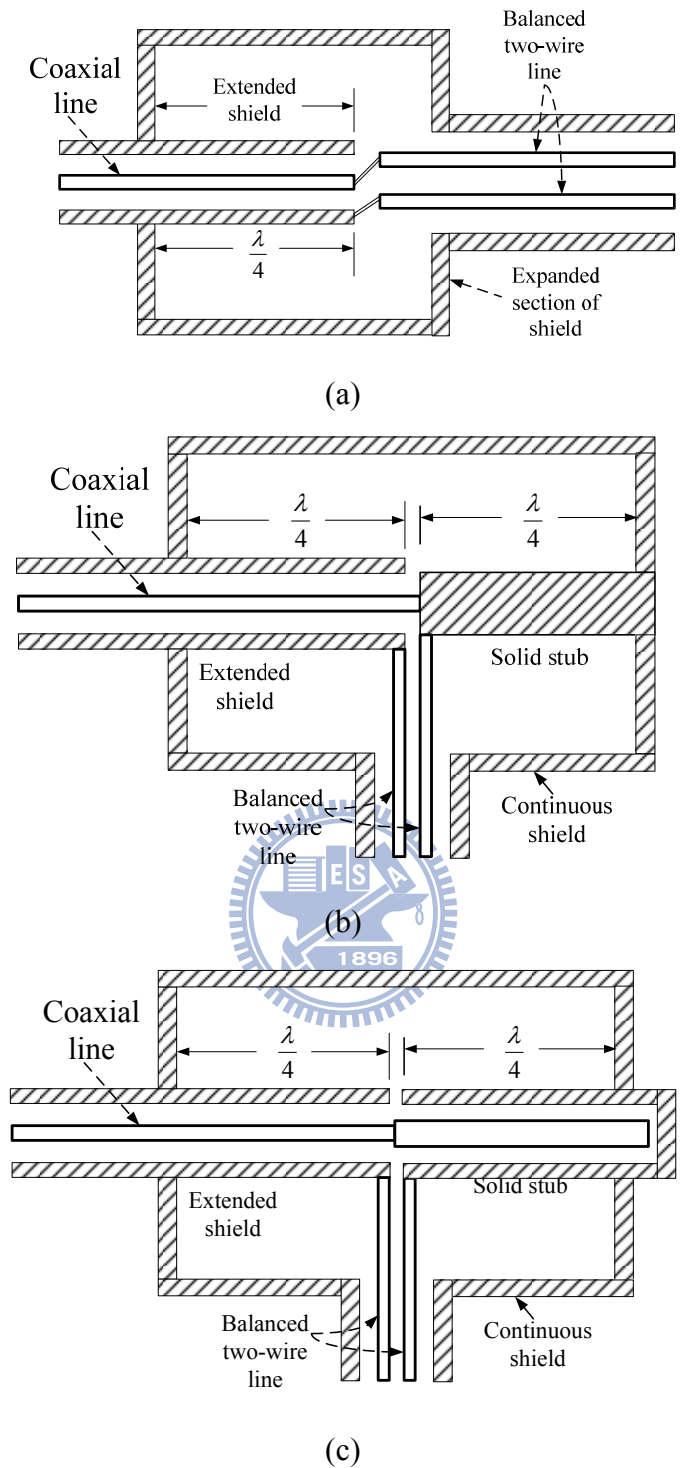


Fig. 1.2. Marchand balun. (a) Type 1. (b) Type 2. (c) Type 3.

shown in Fig. 1.4. Interestingly, the equivalent circuit of this coaxial balun is exactly the same as Marchand's but the author made no reference to Marchand in his paper. However, the Roberts balun is a little easier to construct than Marchand's.

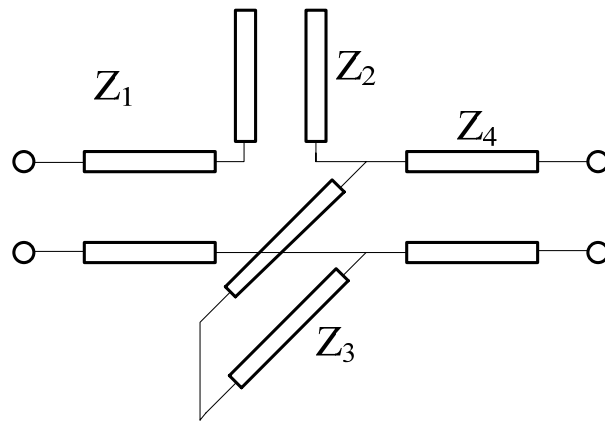


Fig. 1.3. Equivalent circuit of Marchand balun.

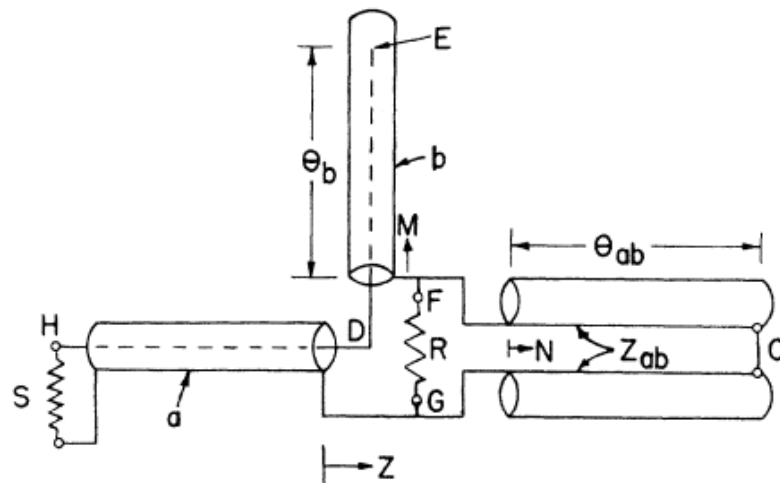


Fig. 1.4. Roberts balun (clipped from Fig. 3 in [103]).

Due to the equivalent circuit prototype shown in Fig. 1.3, the Marchand and Roberts balun are inherently band-pass networks. The simplest design techniques for these two baluns is to set Z_1 and Z_4 to the unbalanced and balanced port impedances, respectively, and then the characteristic impedances of the two stubs can be designed from standard lumped element filter theory [6], [26]. The electrical lengths of the stubs and transmission lines are 90° at the center frequency of the balun. The responses of the baluns can be maximally flat (Butterworth) or equiripple (Tchebyshev) which depend on the values of the characteristic impedances.

In the 1980's, two important papers proposed by Cloete [106], [107] showed graphs of the element values as a function of bandwidth and passband return loss of

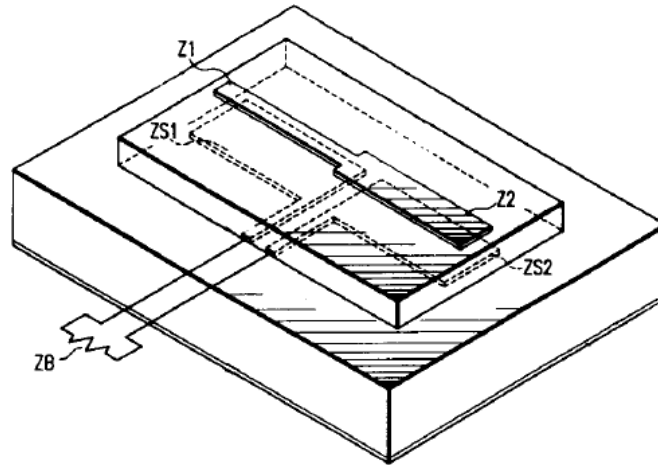


Fig. 1.5. Broadside-coupled balun (clipped from Fig. 2 in [111]).

the Marchand balun. Cloete designed a fourth-order Marchand balun with 15dB return loss over a decade bandwidth. The only limitation to use the design chart is that the balanced and the unbalanced ports can not have the same port resistance, but a 2:1 port resistance ratio. However, this is convenient if an anti-phase power divider is wanted instead of a balun since the 100 Ohms balanced load can be replaced by a 50 Ohm load connected between each of the balanced port's terminals and ground.

There has been much interest in developing a planar structure of the Marchand or Roberts balun for use in monolithic and hybrid integrated circuits. One of the first papers to concern this issue is proposed by Pavio and Kikel [111]. The paper shows a whole view of the proposed structure, and this circuit is similar to Marchand balun. A broadside-coupled stripline structure is used to construct the balun, as shown in Fig. 1.5. The upper dielectric is very thin compared with the lower one, and, thus, considering coupling between the upper conductor and the ground plane could be ignored. So, the structure in Fig. 1.5 could be viewed as simply two transmission lines with upper and middle conductor forming one transmission line, and with the middle and lower conductor forming the other one. However, this structure is inherently a

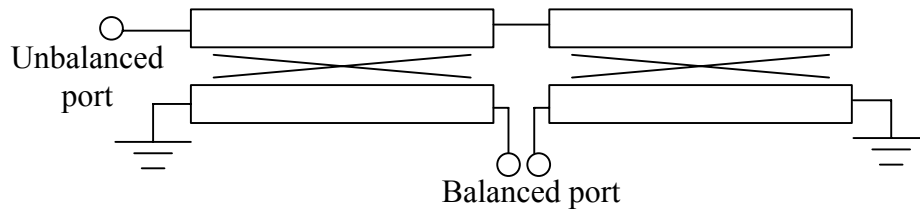


Fig. 1.6. A coupled-line Marchand balun.

three-conductor coupled-line network, and detailed analysis of the structure must be taken into account.

Fig. 1.6 shows the coupled-line form of the edged-coupled planar Marchand balun. Several research works [115], [119], [120], [122], [125], [126] have focused on this edged-coupled version of Marchand balun. Goldsmith *et al.* [115] published the first comprehensive analysis of Fig. 1.6. The key point of analyzing coupled-line Marchand balun is that the two coupled-line sections have the same coupling coefficient. This results in the largely simplified design equations, which can be found in [119]. The design parameters derived by Goldsmith have successfully being connected to the coupling coefficient and even- and odd-mode impedances of the two coupled-line sections, which can be easy transformed into the physical parameters by using ADS or AWR circuit simulators. However, to design a balun having a decade bandwidth is not an easy task based on this coupled-line form of Marchand balun.

1.2.2 Objective and Contribution in the Second Topic of this Dissertation

The objectives of this balun research are to develop higher-order Marchand-type balun and to realize it in planar structure. With the proposed 5-order Marchand balun, a very wide bandwidth (152%) can be achieved, and the novel realization of the balun is to utilize microstrip line, slot line, and coplanar stripline. The 5-order Marchand baluns are synthesized by use of the Richard's transformation and, thus, it means that the responses of the synthesized Marchand balun are exactly predicted at all

frequencies. Two examples of the 5-order Marchand balun are presented to demonstrate the design procedures. In addition, a 6-order Marchand balun is presented to discuss.

1.3 Organization of this Dissertation

This dissertation is organized as follows.

In Chapter 2, the first part is to introduce the basic theory of cross-coupled filters. The model of the cross-coupled filter in low-pass domain is given. The relation between a coupling matrix and S -parameter is derived from the model. Then, how to directly obtain the position of finite transmission zeros to a given coupling matrix is given. A conventional 3-order trisection is taken as an example. Some of interesting coupling schemes are arranged in a Table. A simple recursive formula to determine the generalized Chebyshev polynomials is given. Importantly, a general method for the synthesis of the coupling matrix in the transversal array is discussed. How to transform the coupling matrix from the transversal topology to the wanted coupling schemes by utilizing both eigenvalue approach and optimization is given. Lowpass prototype, generalized bandpass filters, impedance and admittance inverters, and the narrowband equivalence between coupled-line circuits and impedance and admittance inverters with transmission lines are introduced. Furthermore, coupled-resonator theory for extraction of external Q and coupling coefficients is given. To manipulate the spurious responses, the basic characteristics of stepped impedance resonators are discussed. How to obtain the relations between the coupling matrix and design parameters of coupled-resonator filters is presented. Those contents are useful in designing the cross-coupled filters which will be proposed in Chapter 3-5.

The second part in Chapter 2 is to consider distributed transmission line elements. To exactly synthesize the distributed transmission line networks, the Richards variable

and Richard theorem should be concerned and will also be discussed. The basic four Kuroda identities are given. General low- and high-pass S -plane prototype circuits are presented, and its corresponding characteristic functions are given. In addition, a synthesizing procedure is briefly discussed.

In chapter 3, two filters exhibiting quadruplet and canonical-form responses are designed. To extend the bandwidth of stopband, quarter-wave stepped impedance resonators are used. The use of the enhancing line of source-load coupling results in one additional pair of finite transmission zeros.

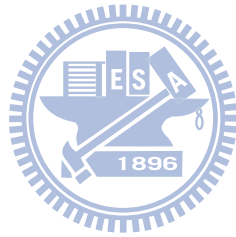
Chapter 4 describes microstrip parallel-coupled filters with generalized Chebyshev responses. The mechanism for generating finite transmission zeros is presented. The design procedures are discussed in detail. Two mixed cascade quadruplet and trisection filters are realized to demonstrate the feasibility. Furthermore, sensitivity analysis and a design guide to show the closest transmission zeros corresponding to realizable physical dimensions are discussed by taking examples.

In chapter 5, new coupling schemes with the properties of bisymmetric coupling matrix, weak cross couplings, and synchronous-tuned or very tiny asynchronous-tuned resonators are presented. Bisymmetric coupling matrices imply symmetric layouts. The comparison between conventional and new proposed coupling schemes are discussed. The proposed bisymmetric coupling schemes can be used for the implementation of generalized Chebyshev filters with transmission zeros very close to the passband in planar technology.

Chapter 6 presents new higher-order Marchand balun with ultra wideband performances. Two network transformations, one is the Kuroda identity and the other is the proposed circuit transformation, are utilized to derive the final S -plane prototype circuit of Marchand balun. The exact synthesis and realization of the

proposed Marchand balun are discussed in detail.

In Chapter 7, conclusions and future works are given.



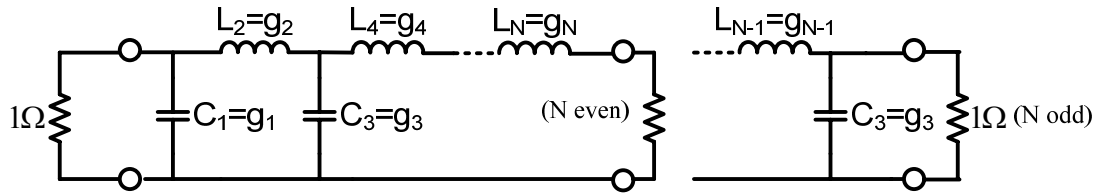
Chapter 2 Theory of Microwave Resonator Filters and Distributed Circuit Design

2.1 Basic Theory Used in Cross-Coupled Filters

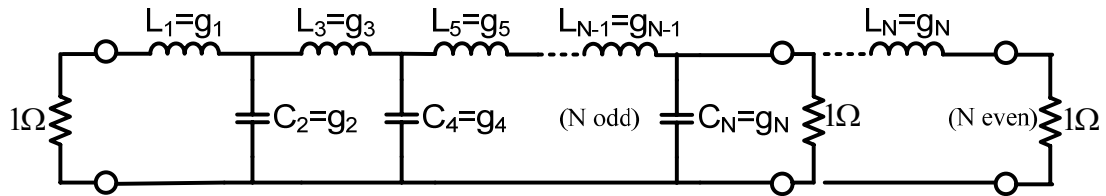
In this section, the basic theory and design techniques for cross-coupled filters will be introduced. At first, the cross-coupled resonators network corresponding to the coupling matrix is analyzed in the normalized frequency domain. The relations between the normalized network parameters and S -parameters are derived. How to obtain the position of finite transmission zeros from coupling topologies is also given. In section 2.1.2, different types of impedance and admittance inverters are introduced, and the corresponding equivalent circuits are also presented. The frequently used coupled-line circuits and their equivalent circuits are provided. The segmentation method which is used to extract the external Q and the coupling coefficients is discussed in Section 2.1.3. Next, the characteristics of step impedance resonators will be reviewed. Finally, how to transform the synthesized coupling matrix to the design parameters of cross-coupled filters will be derived.

2.1.1 Synthesis Theory of Advanced Coupling Matrix in the Normalized Domain

The design of microwave filters normally starts from the synthesis of a low-pass prototype network which is shown in Fig. 2.1. Low-pass prototype networks are two-port network with an angular cutoff frequency of 1 rad/s and operating in a 1- Ω system. This type of lowpass filter can serve as a prototype for designing various practical filters with frequency and element transformations. The corresponding g values with different frequency responses, i.e. Butterworth, Chebyshev, Elliptic function, and Gaussian responses, can be computed [6]. The alternative networks with impedance and admittance inverters as shown in Fig. 2.2 are also used. The networks in Fig. 2.2 can be represented by coupling matrices and are very useful for the design

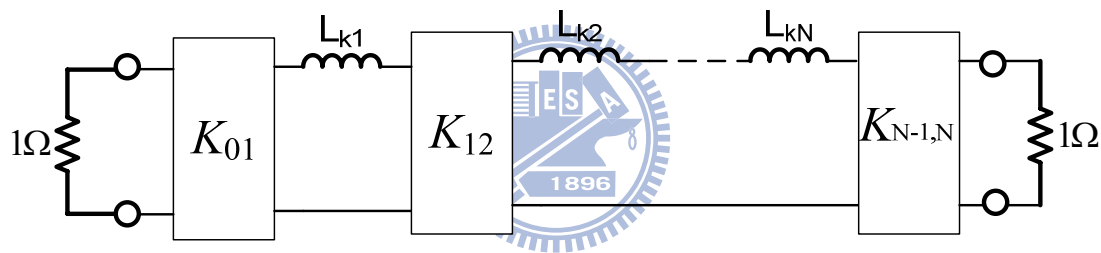


(a)

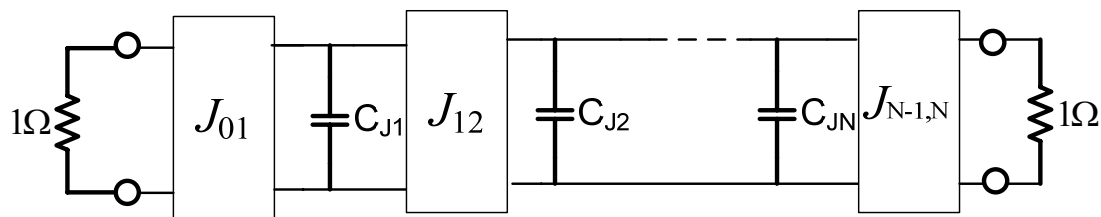


(b)

Fig. 2.1. Lowpass filter prototypes with ladder networks. (a) Begin with a shunt capacitor. (b) Begin with a series inductor.



(a)

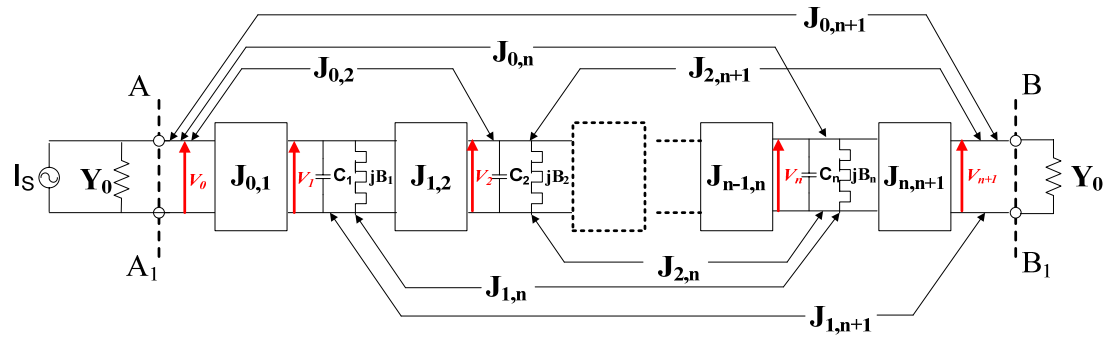


(b)

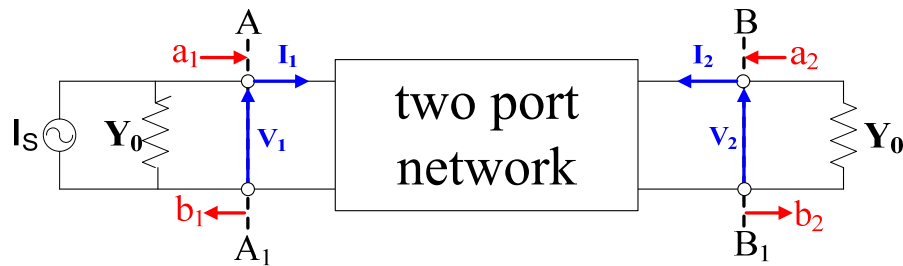
Fig. 2.2. Alternative lowpass prototype networks using inverter. (a) K -inverters. (b) J -inverters.

of narrow band bandpass filter. So far, the cross coupling is not involved.

A general cross-coupled filter prototype of degree n in the lowpass domain is shown in Fig. 2.3 (a) [7], [90]. It is shown that this prototype can be obtained by

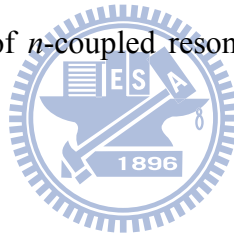


(a)



(b)

Fig. 2.3. (a) Equivalent circuit of n -coupled resonators in low pass domain. (b) Its network representation.



including all possible cross-coupling elements and frequency shifts of resonators. The prototype filter consists of frequency independent impedance inverters $J_{i,j}$ s, capacitors C_i s and susceptances B_i s. The values of all the capacitor and the terminated admittance Y_0 are set equal to one. The capacitors in the low-pass domain correspond to the resonators in the bandpass domain. Thus, the frequency invariant susceptance B_i represent the frequency shift of resonators in the bandpass domain. The values of B_i are zero for the synchronous filters and nonzero for the asynchronous filters. Applying circuit analysis of Kirchhoff's current law to this prototype and stating the algebraic sum of the currents leaving a node in a network is zero, with a driving with a driving or external current of I_s , the node equations for the circuit of Fig. 2.3(a) are shown in (2.1),

$$\begin{bmatrix} Y_0 & jJ_{0,1} & jJ_{0,2} & \cdots & jJ_{0,n+1} \\ jJ_{0,1} & j\Omega + jB_1 & jJ_{1,2} & \cdots & jJ_{1,n+1} \\ jJ_{0,2} & jJ_{1,2} & \ddots & & \vdots \\ \vdots & \vdots & & j\Omega + jB_n & jJ_{n,n+1} \\ jJ_{0,n+1} & jJ_{1,n+1} & \cdots & jJ_{n,n+1} & Y_0 \end{bmatrix}_{(n+2) \times (n+2)} \begin{bmatrix} V_0 \\ V_1 \\ \vdots \\ V_n \\ V_{n+1} \end{bmatrix}_{(n+2) \times 1} = \begin{bmatrix} I_s \\ 0 \\ 0 \\ \vdots \\ 0 \end{bmatrix}_{(n+2) \times 1} \quad (2.1)$$

where Ω is the normalized frequency. The two-port S -parameters of a coupled-resonator filter can be derived by the corresponding two-port network as shown in Fig. 2.3(b). Comparing Fig. 2.3(a) and Fig 2.3(b), one can find that $V_1=V_0$, $V_2=V_{n+1}$, and $I_1=I_s-Y_0V_0$. And

$$a_1 = \frac{I_s}{2}, \quad b_1 = \frac{2V_0 - I_s}{2}$$

$$a_2 = 0, \quad b_2 = V_{n+1}$$

Thus,

$$S_{11} = \left. \frac{b_1}{a_1} \right|_{a_2=0} = -1 + \frac{2V_0}{I_s} \quad (2.2)$$

$$S_{21} = \left. \frac{b_2}{a_1} \right|_{a_2=0} = \frac{2V_{n+1}}{I_s} \quad (2.3)$$

From (2.1), we can obtain

$$\frac{V_0}{I_s} = [Y]_{1,1}^{-1} \quad (2.4)$$

$$\frac{V_{n+1}}{I_s} = [Y]_{(n+2),1}^{-1} \quad (2.5)$$

Substitute (2.4) into (2.2), one can obtain

$$S_{11} = -1 + 2[Y]_{1,1}^{-1} \quad (2.6)$$

Substitute (2.5) into (2.3), thus enable obtaining

$$S_{21} = 2[Y]_{n+2,1}^{-1} \quad (2.7)$$

In the literatures, the matrix

$$\begin{bmatrix} 0 & J_{0,1} & J_{0,2} & \cdots & J_{0,n+1} \\ J_{0,1} & B_1 & J_{1,2} & \cdots & J_{1,n+1} \\ J_{0,2} & J_{1,2} & \ddots & & \vdots \\ \vdots & \vdots & & B_n & J_{n,n+1} \\ J_{0,n+1} & J_{1,n+1} & \cdots & J_{n,n+1} & 0 \end{bmatrix}$$

is called the normalized coupling matrix and denoted as matrix $[M]$.

$$[M] = \begin{bmatrix} 0 & M_{S1} & M_{S2} & \cdots & M_{SL} \\ M_{S1} & M_{11} & M_{12} & \cdots & M_{1L} \\ M_{S2} & M_{12} & \ddots & & \vdots \\ \vdots & \vdots & & M_{nn} & M_{nL} \\ M_{SL} & M_{1L} & \cdots & M_{nL} & 0 \end{bmatrix}$$

where $M_{ij}=J_{i,j}$, $M_{ii}=B_i$. The admittance matrix is related to the normalized coupling matrix, and can be expressed as

$$[Y] = s[I] + j[M] + [G] = j(\Omega[U]_0 + [M] - j[G]) = j[A],$$

where $[A] = \Omega[U]_0 + [M] - j[G]$, $[U_0] \in R^{(n+2) \times (n+2)}$ is identical to the identity matrix, except for the element $[U_0]_{11} = [U_0]_{n+2,n+2} = 0$, and $[G] \in R^{(n+2) \times (n+2)}$ is also a diagonal matrix, $[G] = \text{diag}\{1, 0, \dots, 0, 1\}$. The equations (2.6) and (2.7) can be rewritten as

$$S_{11} = -1 - 2j[A]_{1,1}^{-1} \quad (2.8)$$

$$S_{21} = -2j[A]_{(n+2),1}^{-1} \quad (2.9)$$

Similarly, one can derive

$$S_{22} = -1 - 2j[A]_{n+2,n+2}^{-1} \quad (2.10)$$

The equations (2.8), (2.9) and (2.10) directly related the normalized coupling matrix to the S -parameters.

In the following, it will be shown that the position of finite transmission zeros can be predicted through transfer function. From the equations (2.8) and (2.9), one

can express S_{11} and S_{22} as rational functions,

$$S_{11}(\Omega) = \frac{F(\Omega)}{E(\Omega)} \quad (2.10)$$

$$S_{21}(\Omega) = \frac{P(\Omega)}{E(\Omega)} \quad (2.11)$$

Obviously, the finite transmission zeros are the roots of the equation

$$P(\Omega) = 0 \quad (2.12)$$

Solving the equation (2-12) can help to understand the dependence between the coupling coefficients and finite transmission zeros, thus enabling to get more insight to control the finite transmission zeros. An example to illustrate this procedure would be clear. Take a conventional 3-order trisection coupling scheme shown in Fig. 2.4 as an example.

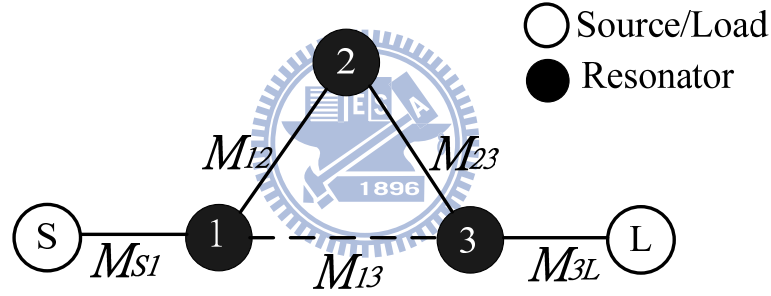


Fig. 2.4. The coupling route of the example filter

The coupling matrix corresponds to the coupling topology of Fig. 2.4 is

$$M = \begin{bmatrix} 0 & M_{S1} & 0 & 0 & 0 \\ M_{S1} & M_{11} & M_{12} & M_{13} & 0 \\ 0 & M_{12} & M_{22} & M_{23} & 0 \\ 0 & M_{13} & M_{23} & M_{33} & M_{3L} \\ 0 & 0 & 0 & M_{3L} & 0 \end{bmatrix} \quad (2.13)$$

By solving $P(\Omega) = 0$, one can find the roots, and it can be expressed as

$$\Omega = -M_{22} + \frac{M_{12}M_{23}}{M_{13}} \quad (2.14)$$

When $-M_{22} + (M_{12}M_{23}/M_{13}) > 0$, a transmission zero on upper stopband occurs.

Coupling schemes		
<p>2-order trisection</p>	<p>3-order trisection</p>	<p>3-order cascade trisection</p>
<p>3-order quadruplet</p>	<p>4-order quadruplet</p>	<p>4-order mixed cascade quadruplet and trisection</p>
<p>4-order canonical form</p>	<p>Doublet</p>	<p>Extended doublet</p>
<p>Box section</p>	<p>Cul-de-sac</p>	<p>5-order cascade quadruplet</p>

Table 2.1 Interesting well-known coupling topologies.

While $-M_{22} + (M_{12}M_{23}/M_{13}) < 0$, a transmission zero on lower stopband is created.

Several interesting well-known coupling schemes [6], [7], [66], [67] are shown in Table 2.1.

From the discussion as described above, we know the cross-coupled filter exhibits finite transmission zeros (attenuation poles), which means the responses of cross-coupled filters may correspond to the generalized Chebyshev responses. In fact, how to generate the $S_{11}(s)$ and $S_{21}(s)$ corresponding to the generalized Chebyshev functions and find the corresponding coupling matrices are important and

well-established. Many synthesis methods for cross-coupled filters have been proposed in [20], [34]-[37]. In this dissertation, we adopted the simple recursion formula [34] proposed by Smain Amari to determine the low-pass prototype with generalized Chebyshev responses and focused on the transversal array method [37] proposed by Richard Cameron to obtain coupling matrices.

The reflection and transfer polynomials of cross-coupled filters with generalized Chebyshev responses can be obtained by using the recursion formula as follows. The transfer function $S_{21}(\omega')$ is

$$|S_{21}(\omega')|^2 = \frac{1}{1 + \varepsilon^2 F_N^2(\omega')} \quad (2.15)$$

where ω' is the frequency variable in a low-pass prototype, ε is a constant related to the inband return loss R which is

$$\varepsilon = [10^{R/10} - 1]^{1/2} \quad (2.16)$$

The characteristic filtering function $F_N(\omega')$ is

$$F_N(\omega') = \cosh\left(\sum_{n=1}^N \cosh^{-1}(x_n)\right), \quad x_n = \frac{\omega' - 1/\omega'_n}{1 - \omega'/\omega'_n} \quad (2.17)$$

where, $s_n = j\omega'_n$ is the location of the n th transmission zero in the low-pass normalized domain, and $|F_N(\omega' = \pm 1)| = 1$ for all value of N . The function $F_N(\omega')$ is a rational function, and it can be expressed as

$$F_N(\omega') = \frac{P_N(\omega')}{\prod_{n=1}^N \left(1 - \frac{\omega'}{\omega'_n}\right)} = \frac{P_N(\omega')}{D_N(\omega')} \quad (2.18)$$

To compute $P_N(\omega')$ a simple recursion relation is established between $P_{N-1}(\omega')$, $P_N(\omega')$ and $P_{N+1}(\omega')$. Using the identity $\cosh(\alpha \pm \beta) = \cosh(\alpha)\cosh(\beta) \mp \sinh(\alpha)\sinh(\beta)$, we can write

$$\frac{P_{N+1}(\omega')}{\left(1 - \frac{\omega'}{\omega'_{N+1}}\right) D_N} = \cosh\left(\sum_{n=1}^N \cosh^{-1}(x_n) + \cosh^{-1}(x_{N+1})\right)$$

$$\begin{aligned}
&= \sinh\left(\sum_{n=1}^N \cosh^{-1}(x_n)\right) \sinh(\cosh^{-1}(x_{N+1})) + \cosh\left(\sum_{n=1}^N \cosh^{-1}(x_n)\right) x_{N+1} \\
&= \sinh\left(\sum_{n=1}^N \cosh^{-1}(x_n)\right) \sinh(\cosh^{-1}(x_{N+1})) + x_{N+1} \frac{P_N(\omega')}{D_N}
\end{aligned} \tag{2.19}$$

Similarly,

$$\frac{\left(1 - \frac{\omega'}{\omega'_N}\right) P_{N-1}(\omega')}{D_N} = -\sinh\left(\sum_{n=1}^N \cosh^{-1}(x_n)\right) \sinh(\cosh^{-1}(x_N)) + x_N \frac{P_N(\omega')}{D_N} \tag{2.20}$$

From equation (2.19) and (2.20), by using hyperbolic identities the recursion relation is obtained as the following equation.

$$\begin{aligned}
P_{N+1}(\omega') &= -P_{N-1}(\omega') \left(1 - \frac{\omega'}{\omega'_N}\right)^2 \frac{(1 - 1/\omega'^2_{N+1})^{1/2}}{(1 - 1/\omega'^2_N)^{1/2}} \\
&\quad + P_N(\omega') \left[\omega' - \frac{1}{\omega'_{N+1}} + \left(\omega' - \frac{1}{\omega'_N}\right) \frac{(1 - 1/\omega'^2_{N+1})^{1/2}}{(1 - 1/\omega'^2_N)^{1/2}} \right]
\end{aligned} \tag{2.21}$$

where the polynomials $P_0(\omega')=1$, $P_1(\omega')=\omega'-1/\omega'_1$. Thus, the transfer and reflection polynomials for the generalized Chebyshev filtering function can be expressed in the form

$$|S_{21}(\omega')|^2 = \frac{D_N^2}{D_N^2 + \varepsilon^2 P_N^2} = \frac{D_N^2}{E_N^2}, \text{ or } S_{21}(\omega') = \frac{D_N}{E_N} \tag{2.22}$$

$$|S_{11}(\omega')|^2 = 1 - |S_{21}(\omega')|^2 = \frac{E_N^2 - D_N^2}{E_N^2} = \frac{F_N^2}{E_N^2}, \text{ or } S_{11}(\omega') = \frac{F_N}{E_N} \tag{2.23}$$

The next step is to synthesize the coupling matrix.

When concerning the canonical transversal topology, considering admittance function is advantageous to synthesize this transversal coupling scheme. The first step is to construct the two-port short-circuit admittance parameter matrix $[Y_N]$ for the overall network. Fig. 2.5 shows a two-port network terminated in a 1Ω resistance, and Fig. 2.6 is the canonical transversal topology.

Following the analytical formula in [37], one can get the transversal matrix having the following form

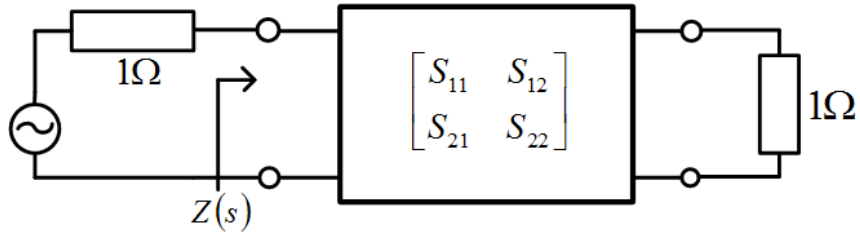


Fig. 2.5. A two-port network.

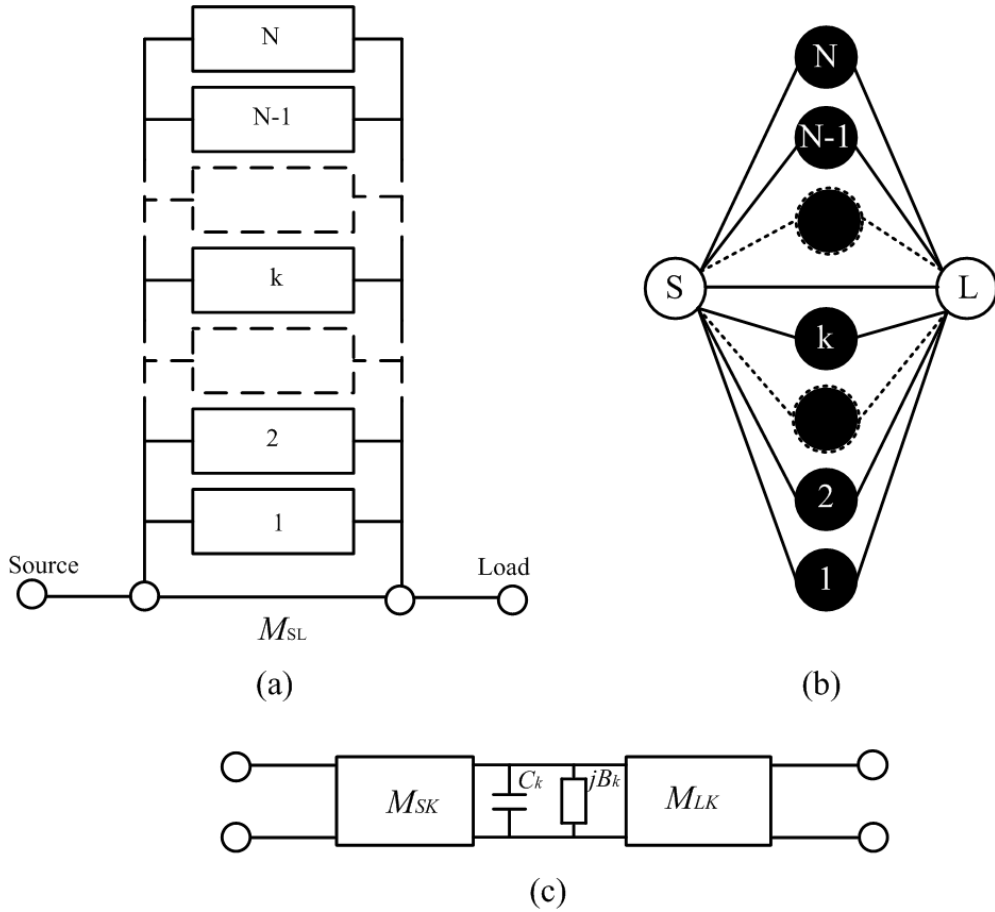


Fig. 2.6. Canonical transversal topology.

$$M = \begin{bmatrix} 0 & M_{S1} & M_{S2} & \cdots & M_{SL} \\ M_{S1} & M_{11} & 0 & \cdots & M_{L1} \\ M_{S2} & 0 & \ddots & \cdots & \vdots \\ \vdots & \vdots & \vdots & M_{nn} & M_{Ln} \\ M_{SL} & M_{L1} & \cdots & M_{Ln} & 0 \end{bmatrix} \quad (2.24)$$

The corresponding coupling route of the transversal topology is shown in Fig. 2.6.

Detailed derivation procedures can be found in [37]. Here, we only summarized important equations and design parameters of the transversal topology. First, the admittance function $[Y_N]$ can be synthesized from the transfer and reflection polynomials in (2.22) and (2.23). The numerator and denominator polynomials for the $y_{21}(s)$ and $y_{22}(s)$ elements of $[Y_N]$ are built up directly from the transfer and reflection polynomials for $S_{21}(s)$ and $S_{11}(s)$. Then, the following equation for the admittance matrix $[Y_N]$ for the overall network:

$$[Y_N] = \begin{bmatrix} y_{11}(s) & y_{12}(s) \\ y_{21}(s) & y_{22}(s) \end{bmatrix} = j \begin{bmatrix} 0 & K_0 \\ K_0 & 0 \end{bmatrix} + \sum_{k=1}^N \frac{1}{(s - j\lambda_k)} \cdot \begin{bmatrix} r_{11k} & r_{12k} \\ r_{21k} & r_{22k} \end{bmatrix} \quad (2.25)$$

Here, the residues r_{21k} and r_{22k} may be found from partial fraction expansions of the denominator and numerator polynomials for $y_{21}(s)$ and $y_{22}(s)$, and the purely real eigenvalues λ_k of the network found by rooting the denominator polynomial common to both $y_{21}(s)$ and $y_{22}(s)$, which has purely imaginary roots $= j\lambda_k$.

Second, another two-port admittance matrix $[Y_N]$ is to cascade the elements in Fig. 2.6(c), thus gives an $ABCD$ transfer matrix for the k th “low-pass resonator” as follows:

$$[ABCD]_k = - \begin{bmatrix} \frac{M_{LK}}{M_{SK}} & \frac{(sC_k + jB_k)}{M_{SK}M_{LK}} \\ 0 & \frac{M_{SK}}{M_{LK}} \end{bmatrix} \quad (2.26)$$

which can then be converted into the equivalent short-circuit y -parameter matrix

$$[y_k] = \frac{1}{(sC_k + jB_k)} \cdot \begin{bmatrix} M_{SK}^2 & M_{SK}M_{LK} \\ M_{SK}M_{LK} & M_{LK}^2 \end{bmatrix} \quad (2.27)$$

The admittance matrix $[Y_N]$ for the parallel-connected transversal array is the sum of the y -parameter matrices for the N individual sections, plus the y -parameters matrix $[y_{SL}]$ for the direct source-load coupling inverter M_{SL}

$$[Y_N] = j \begin{bmatrix} 0 & M_{SL} \\ M_{SL} & 0 \end{bmatrix} + \sum_{k=1}^N \frac{1}{(sC_k + jB_k)} \begin{bmatrix} M_{SK}^2 & M_{SK}M_{LK} \\ M_{SK}M_{LK} & M_{LK}^2 \end{bmatrix} \quad (2.28)$$

Comparison of (2.25) and (2.28) shows

$$\begin{aligned} \frac{r_{21k}}{(s - j\lambda_k)} &= \frac{M_{SK}M_{LK}}{(sC_k + jB_k)} \\ \frac{r_{22k}}{(s - j\lambda_k)} &= \frac{M_{LK}^2}{(sC_k + jB_k)} \end{aligned} \quad (2.29)$$

Thus, by equating the real and imaginary parts in (2.29), important extracted circuit parameters are

$$\begin{aligned} C_k &= 1 \\ B_k (\equiv M_{kk}) &= -\lambda_k \\ M_{LK}^2 &= r_{22k} \\ M_{SK}M_{LK} &= r_{21k} \end{aligned} \quad (2.30)$$

The synthesis of the transversal topology is complete.

Although the coupling matrix of the transversal topology is so far synthesized, the transformations of coupling matrices from the transversal topology to the wanted coupling schemes are necessary due to the easy realization of coupling schemes. Fig. 2.7 shows a diagram describing what topologies is a 3-order transversal topology transformed into. In [37], it is difficult to determine the rotation angles of the sequence of similar transformation. So, the eigenvalue approach [51] to optimizing the coupling matrix of the wanted coupling scheme is adopted in this dissertation. It is very powerful for extracting the coupling matrix of filters with order under 14. A briefly review of this method is discussed as follows.

The transversal coupling matrix (2.24) is denoted as

$$\underline{\underline{M}}_t = \begin{bmatrix} 0 & \underline{r}_S^T & r_{SL} \\ \underline{r}_S & \underline{\underline{\Lambda}} & \underline{r}_L \\ r_{SL} & \underline{r}_L^T & 0 \end{bmatrix} \quad (2.31)$$

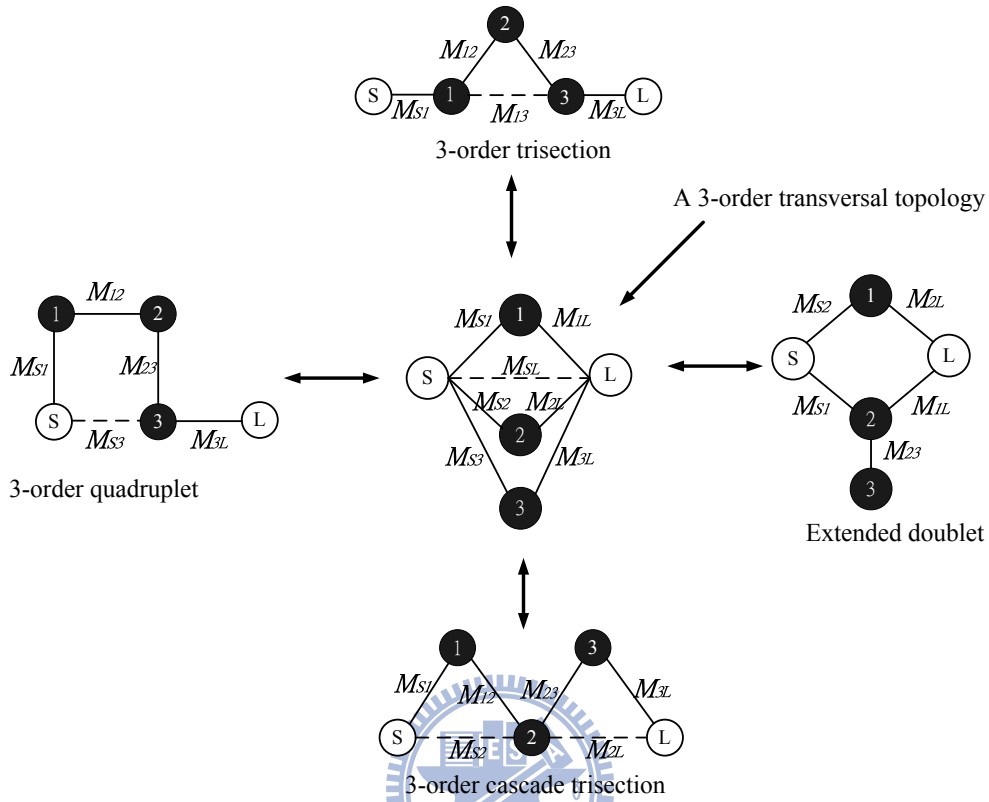


Fig. 2.7. A diagram shows that a 3-order transversal topology transforms into a wanted coupling topology.

Let $\underline{\underline{R}}$ denote the product of elementary plane rotations involving orthogonal rotations among the planes 1 to N

$$\underline{\underline{R}} = \begin{bmatrix} 1 & \underline{\underline{0}}^T & 0 \\ 0 & \underline{\underline{X}} & 0 \\ 0 & \underline{\underline{0}}^T & 1 \end{bmatrix} \quad (2.32)$$

where $\underline{\underline{X}}$ is an orthogonal matrix, and $\underline{\underline{0}}$ represents the zero vector. Applying similarity transformations to the matrix $\underline{\underline{M}}_t$ one obtains desired coupling matrix $\underline{\underline{M}}$ in the form

$$\underline{\underline{M}} = \begin{bmatrix} 1 & \underline{\underline{0}}^T & 0 \\ 0 & \underline{\underline{X}} & 0 \\ 0 & \underline{\underline{0}}^T & 1 \end{bmatrix} \begin{bmatrix} 0 & \underline{\underline{r}}_S^T & r_{SL} \\ \underline{\underline{r}}_S & \underline{\underline{\Lambda}} & \underline{\underline{r}}_L \\ r_{SL} & \underline{\underline{r}}_L^T & 0 \end{bmatrix} \begin{bmatrix} 1 & \underline{\underline{0}}^T & 0 \\ 0 & \underline{\underline{X}} & 0 \\ 0 & \underline{\underline{0}}^T & 1 \end{bmatrix}^T = \begin{bmatrix} 0 & (\underline{\underline{X}}\underline{\underline{r}}_S)^T & r_{SL} \\ \underline{\underline{X}}\underline{\underline{r}}_S & \underline{\underline{X}}\underline{\underline{\Lambda}}\underline{\underline{X}}^T & \underline{\underline{X}}\underline{\underline{r}}_L \\ r_{SL} & (\underline{\underline{X}}\underline{\underline{r}}_L)^T & 0 \end{bmatrix} \quad (2.33)$$

It is important to keep in mind that similarity transformations preserve eigenvalues, so the matrix $\underline{\underline{M}}$ preserves the eigenvalues of the matrix $\underline{\underline{M}}_t$. Let $\underline{\underline{\lambda}} = [\underline{\lambda}^P; \underline{\lambda}^{z1}; \underline{\lambda}^{z2}]$, where λ_i^P are the eigenvalues of the transversal coupling matrix $\underline{\underline{M}}_t$ that is synthesized using the analytic method in [37], λ_i^{z1} are the eigenvalues of upper principal submatrix obtained by deleting the last row and column of matrix $\underline{\underline{M}}_t$ and λ_i^{z2} are the eigenvalues of the lower principal submatrix obtained by deleting the first row and column of the matrix $\underline{\underline{M}}_t$. And let $\hat{\underline{\lambda}} = [\hat{\underline{\lambda}}^P; \hat{\underline{\lambda}}^{z1}; \hat{\underline{\lambda}}^{z2}]$ are the eigenvalues of the coupling matrix created in the course of optimization and its upper and lower principal submatrices, respectively. Then, a cost function may be formulated to be minimized:

$$C = (\hat{\underline{\lambda}} - \underline{\underline{\lambda}})^T (\hat{\underline{\lambda}} - \underline{\underline{\lambda}}) \quad (2.34)$$

This is a least squares optimization problem. Several optimization methods such as Newton method, conjugate gradient method, etc. can minimize the cost function C through the gradient with respect to the coupling elements of $\underline{\underline{M}}$, and thus enable in

$$\hat{\underline{\lambda}} = \underline{\underline{\lambda}}.$$

2.1.2 Useful Impedance and Admittance Inverters and Coupled-Line Circuits

Before introducing impedance and admittance inverters, the prototype of generalized bandpass filters should be mentioned. To begin with, low-pass prototype in Fig. 2.2 is transformed in to bandpass filters by applying the low-pass to bandpass

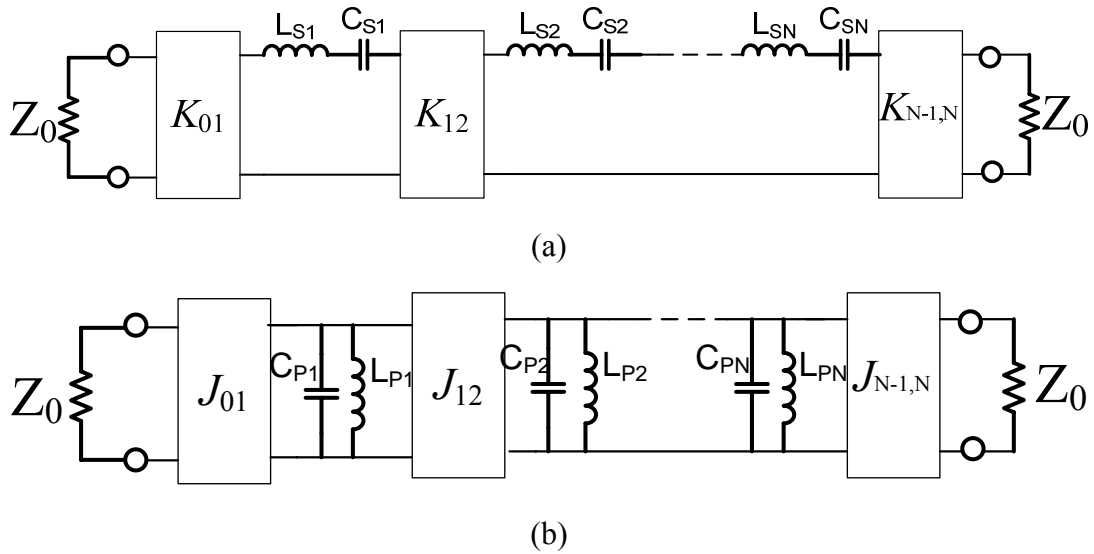


Fig. 2.8. Bandpass filters. (a) Use impedance inverters. (b) Use admittance inverters.

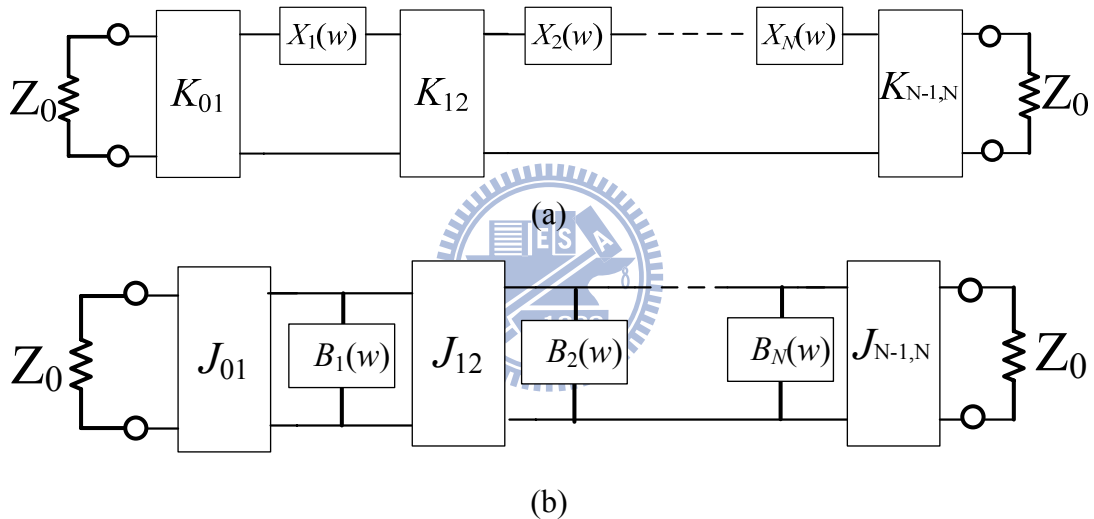


Fig. 2.9. Generalized bandpass filters. (a) K -inverters. (b) J -inverters.

frequency transformation. Fig. 2.8(a) and (b) show the transformed bandpass filters corresponding to Fig. 2.2(a) and (b), respectively.

Actually, for the purpose of general design including not only the lumped LC resonators but also the distributed circuit resonators, two important generalizations for bandpass filter design are shown in Fig. 2.9. Here, two quantities, called the reactance slope parameter and susceptance slope parameter, respectively, are introduced as

$$x_i = \frac{\omega_0}{2} \left. \frac{dX_{ri}(\omega)}{d\omega} \right|_{\omega=\omega_0} \quad (2.35)$$

$$b_i = \frac{\omega_0}{2} \left. \frac{dB_{ri}(\omega)}{d\omega} \right|_{\omega=\omega_0} \quad (2.36)$$

where $X_{ri}(\omega)$ is the reactance of i -th series resonator tank in Fig. 2.9(a) and $B_{ri}(\omega)$ is the susceptance of i -th shunt resonator tank in Fig. 2.9(b).

Therefore, design parameters of generalized bandpass filters in Fig. 2.9(a) and Fig. 2.9(b) are

$$K_{01} = \sqrt{\frac{Z_0 FBW x_1}{g_0 g_1}}, \quad K_{i,i+1} = FBW \sqrt{\frac{x_i x_{i+1}}{g_i g_{i+1}}}_{i=1 \text{ to } N-1}, \quad K_{N,N+1} = \sqrt{\frac{Z_0 FBW x_N}{g_N g_{N+1}}} \quad (2.37)$$

$$J_{01} = \sqrt{\frac{Y_0 FBW b_1}{g_0 g_1}}, \quad J_{i,i+1} = FBW \sqrt{\frac{b_i b_{i+1}}{g_i g_{i+1}}}_{i=1 \text{ to } N-1}, \quad J_{N,N+1} = \sqrt{\frac{Y_0 FBW b_N}{g_N g_{N+1}}} \quad (2.38)$$

where FBW is the fractional bandwidth, and g_0, g_1, \dots, g_{N+1} can be obtained in section 3.21~ section 3.24 of [6] for various filtering functions.

In the following, several numerous equivalent circuits operating as inverters are introduced. All necessarily give an image phase of some odd multiple of ± 90 degree, and some of inverters have good inverting properties over a much wider bandwidth. In addition, some of inverters have the property of the finite frequency pole-producing function.

One of the simplest forms of inverters is a quarter-wavelength of transmission line. In this case, the quarter-wavelength transmission line corresponds to an inverter parameter of $K = Z_0$ Ohms where Z_0 is the characteristic impedance of the line. Similarly, the quarter-wavelength transmission line also serves as an admittance inverter, and the admittance inverter parameter is $J = Y_0$ where Y_0 is the characteristic admittance of the line. The inverter properties of the line are relatively narrow-band in nature.

Other inverters exhibiting a wider bandwidth than that of the quarter-wavelength

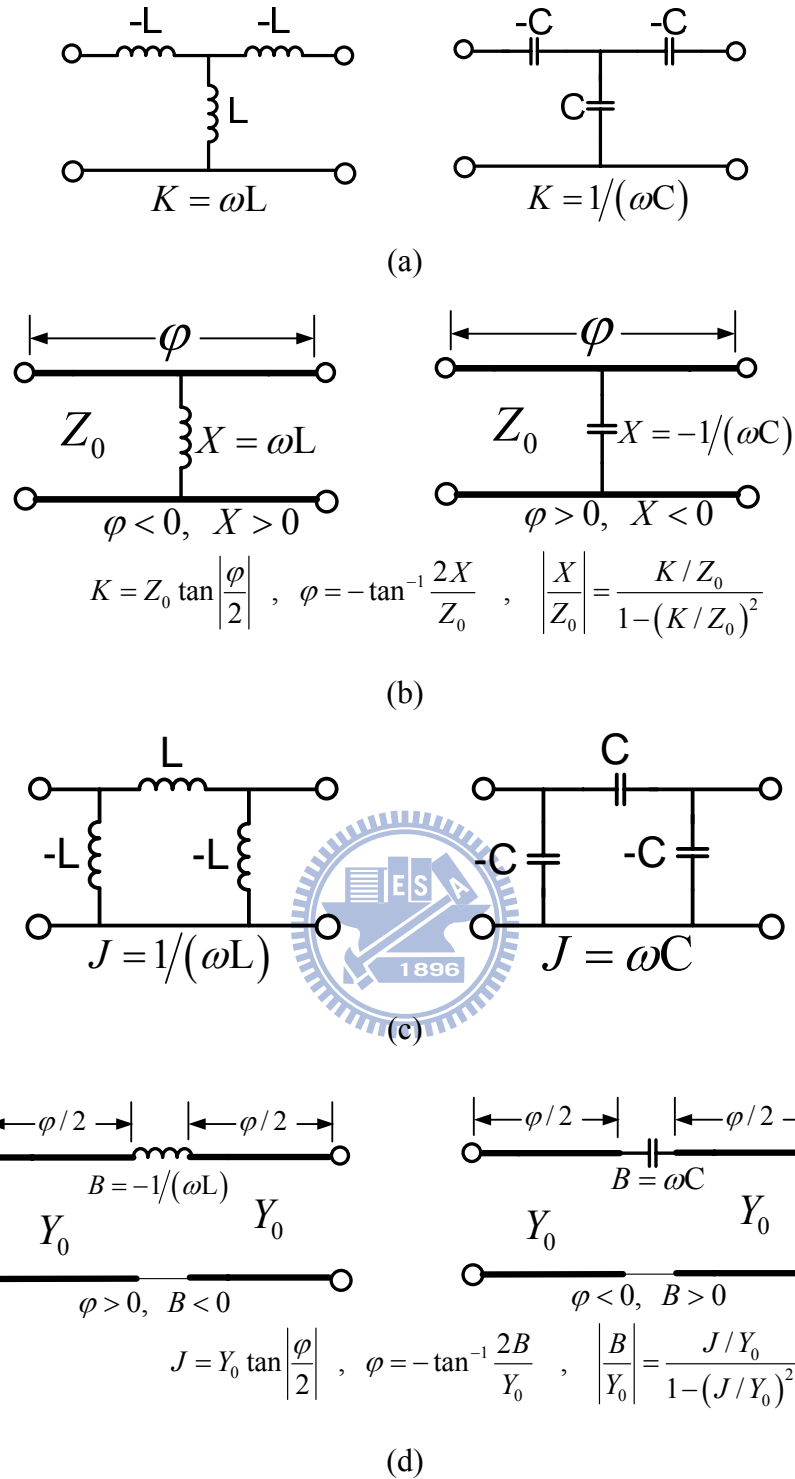


Fig. 2.10. Inverters. (a) Lumped-element K inverters. (b) Lumped- and distributed-elements K inverters. (b) Lumped-element J inverters. (b) Lumped- and distributed-elements J inverters.

transmission line are shown in Fig. 2.10 [27]. For K -inverters, those shown in Fig. 2.10(a) are particularly useful in circuits where the negative L or C can be absorbed

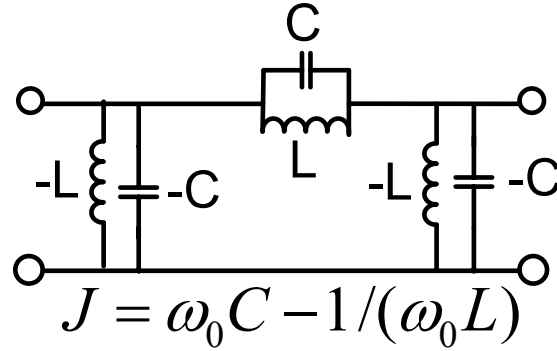


Fig. 2.11. Pole-producing admittance inverters [57].

into adjacent positive series element of the same type so as to give a resulting circuit having all positive elements. The inverters shown in Fig. 2.10(b) are particularly useful in circuits where the line of positive or negative electrical length φ shown in the figures can be added to or subtracted from adjacent lines of the same impedance. Figs. 2.10(c) and (d) show four inverting circuits which are of special interest for use as J inverters. These J -inverter circuits are the dual of K -inverter circuits. The design parameters are provided as shown in the figure.

Recently, a realization of the inverter shown in Fig. 2.11 which is to use a Pi of parallel LC sections is proposed by Levy [57]. This inverter introduces a pole at

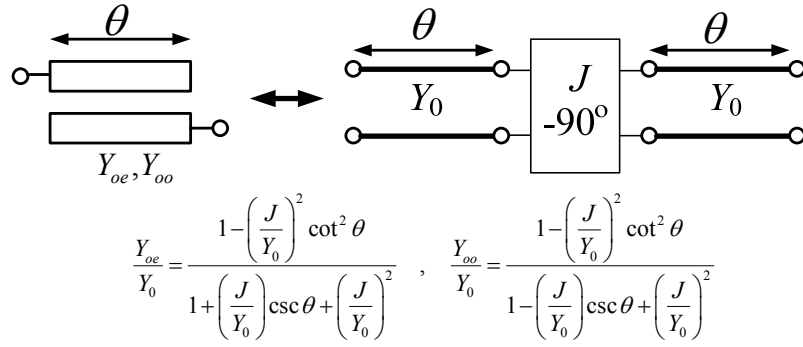
$$\omega_p = 1/\sqrt{LC} \quad (2.39)$$

And the susceptance of the inverter is

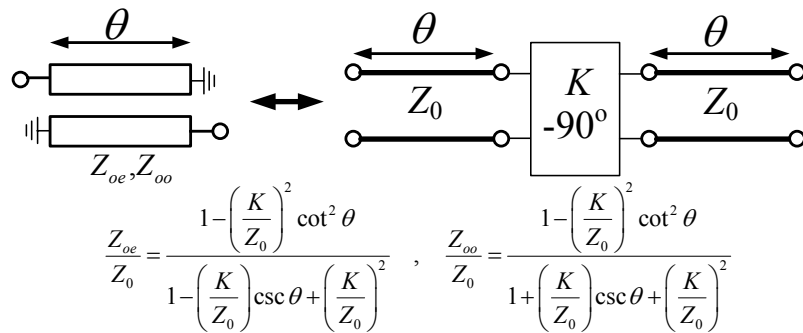
$$\omega_0 C - 1/(\omega_0 L) = J \quad (2.40)$$

where ω_0 is the mid-band or synchronous frequency of the filter to be designed. The values of C and L are then obtained from (2.39) and (2.40).

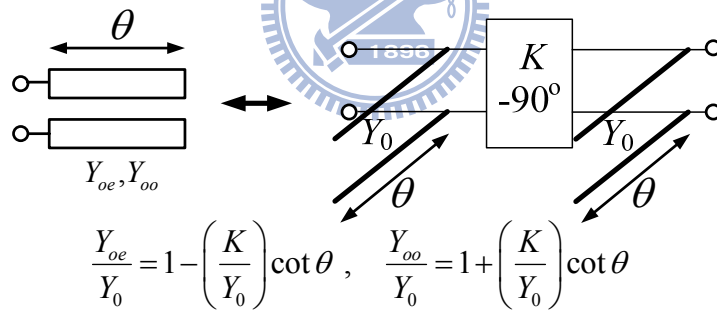
The equivalent circuits of coupled-line circuits in narrowband filter applications are also related to J - K inverters. The four coupled-line circuits [27], [92]-[94] parallel-coupled open-ended and short-ended circuits as well as antiparallel-coupled



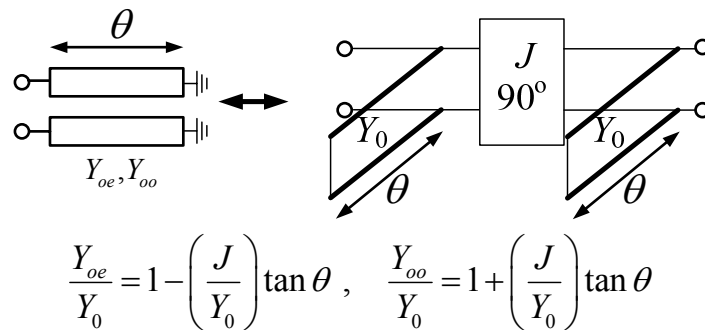
(a)



(b)



(c)



(d)

Fig. 2.12. Parallel- and antiparallel-coupled line circuits and its equivalent circuits.

open-ended and short-ended circuits, which are used as basic building blocks in microwave filters are shown in Fig. 2.12. The electrical parameters of these circuits are expressed by even- and odd-mode impedance Z_{oe} , Z_{oo} , and electrical coupling angle θ . Design parameters of the four coupled-line circuits related to the corresponding equivalent circuits comprising an inverter and two transmission lines are provided in the figure.

2.1.3 Segmentation Method for Coupled Resonator Filters

For coupled resonator filters, segmentation method is frequently used to extract external Q and coupling coefficients, which means to compute input/output (I/O) coupling and coupling strengths between two resonators. In the segmentation method, the coupling strength between resonators is tested pair by pair to obtain the approximated coupling strength. The external coupling, the coupling between the first/last resonator to the source/load, is calculated by excluding other resonators. In fact, this method should be traced back to Dishal's method [38] in 1951. Dishal presented a simple method of tuning up a multiple-resonant-circuit filter quickly and exactly. He described how to extract the external Q and the coupling between r th and $(r+1)$ th adjacent resonators in a waveguide filter. A detail description of Dishal's method to be used in microstrip resonator filters is presented by Hong and Lancaster [6]. In the following, four basic coupling structures, electric coupling, magnetic coupling, mixed coupling, external quality factor of singly loaded resonator, are reviewed.

First, electric coupling is concerned. An equivalent lumped-element circuit shown in Fig. 2.13(a) may be employed to represent two asynchronous-tuned coupled resonators. The resonant frequencies of the two resonators are $\omega_{01} = (L_1 C_1)^{-1/2}$ and $\omega_{02} = (L_2 C_2)^{-1/2}$, respectively, and the two resonators are coupled to each other

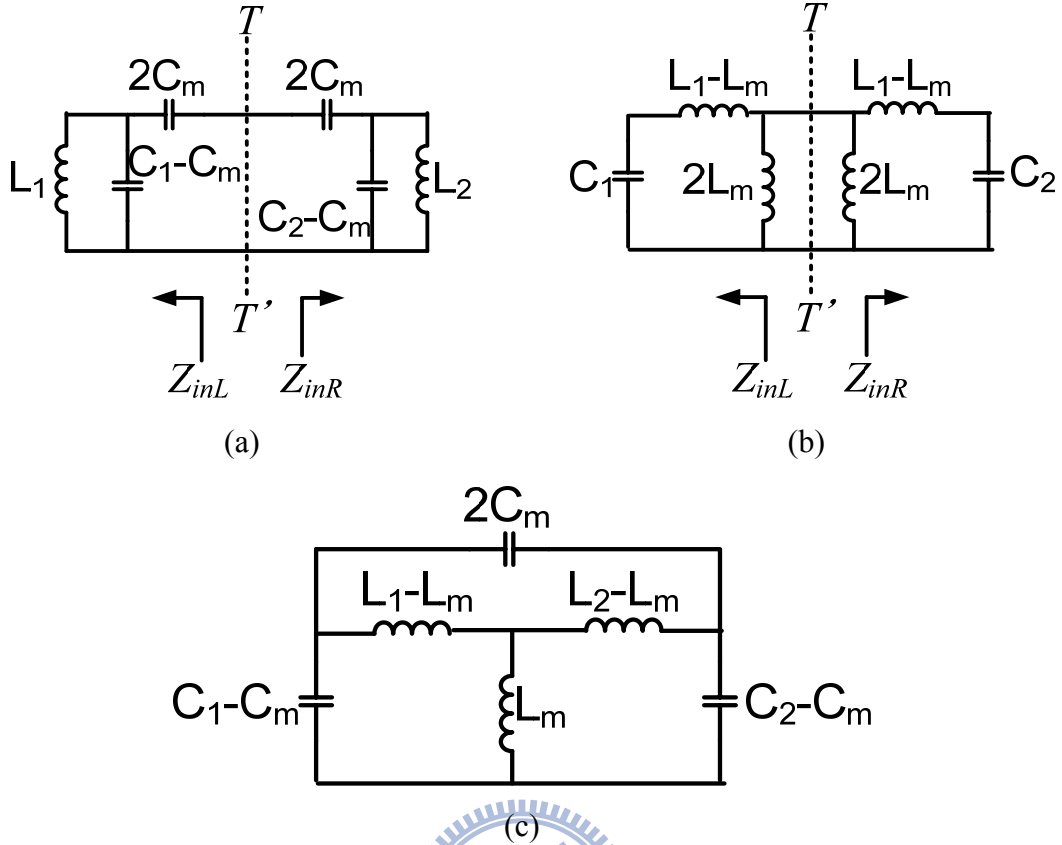


Fig. 2.13. (a) Electrical coupling. (b) Magnetic coupling. (c) Mixed coupling.

electrically through mutual capacitance C_m . The resonant condition of the circuit of Fig. 2.13(a) is

$$Z_{inL} = -Z_{inR} \quad (2.41)$$

where Z_{inR} and Z_{inL} are the input impedances when looking at the right and left of reference plane $T - T'$ of Fig. 2.13(a). From (2.41), an eigenequation is

$$\frac{j\omega L_1}{1 - \omega^2 L_1 (C_1 - C_m)} + \frac{j\omega L_2}{1 - \omega^2 L_2 (C_2 - C_m)} + \frac{1}{j\omega C_m} = 0 \quad (2.42)$$

After some manipulations, (2.42) can be solved as

$$\omega_{1,2} = \sqrt{\frac{(L_1 C_1 + L_2 C_2) \pm \sqrt{(L_1 C_1 - L_2 C_2)^2 + 4L_1 L_2 C_m^2}}{2(L_1 L_2 C_1 C_2 - L_1 L_2 C_m^2)}} \quad (2.43)$$

The electric coupling coefficient is defined as $k_e = C_m / \sqrt{C_1 C_2}$, and then through some manipulations one can obtain the electric coupling coefficient

$$k_e = \frac{C_m}{\sqrt{C_1 C_2}} = \pm \frac{1}{2} \left(\frac{\omega_{02}}{\omega_{01}} + \frac{\omega_{01}}{\omega_{02}} \right) \sqrt{\left(\frac{\omega_2^2 - \omega_1^2}{\omega_2^2 + \omega_1^2} \right)^2 - \left(\frac{\omega_{02}^2 - \omega_{01}^2}{\omega_{02}^2 + \omega_{01}^2} \right)^2} \quad (2.44)$$

in accordance with the ratio of the coupled electric energy to the average stored energy, where the positive sign should be chosen if a positive mutual capacitance is defined.

Similarly, for the magnetic coupling circuit as shown in Fig. 2.13(b), the magnetic coupling coefficient is

$$k_m = \frac{L_m}{\sqrt{L_1 L_2}} = \pm \frac{1}{2} \left(\frac{\omega_{02}}{\omega_{01}} + \frac{\omega_{01}}{\omega_{02}} \right) \sqrt{\left(\frac{\omega_2^2 - \omega_1^2}{\omega_2^2 + \omega_1^2} \right)^2 - \left(\frac{\omega_{02}^2 - \omega_{01}^2}{\omega_{02}^2 + \omega_{01}^2} \right)^2} \quad (2.45)$$

,and for the mixed coupling circuit of Fig. 2.13(c), the mixed coupling coefficient k_x is

$$k_x = k_e - k_m = \pm \frac{1}{2} \left(\frac{\omega_{02}}{\omega_{01}} + \frac{\omega_{01}}{\omega_{02}} \right) \sqrt{\left(\frac{\omega_2^2 - \omega_1^2}{\omega_2^2 + \omega_1^2} \right)^2 - \left(\frac{\omega_{02}^2 - \omega_{01}^2}{\omega_{02}^2 + \omega_{01}^2} \right)^2} \quad (2.46)$$

The detailed derivation is described in [6].

The last one to be concerned is the external quality factor. Shown in Fig. 2.14 is an ideal, lossless LC tank connected to external loads. In this case, power dissipation occurs, and it affects the sharpness of resonant response, which depends upon the ratio of the amount energy stored in the capacitor or inductor to that dissipated in the external load or loads. In Fig. 2.14, the reflection coefficient S_{11} at the excitation port of resonator is

$$S_{11} = \frac{G - Y_{in}}{G + Y_{in}} \quad (2.47)$$

where Y_{in} is the input admittance of the resonator

$$Y_{in} = j\omega C + \frac{1}{j\omega L} = j\omega_0 C \left(\frac{\omega}{\omega_0} - \frac{\omega_0}{\omega} \right) \quad (2.48)$$

Note that $\omega_0 = 1/\sqrt{LC}$ is the resonant frequency of the resonator. Around resonant

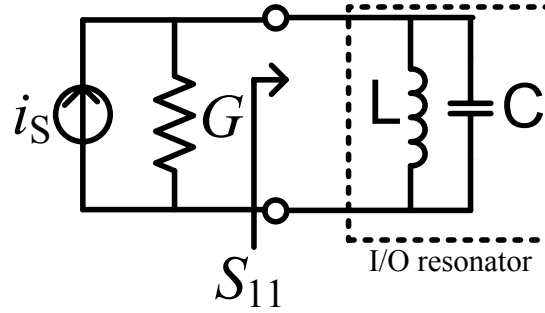


Fig. 2.14. Equivalent circuit of the I/O resonator with single loading.

frequency $\omega = \omega_0 + \Delta\omega$ and definition of the external quality factor $Q_E = \omega_0 C / G = 1 / (\omega_0 L G)$, one can derive

$$S_{11} = \frac{1 - jQ_E(2\Delta\omega/\omega_0)}{1 + jQ_E(2\Delta\omega/\omega_0)} \quad (2.49)$$

Because the resonator is assumed to be lossless, this leads to the unity of S_{11} around resonance. In (2.42), phase responses of S_{11} should be concerned. When $\angle S_{11} = -90^\circ$, implying quantity $Q_E(2\Delta\omega/\omega_0)$ must equal to 1, while $\angle S_{11} = 90^\circ$, implying quantity $Q_E(2\Delta\omega/\omega_0)$ must equal to -1. Therefore, it results in $Q_E(\Delta\omega_{\pm 90}/\omega_0) = 1$.

So, one may extract the corresponding external quality factor from a given loaded resonator through its phase response with respect to frequency

$$Q_E = \frac{\omega_0}{\Delta\omega_{\pm 90}} = \frac{f_0}{\Delta f_{\pm 90}} \quad (2.50)$$

It should be noted that the reference plane of S_{11} in the EM simulation may not exactly match that of equivalent circuit in Fig. 2.14, which leads to an extra phase shift such that the phase of the simulated S_{11} does not equal to zero at resonance. To solve this problem, the resonant frequency can firstly be determined from the peak of the group delay response. Then, find the frequencies at which the phase shifts $\pm 90^\circ$ with respect to the resonant frequency from the phase response. Finally, use (2.50) to compute external quality factor.

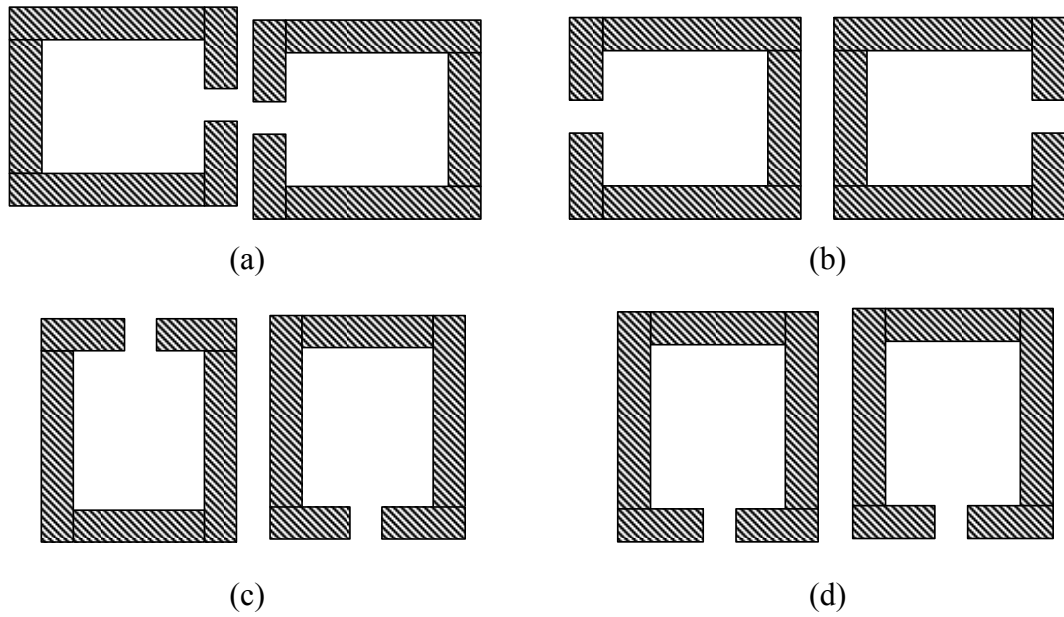


Fig. 2.15. Typical coupling structures of coupled resonators. (a) Electric coupling. (b) Magnetic coupling. (c) and (d) Mixed coupling.

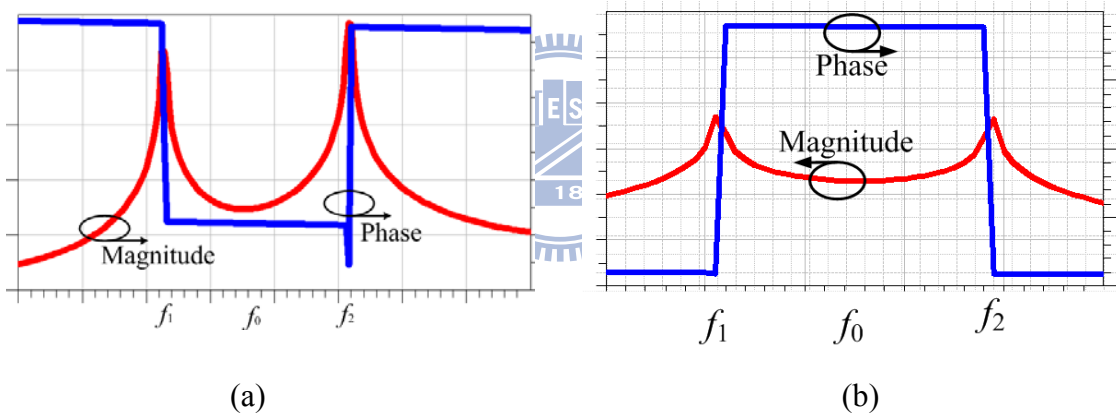


Fig. 2.16. A diagram of simulated responses of (a) electric coupling and (b) magnetic coupling.

Actually, the applications of the above-derived formulas for extracting coupling coefficients and external quality factors have been extensively used in microstrip cross-coupled filters [6], [70]-[73], [75], [80]-[81], [83]. For the purpose of demonstration, the open-loop resonators are taken as examples to the four basic coupling structures. Fig. 2.15 shows typical coupling structures of coupled resonators.

Performing the EM simulations on the circuits shown in Fig. 15, one can observe simulated resonator's frequency responses of the electric coupling and magnetic

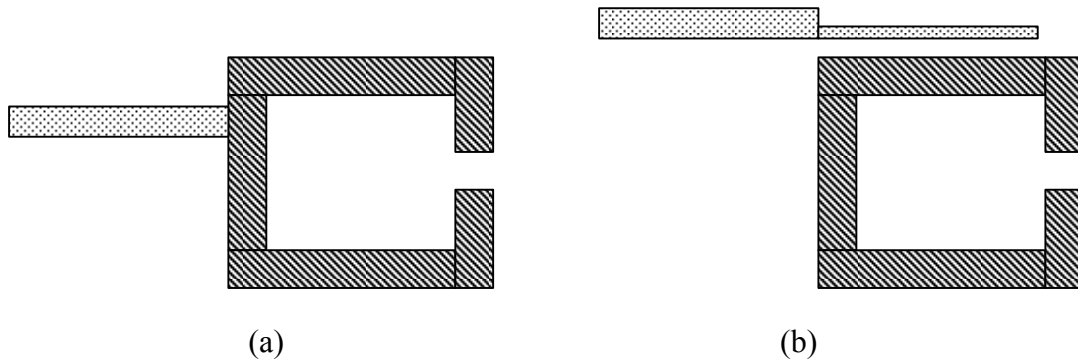


Fig. 2.17. Two typical feeding structures of coupled-resonator filters. (a) Tapped-line coupling. (b) Coupled-line coupling.

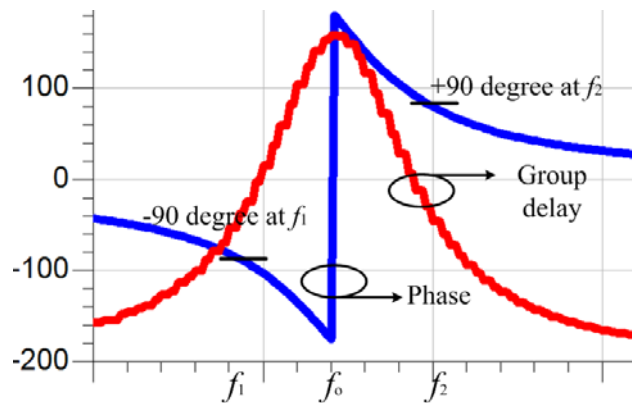


Fig. 2.18. A diagram of simulated responses of the circuits in Fig. 2.17(b)

coupling, which are shown in Fig. 2.16(a) and (b), respectively. The responses of the mixed coupling are either Fig. 2.16(a) or Fig. 2.16(b). Based on (2.44) ~ (2.46), one may extract coupling coefficients between two coupled resonators.

Shown in Fig. 2.17 are two typical feeding structures for coupled-resonator filters. Performing the EM simulations on the circuits, the simulated responses are shown in Fig. 2.18. Based on (2.50), one may extract external quality factor Q .

2.1.4 Stepped Impedance Resonators

In this section, the characteristics and important design parameters of the stepped impedance resonators will be briefly reviewed. The stepped impedance resonator is a TEM or quasi-TEM mode resonator composed of more than two transmission lines with different characteristic impedance. In this dissertation, only the stepped impedan-

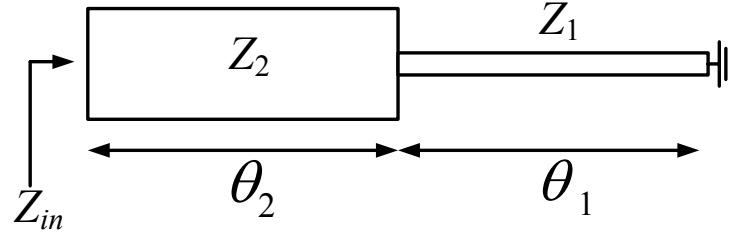


Fig. 2.19. Quarter-wavelength stepped impedance resonator type.

ce resonator comprising two transmission lines with two different characteristic impedances is considered. Fig. 2.19 shows a quarter-wavelength stepped-impedance resonator. Based on the theory of transmission line, the input impedance Z_{in} is

$$Z_{in} = jZ_2 \frac{Z_1 \tan \theta_1 + Z_2 \tan \theta_2}{Z_2 - Z_1 \tan \theta_1 \tan \theta_2} \quad (2.51)$$

The parallel resonance occurs when $Y_{in} = 1/Z_{in} = 0$. Then, the resonant condition is

$$R_Z = \tan \theta_1 \tan \theta_2 \quad (2.52)$$

where $R_Z = Z_2/Z_1$. This resonant condition is useful in obtaining the fundamental and spurious resonances. The overall electrical length of the stepped impedance resonator in Fig. 2.19 is

$$\theta_{TA} = \theta_1 + \theta_2 = \theta_1 + \tan^{-1}(R_Z / \tan \theta_1) \quad (2.53)$$

A special condition is to assume $\theta_1 = \theta_2 = \theta_0 = \tan^{-1} \sqrt{R_Z}$ as the structure of stepped impedance resonator. Thus, when $R_Z < 1$, θ_{TA} attains a minimum value of

$$(\theta_{TA})_{\min} = \tan^{-1} \left(\frac{2\sqrt{R_Z}}{1 - R_Z} \right) \quad (2.54)$$

When $R_Z > 1$, θ_{TA} attains a maximum value of

$$(\theta_{TA})_{\max} = \tan^{-1} \left(\frac{2\sqrt{R_Z}}{1 - R_Z} \right) \quad (2.55)$$

With the knowledge of θ_{TA} , the first spurious frequency f_{SA} can be obtained as

$$f_{SA} = \left(\frac{\pi}{\tan^{-1} \sqrt{R_Z}} - 1 \right) f_0 \quad (2.56)$$

More detailed descriptions of the stepped impedance resonator can be found in [92].

2.1.5 Relations between the Coupling Matrix and Design Parameters of Coupled-Resonator Filters

Consider the circuit of Fig. 2.9(b) in section 2.1.2. The generalized bandpass filter circuit using admittance inverters can be related to the corresponding coupling matrix.

First, for experimental determination of couplings, the input/output external quality factors and coupling coefficients are defined as

$$Q_{e,in} = \frac{b_1}{J_{01}^2/Y_0}, \quad Q_{e,out} = \frac{b_n}{J_{n,n+1}^2/Y_0} \quad (2.57)$$

$$k_{j,j+1} \Big|_{j=1to(n-1)} = \frac{J_{j,j+1}}{\sqrt{b_j b_{j+1}}} \quad (2.58)$$

Where b_i is susceptance slope parameter which is defined as

$$b_i = \frac{\omega_0}{2} \frac{dB_i(\omega)}{d\omega} \Big|_{\omega=\omega_0} \quad (2.59)$$

It should be noted that obtaining the inverter parameters from coupling coefficients need to know the slope parameter of the resonators. The inverter parameter is more useful for filter design analysis because it contains more information than coupling coefficient.

Then, consider the equivalent circuit of n -coupled resonators in low pass domain as shown in Fig. 2.3(a). Here, for simplicity, 2-order coupled resonators are taken as an example. Applying lowpass to bandpass transformation

$$\Omega = \frac{1}{FBW} (f/f_0 - f_0/f) \quad (2.60)$$

the bandpass filter circuit is shown in Fig. 2.20 with

$$\begin{aligned}
L_1 = L_2 = L &= FBW / \omega_0 \\
C_1 = C_2 = C &= \frac{1}{FBW * \omega_0} \\
\omega_0 L &= \frac{1}{\omega_0 C} = FBW
\end{aligned} \tag{2.61}$$

The use of (2.59) can derive the slope parameter of the resonators as

$$b_i = \omega_0 C = \frac{1}{FBW} \tag{2.62}$$

Thus, the external quality factor of the first and last resonator is

$$Q_{e,in} = \frac{1}{M_{S1}^2 * FBW}, \quad Q_{e,out} = \frac{1}{M_{2L}^2 * FBW} \tag{2.63}$$

Note that the admittance inverter J_{01} before impedance scaling is denoted as M_{S1} .

Coupling coefficients can also be derived as

$$k_{12} = \frac{J_{12}}{\sqrt{b_1 b_2}} = J_{12} * FBW = M_{12} * FBW \tag{2.64}$$

The use of (2.57)~(2.59) and (2.63)~(2.64) can design a filter with knowledge of slope parameters which contain more information on filters.

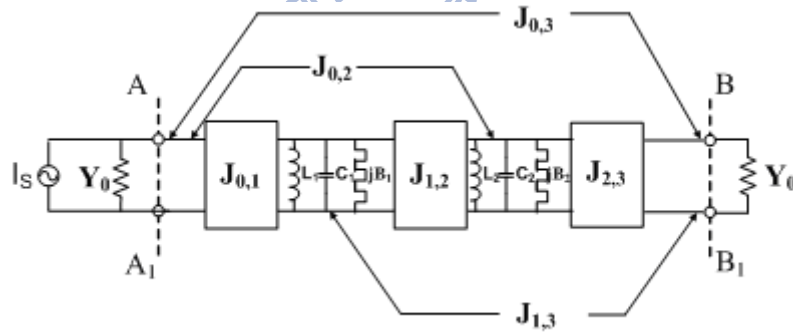


Fig. 2.20. A 2-order cross-coupled bandpass filter circuit.

2.2 Distributed Circuits with Transmission Line Elements

A common approach to the design of a practical distributed circuit is to explore some approximate equivalence between it and a lumped element and other distributed circuit. Actually, some of possible equivalences have already been discussed in connection with the design of low- and high-pass filters. In the following, how

distributed transmission line functions to be treated as lumped inductor and capacitor elements and unit element will be introduced. This also includes the famous Kuroda identities, Richards theorem, and the synthesis procedures of the distributed transmission line.

2.2.1 Richards Variable and Transmission Line Networks

Due to the use of distributed transmission line, transmission line equation should be concerned

$$Z_{in}(\theta) = Z_0 \frac{Z_L + jZ_0 \tan \theta}{Z_0 + jZ_L \tan \theta} \quad (2.65)$$

Here, the transmission line assumed to be lossless. In (2.65), it shows the input impedance of the transmission line with characteristic impedance Z_0 and to be terminated with a load impedance Z_L .

Based on (2.65), Richard proposed a frequency transformation that is

$$S = j\Omega = j \tan \theta = j \tan \left(\frac{\pi\omega}{2\omega_0} \right) \quad (2.66)$$

where ω is the usual real radian frequency variable, ω_0 is the radian frequency at which all line lengths are a quarter-wave long, Ω is the distributed radian frequency variable, and S is called Richards variable.

It is interesting to show the mapping of this frequency transformation (2.66). Fig. 2.21 shows the relationship between ω and Ω . The response of the distributed circuit repeats in frequency intervals of $2\omega_0$. This mapping is theoretically exact at all frequencies.

By replacing the reactance elements, a lumped element LC network with a realizable impedance $Z(s)$ in the s plane, where $s = j\omega$, may be converted into one consisting of uniform sections with an impedance $Z(S)$ in the S plane, where

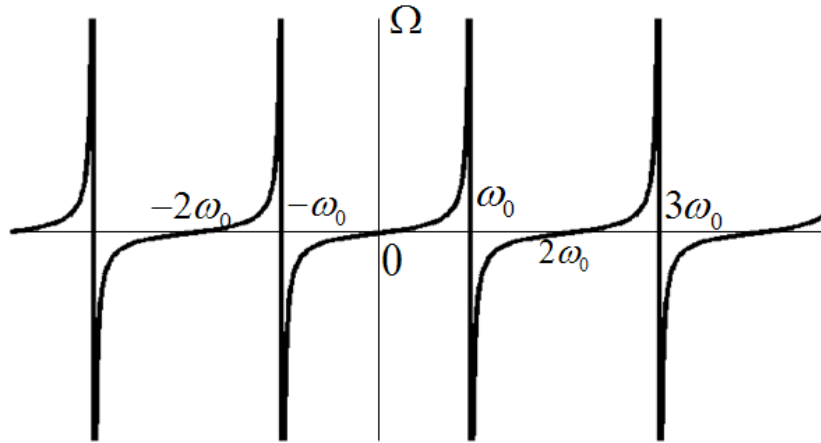


Fig. 2.21. Mapping between real frequency variable ω and distributed frequency variable Ω .

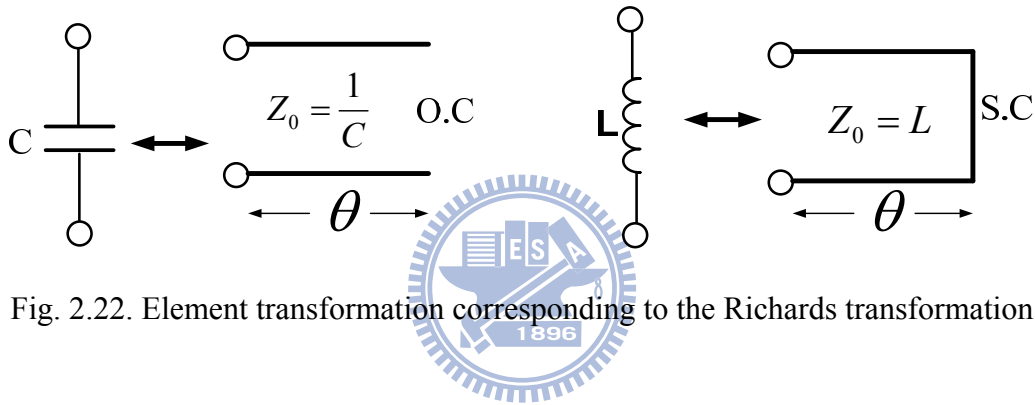


Fig. 2.22. Element transformation corresponding to the Richards transformation

$S = j \tan(\pi\omega/2\omega_0)$. Fig. 2.22 depicts the equivalence between the lumped and distributed circuits in the s and S planes. The impedance of a lumped inductor L in the s plane is $Z(s) = sL$, while considering a short-circuited line of characteristic impedance Z_0 the impedance of the short-circuited line is

$$Z(S) = jZ_0 \tan \theta = SZ_0 \quad (2.67)$$

which is derived by using (2.65). Thus, the S -plane inductor with inductance value Z_0 is recognized as the input impedance of a short-circuited line of characteristic impedance Z_0 in the s plane. Similarly, for the S -plane capacitor with capacitance value $1/Z_0$ is recognized as the input impedance of an open-circuited line of characteristic impedance Z_0 in the s plane. Thus, the impedance of the open-

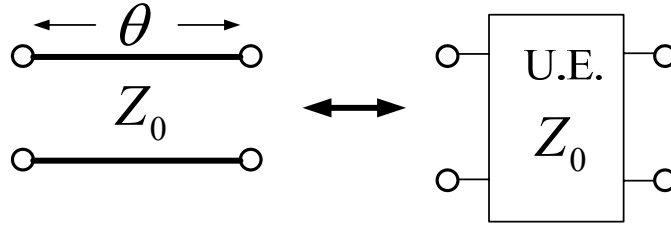


Fig. 2.23. Richards transformation applied to an interconnecting transmission line.

circuited line is

$$Z(S) = \frac{Z_0}{j \tan \theta} \quad (2.68)$$

Another concerned network is an interconnecting transmission line in the s plane. The effect of the Richards transformation on the interconnecting transmission line is to turn it into a unit element (U.E.), which is shown in Fig. 2.23. The transformation can be further illustrated by considering the $ABCD$ matrix of the interconnecting transmission line of the form

$$\begin{bmatrix} A & B \\ C & D \end{bmatrix} = \begin{bmatrix} \cos \theta & jZ_0 \sin \theta \\ jY_0 \sin \theta & \cos \theta \end{bmatrix} \quad (2.69)$$

which transforms into a unit element in the S -plane with an $ABCD$ matrix:

$$\begin{bmatrix} A & B \\ C & D \end{bmatrix}_{U.E.} = \frac{1}{\sqrt{1-S^2}} \begin{bmatrix} 1 & Z_0 S \\ Y_0 S & 1 \end{bmatrix} \quad (2.70)$$

after dividing each matrix element by $\cos \theta$ and substituting S for $j \tan \theta$. Related discussions on a unit element will be introduced in the following subsections.

2.2.2 Richards Theorem and Kuroda Identities

In addition to the basic S -plane distributed inductors and capacitors defined by the Richards transformation, a unit element (U.E.) may also be defined. UEs are commensurate sections of transmission line which may be employed to separate circuit elements in the high-frequency circuits. The Richards theorem states a UE may always be extracted from a distributed S -plane reactance function and the remainder

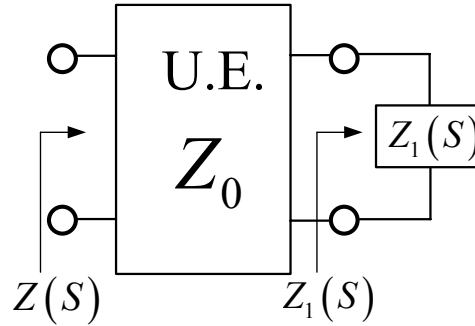


Fig. 2.24. A circuit used to illustrate the Richards theorem.

function is guaranteed to be positive real and of one degree less than the original one. The characteristic impedance of this UE has the value of the one-port immittance with S replaced by unity. The Richards theorem permits a canonical realization of a reactance function as a cascade of UEs terminated in either an open circuit or a short circuit [130].

The observation of the matrix in (2.70) shows that the unit element must create a half-order transmission zero at $S = \pm 1$. The unit element, therefore, does produce a transmission zero, but the zero occurs at $S = \pm 1$ on the real axis of the S -plane. In other words, there is no transmission zero on the $j\Omega$ axis of the S -plane. The following statement will give a clear description of Richards theorem (unit element).

Fig. 2.24 shows the input impedance $Z(S)$ of a transmission line of characteristic impedance Z_0 terminated in an impedance $Z_1(S)$ is given from transmission line theory (see from (2.65)) by

$$Z(S) = Z_0 (Z_1(S) + SZ_0) / (SZ_1(S) + Z_0) \quad (2.71)$$

After manipulation, (2.71) becomes

$$Z_1(S) = Z_0 \frac{Z(S) - SZ_0}{Z_0 - SZ(S)} \quad (2.72)$$

Again, the Richards theorem states that a unit element $Z(1)$ may always be extracted from an impedance function and the remainder impedance $Z_1(S)$ is positive real and in the reactance function $Z_1(S)$ of one degree less than $Z(S)$. Let $S=1$ in (2.71) lead to $Z(1)=Z_0$. Indeed, the characteristic impedance of the unit element shown in Fig. 2.24 is Z_0 .

Combining (2.72) and $Z(1)=Z_0$ yields

$$Z_1(S) = Z(1) \frac{Z(S) - SZ(1)}{Z(1) - SZ(S)} \quad (2.73)$$

From (2.73) it can be shown that a common factor $(S^2 - 1)$ can be cancelled in both numerator and denominator polynomials of $Z_1(S)$, and the reactance function $Z_1(S)$ can then be obtained. At this time, the extraction of the unit element is complete.

As shown in Fig. 2.25, there are four different Kuroda identities [131], which facilitate the movement of one of the four basic types of reactance branches through a single unit element. The first and second identities shown in Figs. 2.25(a) and (b) respectively are called the first type of Kuroda identities, while the third and fourth identities shown in Figs. 2.25(c) and (d) respectively are called the second type of Kuroda identities. The first identity provides equivalence between a shunt capacitor and a UE circuit to a UE and series inductor, and in the case of the second, a series inductor is transformed into a shunt capacitor on the opposite side of the UE. The third identity shows that a shunt inductor transforms into another shunt inductor and an ideal transformer with a turns ratio of $1:n^2$, and in the case of the fourth, a series capacitor transforms into another series capacitor and an ideal transformer with a

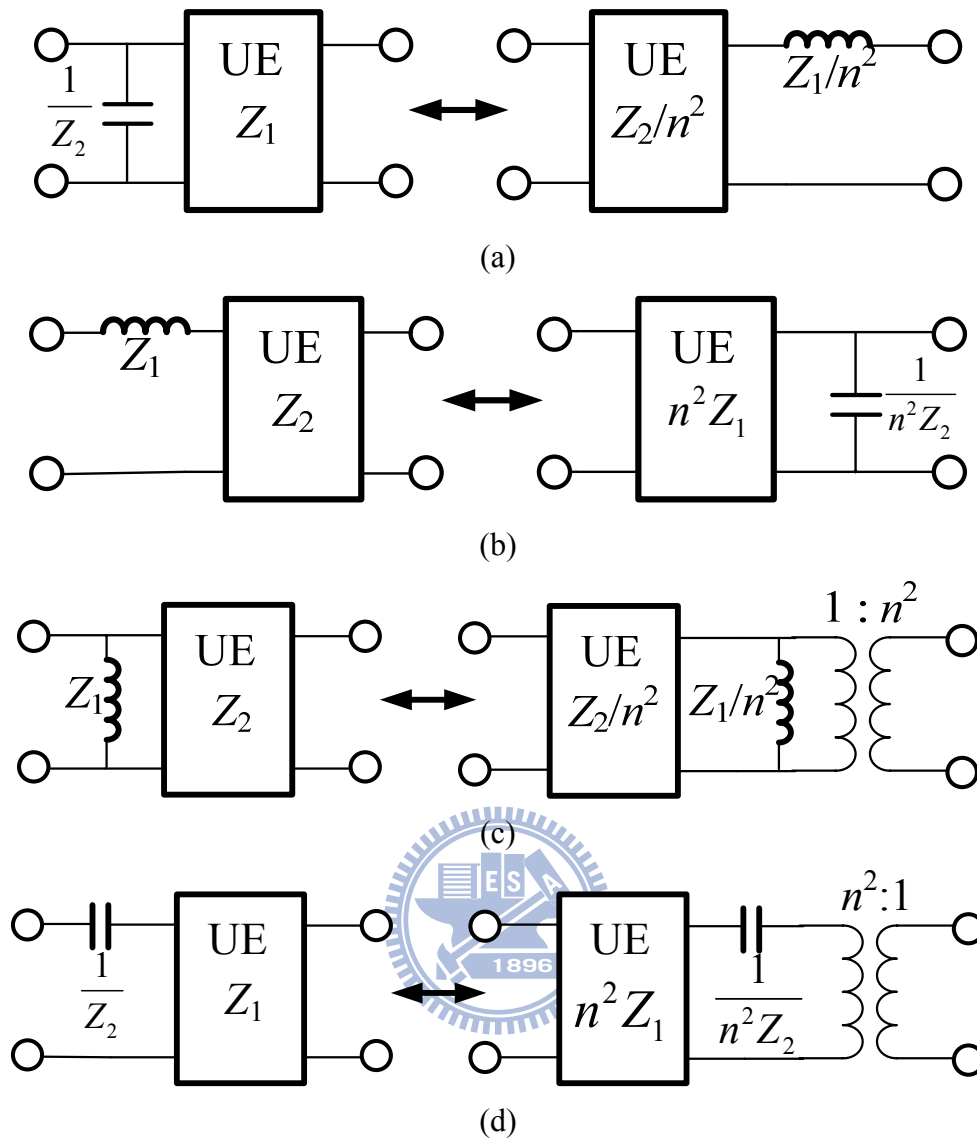


Fig. 2.25. The four Kuroda identities where $n^2 = 1 + Z_2/Z_1$.

turns ratio of $n^2 : 1$.

It should be emphasized here that the Kuroda identities apply specifically to S -plane networks. This means that in terms of the equivalent distributed s -plane elements, the lengths of the reactive stubs (equivalent to the S -plane inductors and capacitors) and the adjacent transmission lines (equivalent to the unit elements) must all be identical.

2.2.3 Transmission Line Approximating Functions and Synthesis Procedure

In this dissertation, due to the concerned network as shown in Fig. 1.3, Marchand balun is inherently a band-pass network. Thus, filter theorem can be adopted to synthesize the Marchand balun. The key point is to determine the polynomial of reflection coefficient for a cascade of unit elements and prototype LC distributed elements. Table 2.2 provides each of the distributed L , C and U.E. and its corresponding $ABCD$ matrices. For showing how to obtain the reflection coefficient, a prototype circuit shown in Fig. 2.26 is taken as an example. The first is to utilize the $ABCD$ parameter in Table 2.2 and obtain the overall cascaded $ABCD$ matrices

$$\begin{aligned} \begin{bmatrix} A(S) & B(S) \\ C(S) & D(S) \end{bmatrix}_{all} &= \begin{bmatrix} 1 & 0 \\ SC & 1 \end{bmatrix} \begin{bmatrix} 1 & 0 \\ 1/SL & 1 \end{bmatrix} \frac{1}{\sqrt{1-S^2}} \begin{bmatrix} 1 & Z_{01}S \\ Y_{01}S & 1 \end{bmatrix} \dots \\ &\dots \frac{1}{\sqrt{1-S^2}} \begin{bmatrix} 1 & Z_{03}S \\ Y_{03}S & 1 \end{bmatrix} \end{aligned} \quad (2.74)$$

Then, the reflection coefficient is given by the well-known formula

$$S_{11}(S) = \frac{A(S) + B(S) - C(S) - D(S)}{A(S) + B(S) + C(S) + D(S)} \quad (2.75)$$

Actually, in [132]-[136] distributed transmission line elements have been studied and some approximating functions are obtained to be suitable to the corresponding circuit networks. For the concerned prototype circuits shown in Fig. 2.26, the generalized magnitude squared high- and low-pass transfer functions with Chebyshev responses are described and summarized by Horton and Wenzel [135]. The characteristic functions associated with the high- and low-pass prototype circuits are given by

$$K(S^2) = \left[T_m \left(\frac{S_C}{S} \right) T_n \left(\frac{\sqrt{1-S_C^2}}{\sqrt{1-S^2}} \right) - U_m \left(\frac{S_C}{S} \right) U_n \left(\frac{\sqrt{1-S_C^2}}{\sqrt{1-S^2}} \right) \right]^2 \quad (2.76)$$

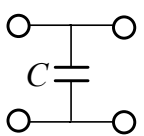
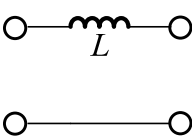
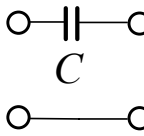
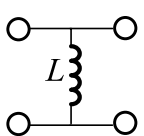
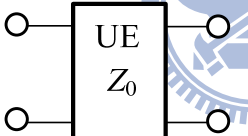
Filter elements	$ABCD$
	$\begin{bmatrix} 1 & 0 \\ SC & 1 \end{bmatrix}$
	$\begin{bmatrix} 1 & SL \\ 0 & 1 \end{bmatrix}$
	$\begin{bmatrix} 1 & \frac{1}{SC} \\ 0 & 1 \end{bmatrix}$
	$\begin{bmatrix} 1 & 0 \\ \frac{1}{SL} & 1 \end{bmatrix}$
	$\frac{1}{\sqrt{1-S^2}} \begin{bmatrix} 1 & Z_0 S \\ Y_0 S & 1 \end{bmatrix}$

Table 2.2. $ABCD$ matrices for distributed LC ladder and a unit element.

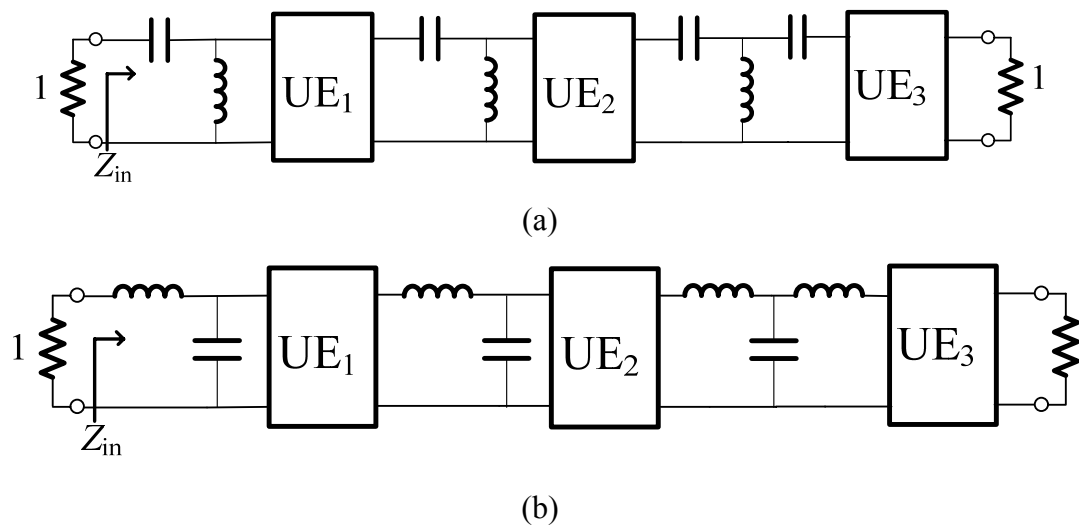


Fig. 2.26. (a) A possible high-pass prototype circuit. (b) A possible low-pass prototype circuit

and

$$K(S^2) = \left[T_m \left(\frac{S}{S_c} \right) T_n \left(\frac{S\sqrt{1-S_c^2}}{S_c\sqrt{1-S^2}} \right) - U_m \left(\frac{S}{S_c} \right) U_n \left(\frac{S\sqrt{1-S_c^2}}{S_c\sqrt{1-S^2}} \right) \right]^2 \quad (2.77)$$

respectively, where $T_n(x)$ and $U_n(x)$ are the unnormalized Chebyshev polynomials of the first and second kind of order n :

$$\begin{aligned} T_n(x) &= \cos(n \cos^{-1} x) \\ U_n(x) &= \sin(n \cos^{-1} x) \end{aligned} \quad (2.78)$$

, $S_c = j\Omega_c$, Ω_c is the cutoff frequency which occurs at half power (-3dB), and m is the number of a mixed cascade ladder elements and n is the number of unit elements.

Furthermore, it is recalled that the scattering parameters are related to the characteristic function $K(S^2)$ and the ripple level ε of the circuit by

$$|S_{21}(S)|^2 = \frac{1}{1 + \varepsilon^2 K(S^2)} \quad (2.79)$$

$$|S_{11}(S)|^2 = \frac{\varepsilon^2 K(S^2)}{1 + \varepsilon^2 K(S^2)} \quad (2.80)$$

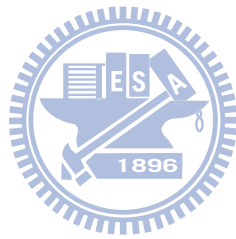
Then the appropriate poles and zeros of $|S_{11}(S)|^2$ must be assigned to $S_{11}(S)$ and $S_{11}(-S)$ with the knowledge that

$$|S_{11}(S)|^2 = S_{11}(S) * S_{11}(-S) \quad (2.81)$$

The next step is to derive the input impedance function $Z_{in}(S)$ shown in Fig. 2.26. The source resistance is assumed to be unity. The relationship between $S_{11}(S)$ and $Z_{in}(S)$ is expressed as

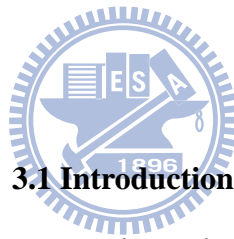
$$Z_{in}(S) = \frac{1 + S_{11}(S)}{1 - S_{11}(S)} \quad (2.82)$$

Finally, the circuit networks shown in Fig. 2.26 are synthesized using the method of standard element extraction which can be found in [135]-[137].



Chapter 3 Quarter-Wave Stepped-Impedance Resonator Filters with Quadruplet and Canonical Form Responses

In this chapter, compact microstrip quarter-wave stepped-impedance resonator (SIR) bandpass filters with quadruplet and canonical form responses are proposed. The proposed quadruplet filter can be designed to have a pair of transmission zeros to achieve sharp selectivity. In addition, by applying an extra source-load coupling, two additional transmission zeros on both side of passband are created to further enhance the selectivity. Because the quarter-wave SIRs are adopted, the circuit size of the filters can be largely reduced and the upper stopband can be extended. Two generalized Chebyshev filters corresponding to quadruplet and canonical form coupling schemes are fabricated. Simulated and measured results are matched very well.



3.1 Introduction

Compact and high-performance microstrip bandpass filters are important building blocks in wireless and mobile communications due to their small size, ease of fabrication and light weight. In many literatures, half-wave or quarter-wave resonators are utilized to design microstrip bandpass filters. The conventional parallel-coupled filters using half-wave resonators have a large circuit size, and they don't exhibit generalized Chebyshev responses for high selectivity [69], [97]. The hairpin and quarter-wave resonators with cross couplings are proposed to solve the problems [72], [75]-[77]. However, these filters still suffer from spurious responses due to the distributed nature. The filters with half-wave resonators depict spurious responses at twice of the center frequency, and the filters with quarter-wavelength resonators have spurious responses at three times of the center frequency.

Recently, many efforts focus on the half-wave and the quarter-wave SIRs to design cross-coupled filters [78]-[80]. In [78], the fourth order filter utilizing both $\lambda/2$ and $\lambda/4$ resonators shows a good rejection bandwidth and high selectivity. However, control of the physical parameters of the open stubs of the $\lambda/2$ SIR-like resonators (resonator 1 and 4) are not easy because they not only suppress the high-order resonances but also implement the external coupling to maintain the appropriate passband performance. In [79], although a good selectivity is obtained, both the coupling routes and the physical layout are too complicated so that the synthesis of the coupling matrix and final fine tuning of the physical layout are too time consuming. In [80], the $\lambda/4$ SIR filter shows good selectivity. However, to design the locations of the transmission zeros is very complicated and too much depends on experience.

In this chapter, we propose two microstrip $\lambda/4$ SIR filters both with generalized Chebyshev responses. The proposed filters can overcome the above problems. Fig. 3.1(a) and Fig. 3.1(b) show two fourth-order filters with cross coupling that one is without source-load coupling and the other is with source-load coupling. The filter in Fig. 3.1(a) has a pair of transmission zeros due to quadruplet coupling scheme whereas the filter in Fig. 3.1(b) has two pairs of transmission zeros due to canonical form coupling scheme. A coupling enhancement line between source and load in Fig. 3.1(b) is used to control the source-load coupling strength. Thus, with the coupling enhancement line, two extra transmission zeros can be controlled easily with a little influence on passband performance. In addition, the $\lambda/4$ stepped impedance resonators are used to obtain compact size and to push the high order spurious frequencies to as high as possible. Therefore, the proposed filters are suitable for bandpass filters with small size, wide stopband and sharp selectivity in a modern communication system.

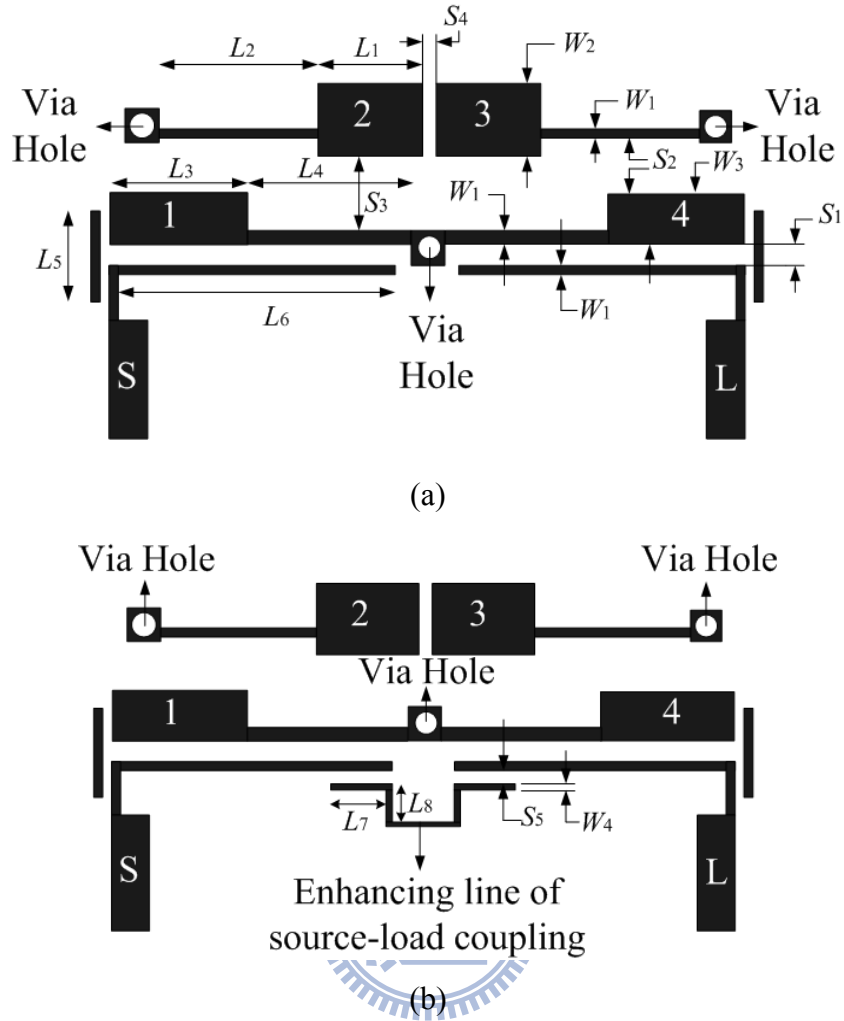


Fig. 3.1. The circuit layouts of the proposed microstrip quarter-wave SIR filters. (a) The fourth-order quadruplet filter. (b) The fourth-order quadruplet filter with source-load coupling.

3.2 Coupling Schemes and Stepped Impedance Resonators

The circuit layout in Fig. 3.1(a) and Fig. 3.1(b) can be modeled as the quadruplet coupling scheme shown in Fig. 3.2(a) and the canonical coupling scheme depicted in Fig. 3.2(b) respectively. Here, the resonators are represented by dark dots, the source and load are empty dots, the solid lines between resonators indicate main coupling, and the broken lines indicate the cross coupling. As shown in Fig. 3.1(a) and Fig. 3.1(b), the unwanted cross coupling exists and leads the coupling route to be complicated. Thus, to avoid the design complexity, we ignore the unwanted cross

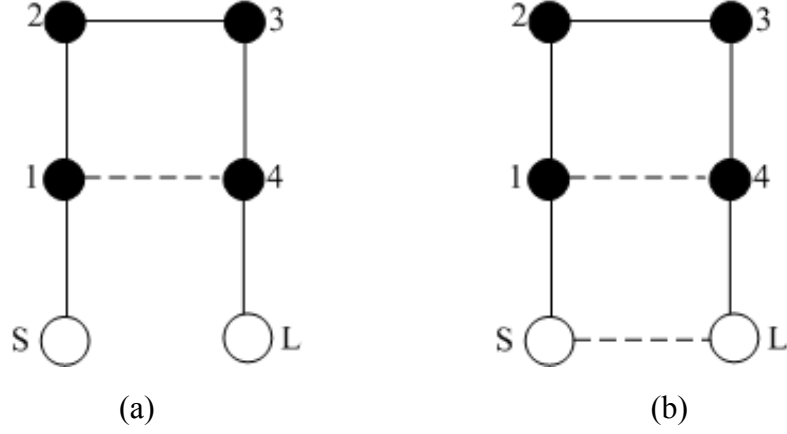


Fig. 3.2. Coupling schemes for the bandpass filters proposed in this chapter. (a) Quadruplet. (b) Canonical form.

coupling in the coupling scheme when designing the filter. This would simplify the coupling matrix.

When designing a cross-coupled filter with the corresponding coupling scheme shown in Fig. 3.2(a), the first step is to extract a coupling matrix which satisfies the specification. In our designed case, the quadruplet filter without source-load coupling is realized to have one pair of real frequency transmission zeros at normalized frequency $\Omega = \pm 2$ for selectivity. The center frequency, fractional bandwidth, and maximum in-band return loss of both filters are 2.45 GHz, 8%, and 20dB, respectively. By using the synthesis technique in [37], the coupling matrix is obtained as

$$M = \begin{bmatrix} 0 & 1.0236 & 0 & 0 & 0 & 0 \\ 1.0236 & 0 & 0.8706 & 0 & -0.1705 & 0 \\ 0 & 0.8706 & 0 & 0.7673 & 0 & 0 \\ 0 & 0 & 0.7673 & 0 & 0.8706 & 0 \\ 0 & -0.1705 & 0 & 0.8706 & 0 & 1.0236 \\ 0 & 0 & 0 & 0 & 1.0236 & 0 \end{bmatrix} \quad (3.1)$$

The next step is to implement the coupling matrix in microstrip technology. For compact size and wide upper stopband, the $\lambda/4$ SIR is a good choice to realize the proposed filter. In the following, we would briefly illustrate basic properties of the SIR.

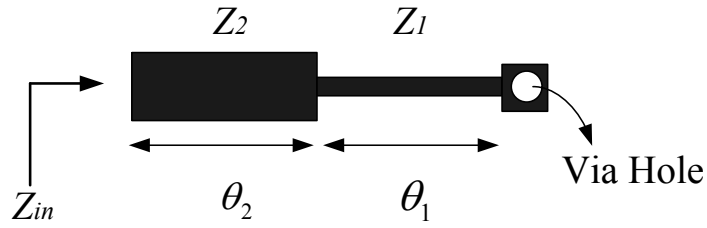


Fig. 3.3. The basic structure of the quarter-wave SIR.

Fig. 3.3 is a basic structure of the quarter-wave stepped impedance resonator ($\lambda/4$ SIR). This resonator comprises two transmission lines with different characteristic impedances. The transmission line of the high impedance Z_1 and the electrical length θ_1 is connected to ground through a via-hole. The transmission line of the low impedance Z_2 and the electrical length θ_2 is connected to the high impedance transmission line and the other end is open circuited. The input impedance of the $\lambda/4$ SIR can be derived easily as follows [92]

$$Z_{in} = jZ_2 \frac{Z_1 \tan \theta_1 + Z_2 \tan \theta_2}{Z_2 - Z_1 \tan \theta_1 \tan \theta_2} \quad (3.2)$$

The parallel resonance occurs when $Y_{in} = 1/Z_{in} = 0$, then we can obtain a useful equation as follows

$$R_Z = \tan \theta_1 \tan \theta_2 \quad (3.3)$$

where R_Z is the impedance ratio of the SIR given as

$$R_Z = \frac{Z_2}{Z_1} \quad (3.4)$$

It can be seen from (3.3) and (3.4) that the important parameters of the resonance condition of SIR are θ_1 , θ_2 and R_Z . When $\theta_1 = \theta_2$, the overall electrical length $\theta_{TA} (= \theta_1 + \theta_2)$ of the resonator and the first spurious frequency f_{SA} are obtained as

$$\theta_{TA} = \tan^{-1} \left(\frac{2\sqrt{R_Z}}{1-R_Z} \right) \quad (3.5)$$

$$f_{SA} = \left(\frac{\pi}{\tan^{-1} \sqrt{R_Z}} - 1 \right) f_0 \quad (3.6)$$

For designing the quadruplet filter proposed in this chapter, we would consider different coupling mechanisms. Figs. 3.4(a)-(c) show three types of coupled microstrip SIRs. The coupling between two resonators in Fig. 3.4(a) is electric coupling due to the stronger electric field around the coupling gap. The coupling in Fig. 3.4(b), on the other hand, is a magnetic coupling due to the inductance contributed by the via-hole. For the coupling of the structure in Fig. 3.4(c), both the electric and magnetic couplings occur at both the coupling sides, and it is a mixed coupling.

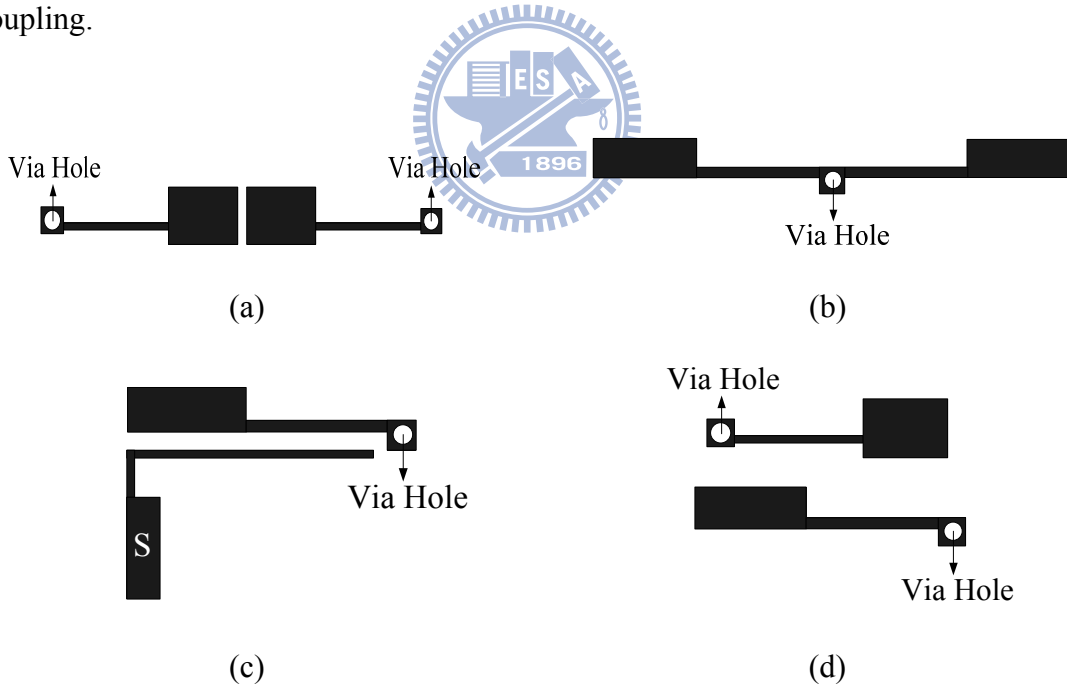


Fig. 3.4. Basic coupling structures of the proposed filters. (a) The electric coupling. (b) The magnetic coupling. (c) The mixed coupling. (d) The coupled-line coupling for input/output coupling.

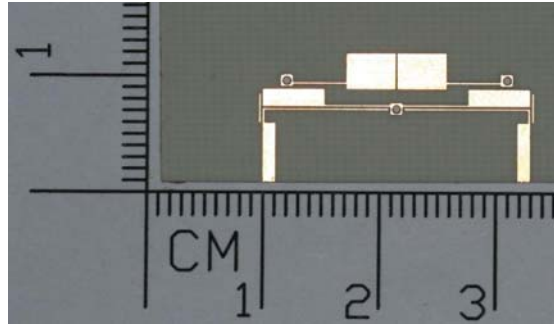
Once the coupling matrix, the type of the resonators and the circuit layout of the filter are determined, we could follow the procedure defined in [6] to determine the

length of each $\lambda/4$ SIR and the spacing between two $\lambda/4$ SIRs so as to get the initial physical parameters. The length of the SIR might be adjusted until the resonance occurs at the center frequency. The spacing between two resonators in Figs. 3.4(a) and 3.4(c) can be determined from the two resonant peaks in the transmission coefficients. In Fig. 3.4(b), the two $\lambda/4$ SIRs couple through the via hole inductance, and the coupling coefficient can also be obtained. The input and output coupling coefficients in Fig. 3.4(d) are determined by observing the phase of the reflection coefficient. It should be pointed out that in Fig. 3.1(a) two short transmission lines are used to enhance the coupling between source and resonator 1 and load and resonator 4, respectively. Therefore, we can roughly obtain each element of the coupling matrix shown in (3.1).

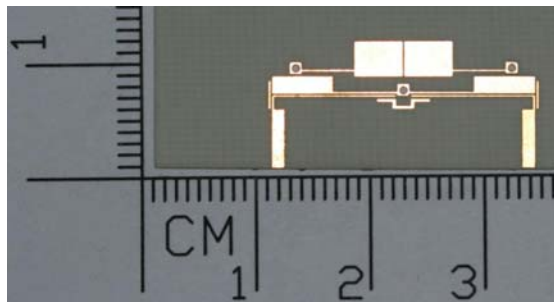
3.3 Filter Design Examples and Results

The proposed filters are built on a 20-mil-thick Rogers RO4003 substrate with $\epsilon_r = 3.38$, $\tan\delta = 0.0021$. The commercial EM-simulation software Sonnet 9.0 [100] is used to perform the actual computation as described above. The specifications of the filter in Fig. 3.1(a) are described in previous section. Here, the dimensions of the resonator 1 are the same as the resonator 4 and the resonator 2 are the same as the resonator 3. The values of Z_1 and Z_2 for resonator 1 and 4 are chosen as 121 and 41.78 Ω , respectively. The values of Z_1 and Z_2 for resonator 2 and 3 are chosen as 121 and 24.93 Ω , respectively. Thus, from (3.3)-(3.6), the values of R_Z and θ_1 for resonator 1 are 0.206 and 24.41 degree, respectively, and the values of R_Z and θ_1 for resonator 2 are 0.3453 and 30.44 degree, respectively.

The initial dimensions are then fine tuned to achieve the original specifications. The dimensions (mm) of the filter shown in Fig. 3.1(a) are $W_1=0.15$, $W_2=3.10$, $W_3=1.52$, $L_1=4.27$, $L_2=4.82$, $L_3=5.28$, $L_4=5.87$, $S_1=0.13$, $S_2=0.38$, $S_3=1.29$, $S_4=0.15$, $L_5=2.54$, $L_6=10.82$. The diameter of the via-hole is 0.81 mm. The second filter shown



(a)

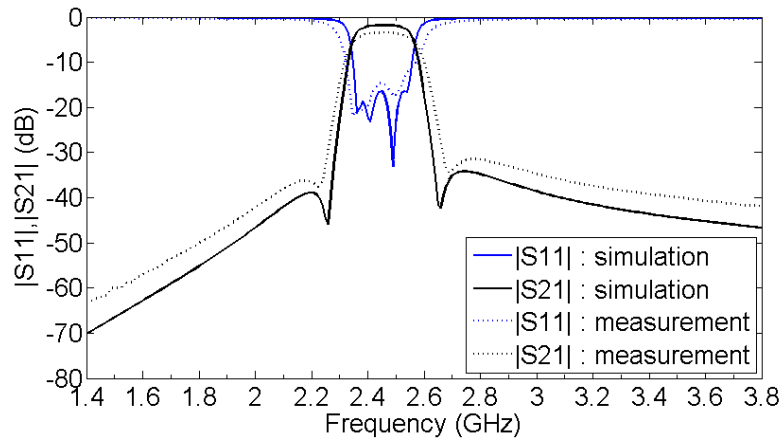


(b)

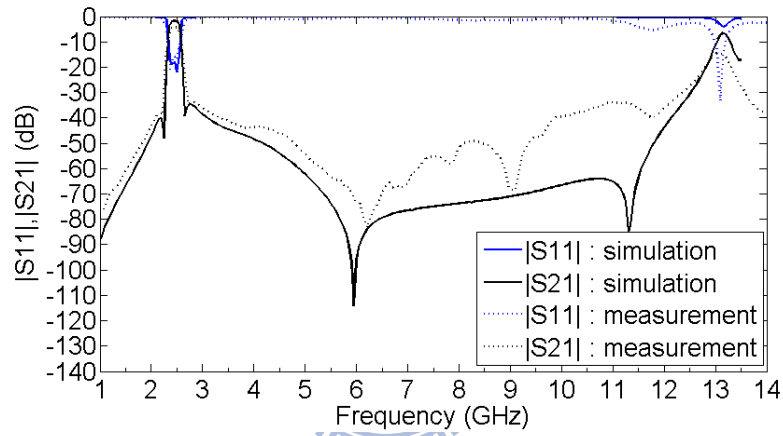
Fig. 3.5. The constructed filters. (a) The quadruplet filter. (b) The quadruplet filter with source/load coupling.

in Fig. 3.1(b) is a canonical form filter that two cross couplings one between resonator 1 and 4 the other one between source and load are included. This would create two extra finite transmission zeros to improve selectivity. Fortunately, one can add the source-load coupling as a perturbation that other portion of the filter could keep unchanged. Therefore, all of the dimensions of the filter in Fig. 3.1(b) are the same as Fig. 3.1(a) except for the source-load coupling enhancement line. The dimensions (mm) of the second filter are $W_4=0.2$, $S_5=0.25$, $L_7=1.17$, $L_8=0.61$. Figs. 3.5(a) and 3.5(b) show the pictures of the two constructed filters.

Fig. 3.6(a) shows the measured in-band performance of the first constructed filter. Good agreement between the simulated and measured results is observed. The midband insertion loss is 2.7 dB and the return loss is greater than 14 dB. The simulated and measured wide-band performances of the filter from 1 GHz up to 14



(a)

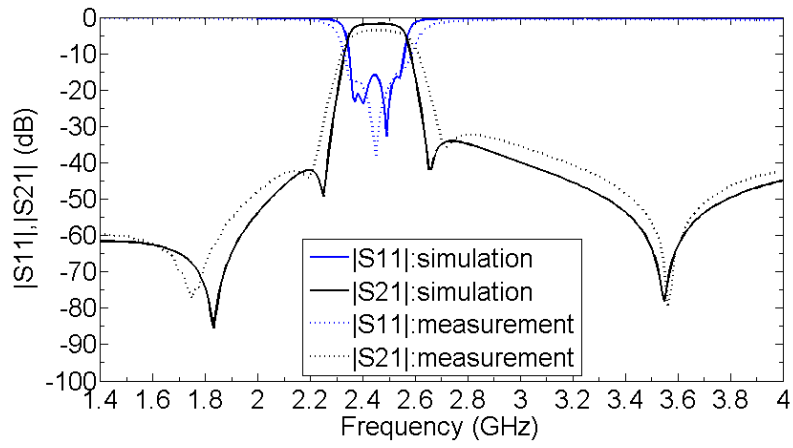


(b)

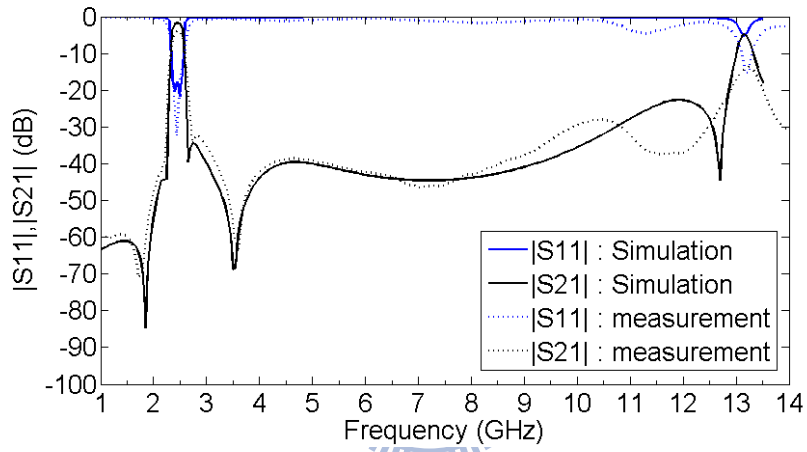
Fig. 3.6. Measured and simulated performances of the quadruplet filter of Fig. 4.5(a). (a) In a narrow-band. (b) In a wide band.

GHz are illustrated in Fig. 3.6(b). The measured transmission performance of the filter is with a rejection level better than 30 dB up to 12.5 GHz.

The in-band performance of the second constructed filter is shown in Fig. 3.7(a). The measured positions of the two additional transmission zeros contributed by source-load coupling are just a little drift compared with the simulated results. The measured insertion loss is 2.75 dB and the return loss is greater than 17 dB. The measured upper stopband performance of the filter shown in Fig. 3.7(b) follows the simulation and achieves an attenuation level exceeding 27 dB up to 12.7 GHz.



(a)



(b)

Fig. 3.7. Measured and simulated performances of the quadruplet filter with source/load coupling in Fig. 3.5(b). (a) In a narrow-band. (b) In a wide band.

Chapter 4 Microstrip Parallel-Coupled Filters with Cascade Trisection and Quadruplet Responses

Microstrip parallel-coupled filters with generalized Chebyshev responses are presented. The basic structure of the proposed filter is a conventional parallel-coupled filter which the physical dimensions can be easily obtained by the well-known analytical method. With the aid of the equivalent circuit corresponding to a conventional parallel-coupled filter, the relative insertion phase from source or load to each open-end of resonators can be easily obtained by observing the two-port admittance matrix. Applying the cross coupling from source or load to a proper nonadjacent resonator, a trisection or a quadruplet coupling scheme can be realized with prescribed transmission zeros. More importantly, the proposed trisection can be designed to have a transmission zero on the lower or upper stopband by just adjusting the length of the cross coupling strip. Using the proposed structure, the conventional time-consuming adjusting procedure to obtain initial physical dimensions of filters is no longer required. In this chapter, a fourth-order parallel-coupled filter is used as the basic structure to demonstrate various combinations of transmission zeros. Simulated and measured results are well matched.

4.1 Introduction

High performance microwave filters are essential circuits in many microwave systems where they serve to pass the wanted signals and suppress unwanted ones in frequency domain [26]. Cross-coupled filters are attractive since they exhibit highly selective responses which are required in modern communication system. Among these cross-coupled filters, the cascade trisections (CT) and cascade quadruplets (CQ) [6], [71], [73], [81], [82], [95] are two of the most commonly used coupling schemes.

Besides the cross-coupled coupling schemes, other coupling topologies such as doublet, extended doublet and box-section were also found interesting [66], [86] and have been successfully implemented in microstrip form [88], [89]. In brief, all of the mentioned filters are designed to have finite transmission zeros for better selectivity.

To design a cross-coupled filter such as the filters in [6], [71], [73], [81], [95], the following procedures are usually taken. The first step is to synthesize a coupling matrix corresponding to a desired response. Secondly, decide the suitable physical layout of the resonator. Thirdly, adjust distance and orientation of two neighboring resonators two by two to get proper signs and magnitudes of the corresponding coupling coefficients. In this step, the Dishal's method [38] is usually used. A detailed description of Dishal's method is given in [6]. Finally, fine tune the whole circuit. The third and final steps are the most tedious and time-consuming steps because, in the third step, they need to generate design curves of coupling and external Q from an EM field solver and, in the final step, one resonator may have many neighbors that when adjusts the distance and orientation against one neighbor the coupling strength with other neighbors may change. Therefore, the iterative adjusting procedure might require. Another drawback to design the conventional cross-coupled filter is that if one coupling coefficient in the coupling matrix changes sign, the physical layout must be reconfigured. For example, in the case of cascade trisection filters of [73], completely different orientations of the resonators must be adopted for a trisection having a lower stopband transmission zero and a trisection having an upper stopband transmission zero because there is one coupling coefficient changed sign. This means that the time-consuming adjusting step described above must be done separately in two cases.

Another interesting cross-coupled filter based on a parallel-coupled filter structure was proposed by Hong and Lancaster [96]. In [96], an extra microstrip line

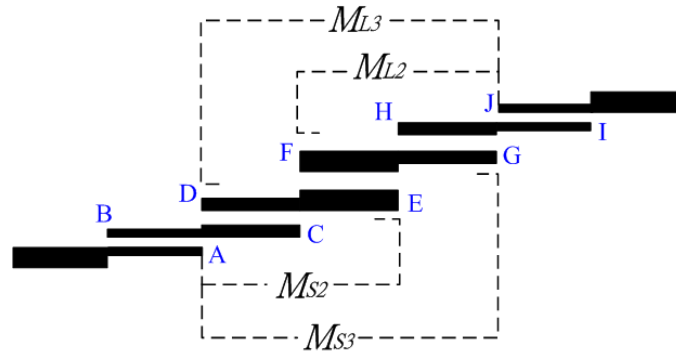
couples the nonadjacent resonators (resonator 1 and 4 in the paper) to produce transmission zeros. By adjusting the length of this extra coupling microstrip line and gaps of the coupling sections, the locations of the transmission zeros can be manipulated. This kind of filter has the benefit of simple layout, manageable transmission zeros, and much less time for adjusting layout than conventional cross-coupled filters. However, it has some problems. The extra coupling microstrip line has its own resonant frequencies. If the electrical length of this extra coupling microstrip line is not integer multiples of 180° , spurious responses appear at these resonant frequencies on lower or upper stopband. The spurious resonance can seriously degrade the stopband performance of the filter. The situation becomes more severe as the extra coupling line becomes longer. If the electrical length of this extra coupling microstrip line is integer multiples of 180° , it becomes an extra resonant node in the coupling route. This extra-resonant node causes the coupling diagram more complex when synthesizing a proper coupling matrix corresponding to a desired response. One way to solve this problem is to use source or load to nonadjacent resonators cross couplings [82]. Unlike [96], the extra coupling line in [82] is directly connected to source or load so that no self-resonance of this extra coupling line will occur. The filter in [82] can largely simplify the design procedures of a CT filter due to its conventional microstrip parallel-coupled filter structure. The CT filter in [82] introduces cross couplings of $M_{S,2}$ and $M_{L,n-1}$ to generate two trisections that two independently controllable transmission zeros on upper stopband are produced. However, the realizable response of the filter in [82] is limited to be the CT filter with two upper stopband transmission zeros.

In spite of the cross-coupled schemes, the coupling schemes such as doublet, extended doublet and box-section are introduced [66], [86]. The main characteristic of these coupling schemes is the ability to shift a transmission zero from one side of

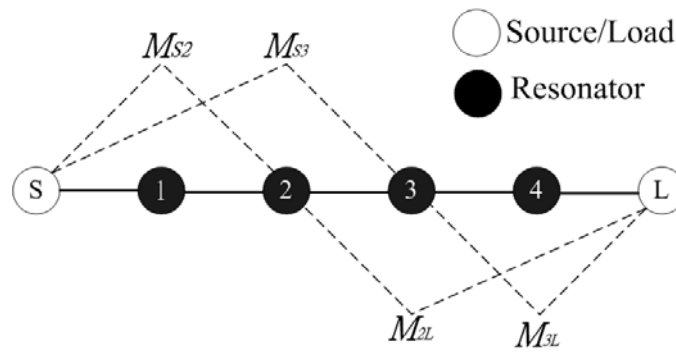
passband to the other by just adjusting the resonant frequencies of resonators in the box portion of the coupling scheme, and this is so-called zero shifting characteristic. Recently, a fourth-order box-section filter proposed by Amari *et al.* [88] and filters with box-like coupling schemes proposed by Liao *et al.* [89] have been successfully implemented using microstrip lines. The drawback of the former is that it needs to use the Dishal's method as described above. The latter used an E-shaped two-mode resonator, namely even- and odd-mode, to support corresponding coupling schemes such as doublet, extended doublet, and box-section. Unfortunately, when designing such a two-mode filter, the physical dimensions of the resonators are very sensitive especially the dimensions of the two-mode resonator. While tuning the filter, carefully adjusting physical parameters of the two-mode resonator is required because some dimensions of the two-mode resonator influence not only the position of the transmission zero but also the in-band return loss. It means that designer should spend much time to tune.



In this chapter, we propose new cross-coupled filters based on a conventional parallel-coupled filter, and all of the shortcomings described above can be solved. Basically, this newly proposed filter structure takes the advantages of the Hong's filter [96] and Liao's filter [82]. Fig. 4.1(a) shows the schematic layout of the proposed filter with a fourth order filter as an example where the crossing coupling between source or load and nonadjacent resonators are presented by dotted lines. Its equivalent coupling diagram is shown in Fig. 4.1(b). The filter has the advantage of using the simple synthesis procedure presented in [97] to serve as the initial design. In Figs. 4.1(a) and (b), although the figures show multiple cross coupling routes from source to nonadjacent resonators, only one of them is chosen in the design procedures. Similar situation occurs in the load end. Then, by observing the relative phase shifts of main and cross-coupled paths between source or load and one of the nodes of the



(a)



(b)

Fig. 4.1. The cross-coupled parallel coupled filter. (a) The schematic layout. (b) Coupling and routing scheme corresponding to (a).

interested resonator, filters with generalized Chebyshev responses can be implemented. Applying suitable cross coupling paths and phases, the proposed filter could be CT, CQ, or combination of quadruplet and trisection. It is important to note that in the trisection configuration the transmission zero can be located on either lower or upper stopband by just applying the suitable cross coupling in Fig. 4.1(a). Therefore, the design procedures of the proposed filter are easy without using of the Dishal's method or the method presented in [6]. Besides, it is more flexible to locate the transmission zeros.

4.2 Phase Relationships and Generation of Finite Transmission Zeros

The purpose in this section is to explore the relative phase shifts of the main

coupling path from source or load to resonators and to apply suitable phase shifts of the cross coupling paths to generate finite frequency transmission zeros on either upper stopband, or lower stopband, or both of the stopbands. Let us take a fourth order filter as an example.

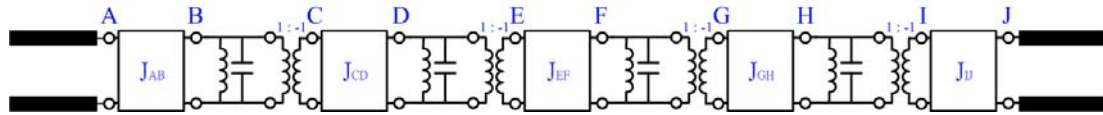


Fig. 4.2. The equivalent lumped-element circuit of a fourth-order parallel coupled filter.

In the beginning, the initial design of the proposed filters is based on the conventional parallel-coupled filter presented by Cohn [97]. Fig. 4.2 shows the lumped-element equivalent circuit of a fourth-order parallel-coupled filter shown in Fig. 4.1(a). Cross couplings are not introduced at this moment. Here, it should be pointed out that the lumped-element equivalent circuit should include the phase-reversing transformer in every resonator. Although the phase-reversing transformer is often omitted in a conventional parallel-coupled filter due to no effect on the magnitude of filter response, it is, however, very important in the proposed cross-coupled filters. Let us now check phase relationships from source or load to resonators. In order to observe the relative phase conveniently, we sequentially number the corresponding nodes of Figs. 4.1(a) and 4.2 as A-J from source to load. Therefore, the relative phases in the lumped-element circuit model of Fig. 4.2 can be determined, and all of the insertion phases between node A and nodes B-J in Fig. 4.1(a) are obtained easily. Consider each box in Fig. 4.2 which represents an ideal admittance inverter having constant image admittance and constant phase shift of -90° for all frequencies. Let nodes A and B to be the input and output ports of the admittance inverter J_{AB} . The matrix element Y_{BA} of the two-port admittance matrix can

then be determined. Thus, the phase of Y_{BA} is -90° over both the frequency ranges $f < f_0$ and $f > f_0$ where f_0 is the center frequency of the filter. Also, the phase shift of the phase-reversing transformer is -180° for all frequencies. Consequently, the phase of Y_{CA} is -270° over both the frequency ranges $f < f_0$ and $f > f_0$. Next, consider Y_{DA} that the shunt inductor/capacitor pair as shown in Fig. 4.2 is a resonator. The phase shift of a resonator at off-resonance frequencies is dependent on whether the frequency is above or below resonance. As $f < f_0$ the admittance of the resonator is inductive and the phase shift should be -90° . Similarly, as $f > f_0$, the admittance of the resonator is capacitive and the phase shift should be $+90^\circ$. As a result, the phase shift of Y_{DA} is -90° when $f < f_0$ ($-90^\circ - 90^\circ - 180^\circ - 90^\circ = -450^\circ = -90^\circ$) and $+90^\circ$ when $f > f_0$ ($-90^\circ + 90^\circ - 180^\circ - 90^\circ = -270^\circ = +90^\circ$). Following similar analyzing procedures described above, one can observe every relative phase shift between node A and nodes B-J. The phase relationships from source or load to resonators can be easily observed by using any commercial circuit simulator. Table 4.1 summarizes the phase relationships between node A and nodes B-J as $f < f_0$ and $f > f_0$. The method is applicable to any order of a parallel-coupled filter. As a result, the relative phase shifts between node A and nodes B-J in Fig. 4.1(a) are identical to those of the lumped-element filter in Fig. 4.2







Next, the cross coupling paths will be studied. When a cross coupling path is applied to node A and another node in the nonadjacent resonator and its phase delay is 180° out of phase with the main path, a transmission zero appears.

The trisection coupling scheme in this filter can be formed by adding a cross coupling path from source to the second resonator. The two ends of the second resonator corresponds to node D and node E. Assume the cross coupling path is applied from source to node D. Because the phase of the main coupling path Y_{DA} is $+90^\circ$ as $f > f_0$, the phase of the cross coupling path from source to node D should

be -90° as $f > f_0$ in order to have an upper stopband transmission zero. On the other hand, if the cross coupling path is applied between source and node E, the filter can also have an upper stopband transmission zero when the phase of cross coupling path Y_{EA} is $+90^\circ$ as $f > f_0$ due to -90° of phase in the main path Y_{EA} as $f > f_0$. In contrast to an upper stopband transmission zero as discussed above, a lower stopband transmission zero could also be possible by applying -90° phase shifts of the cross coupling path Y_{EA} as $f < f_0$ where it is 180° out of phase with that of the main path Y_{EA} . In spite of the source, the load can also be cross-coupled to the third resonator in Fig. 4.1(a) to form another trisection.

Another popular coupling scheme is so called quadruplet where two transmission zeros, one on upper stopband and the other on lower stopband, are generated by applying just one cross coupling path. The quadruplet cross coupling could be from source to the third resonator or from load to the second resonator. Utilizing similar phase analysis method as trisection, the phase relationship of the quadruplet coupling scheme can be easily obtained. Let us use the cross coupling path from source to node G as an example. The phase shift of the main path Y_{GA} is $+90^\circ$ as $f < f_0$ and $f > f_0$. As mentioned above, as long as the phase shift of the cross coupling path Y_{GA} is -90° , two transmission zeros on both lower and upper stopband should appear. Similarly, the quadruplet cross coupling path could also be formed from source to node F.

Table 4.1 summarizes the phase relationships that may help a designer to judge the relative phase of the main coupling from source or load to each node and to apply proper phase of the cross coupling to create desired transmission zeros. After the positions of the transmission zeros being qualitatively determined, the proper strength of the cross coupling should be quantitatively determined for a desired specification. Full discussion will be presented in section 4.3.

	The main coupling path		The cross coupling path		Response	Delay line electrical length	Frequency response predicted
	$f < f_0$	$f > f_0$	$f < f_0$	$f > f_0$			
$Y_{BA}(Y_{BI})$	-90	-90	Not applicable	Not applicable			
$Y_{CA}(Y_{CI})$	+90	+90	Not applicable	Not applicable			
$Y_{DA}(Y_{DI})$	-90	+90	-90	-90	Trisection with a TZ on upper stopband	0° or 360°	
$Y_{DA}(Y_{DI})$	-90	+90	+90	+90	Trisection with a TZ on lower stopband	180°	
$Y_{EA}(Y_{EI})$	+90	-90	-90	-90	Trisection with a TZ on lower stopband	0° or 360°	
$Y_{EA}(Y_{EI})$	+90	-90	+90	+90	Trisection with a TZ on upper stopband	180°	
$Y_{FA}(Y_{FI})$	-90	-90	+90	+90	Quadruplet	180°	
$Y_{GA}(Y_{GI})$	+90	+90	-90	-90	Quadruplet	360°	
$Y_{HA}(Y_{HI})$	-90	+90			*		
$Y_{IA}(Y_{II})$	+90	-90			*		
$Y_{JA}(Y_{JI})$	-90	-90			*		

* : it is a cross coupling not belongs to trisection or quadruplet and beyond the scope of this research.

Table 4.1. The relative phase shifts of the main coupling path, the proper phases of the cross coupling paths to generate transmission zeros, corresponding responses, and delay line electrical length.

4.3 Cross-Coupling Schemes

Two coupling schemes, namely the CT and the mixed cascade quadruplet and trisection [65], are possible for our fourth-order examples. Fig. 4.3(a) and Fig. 4.4(a) show the CT and the mixed cascade quadruplet and trisection coupling schemes respectively. Although the CT and the mixed cascade quadruplet and trisection

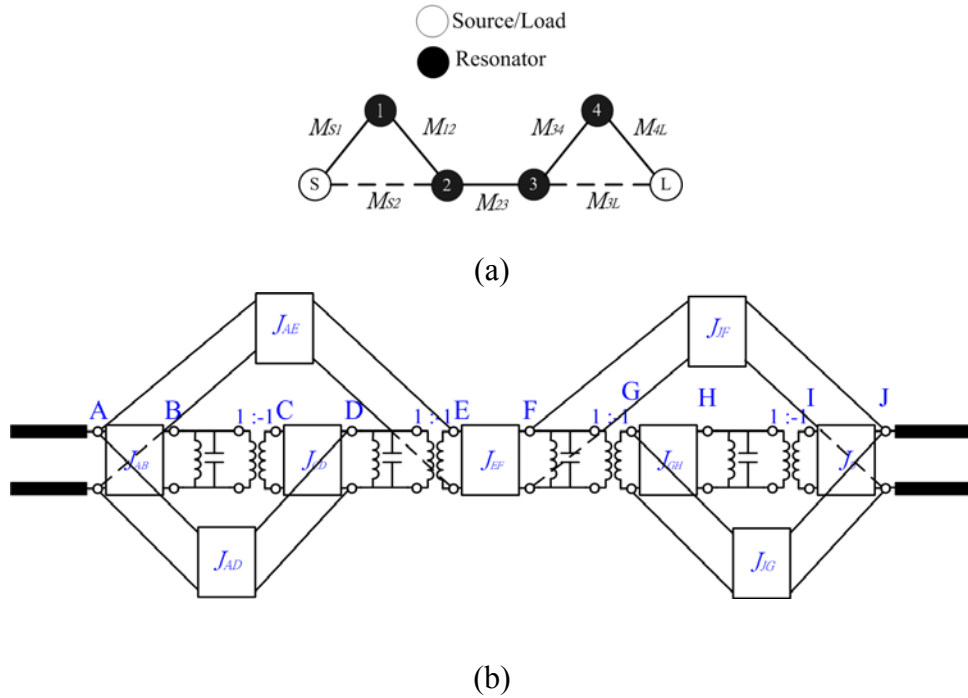


Fig. 4.3. The cascaded trisection filter. (a) The coupling scheme. (b) The corresponding equivalent lumped-element circuit of a fourth-order parallel coupled filter with cross couplings. Either the inverter J_{AD} or J_{AE} corresponds to M_{S2} and either the inverter J_{JF} or J_{JG} corresponds to M_{3L} .

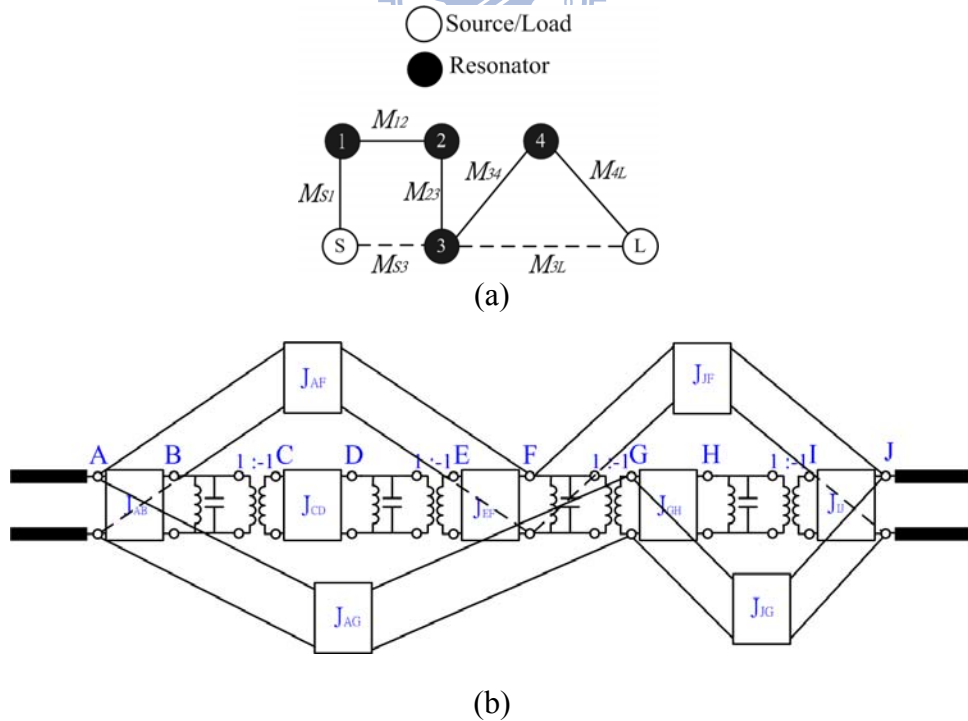


Fig. 4.4. The mixed cascaded quadruplet and trisection filter. (a) The coupling scheme. (b) The corresponding equivalent lumped-element circuit of a fourth-order parallel coupled filter with cross coupling. Either the inverter J_{AF} or J_{AG} corresponds to M_{S3} and either the inverter J_{JF} or J_{JG} corresponds to M_{3L} .

coupling schemes have already proposed in literatures, the microstrip implementation using parallel-coupled structure is first proposed in this research. Here, the resonators are represented by dark dots, the source and load are empty dots, the solid lines between resonators indicate the main coupling, and the broken lines indicate the cross coupling.

The lumped-element equivalent circuit of the fourth-order parallel-coupled filter with CT cross coupling scheme is shown in Fig. 4.3(b). Either the inverter J_{AE} or inverter J_{AD} in Fig. 4.3(b) corresponds to the cross coupling M_{S2} in Fig. 4.3(a), and similar situation applies to the inverter J_{JF} and the inverter J_{JG} . Choosing either J_{AE} or J_{AD} in the source end and either J_{JF} or J_{JG} in the load end, different signs of M_{S2} and M_{3L} can be implemented. Thus, two trisections are formed and each trisection can create a transmission zero on either lower or upper stopband. To demonstrate the mentioned properties, three CT filters are discussed as examples.

The first CT filter is with the following parameters. Its low-pass prototype is with two transmission zeros at $\Omega=3$ and $\Omega=-2$, and a maximum in-band return loss of 20dB. The coupling matrix corresponding to Fig. 4.3(a) is shown in (4.1) where the synthesizing techniques in [37] are used.

$$M = \begin{bmatrix} 0 & 0.9024 & -0.4910 & 0 & 0 & 0 \\ 0.9024 & 0.7905 & 0.6581 & 0 & 0 & 0 \\ -0.4910 & 0.6581 & -0.3186 & 0.7285 & 0 & 0 \\ 0 & 0 & 0.7285 & 0.1845 & 0.7990 & 0.3197 \\ 0 & 0 & 0 & 0.7990 & -0.5601 & 0.9763 \\ 0 & 0 & 0 & 0.3197 & 0.9763 & 0 \end{bmatrix} \quad (4.1)$$

In the coupling matrix, $M_{S2} = -0.4910$ and $M_{3L} = 0.3197$ are in different sign because one transmission zero on upperstopband is due to M_{3L} and the other transmission zero on lower stopband is due to M_{S2} . Because a capacitive coupling provides -90° of phase shift for $f < f_0$ and $f > f_0$, from Table 4.1, an upper stopband transmission zero would be created if a capacitive cross coupling is applied between

nodes J and G. Therefore, J_{JG} could be chosen capacitive to realize M_{3L} . Similarly, if a capacitive cross coupling existed between nodes A and E, there would be a finite transmission zero on the lower stopband. Thus, one may choose J_{AE} with capacitive cross coupling to implement M_{S2} . Due to the physical distance of node A to node E, a delay line is introduced to implement cross coupling between nodes A and E. Thanks to this delay line, more flexible design can be achieved. When capacitive coupling in cooperation with a delay line of electrical length 360° , the overall relative phase shift of the cross coupling is still -90° ($-360^\circ - 90^\circ = -90^\circ$) for $f < f_0$ and $f > f_0$. And in Table 4.1, relative phase shift of the main coupling path from node A to E is 90° on $f < f_0$. Consequently, a finite transmission zero on the lower stopband is generated.

The second CT filter is with two transmission zeros at $\Omega=3$ and $\Omega=2$ in the lowpass domain, and with similar in band return loss of 20dB. The synthesized coupling matrix is depicted in (4.2).

$$M = \begin{bmatrix} 0 & 0.9167 & 0.4889 & 0 & 0 & 0 \\ 0.9167 & -0.7411 & 0.6714 & 0 & 0 & 0 \\ 0.4889 & 0.6714 & 0.4288 & 0.7357 & 0 & 0 \\ 0 & 0 & 0.7357 & 0.3471 & 0.8118 & 0.3179 \\ 0 & 0 & 0 & 0.8118 & -0.4744 & 0.9891 \\ 0 & 0 & 0 & 0.3179 & 0.9891 & 0 \end{bmatrix} \quad (4.2)$$

Note that the sign of M_{S2} changes from negative to positive. Therefore, one may choose J_{AD} as a capacitive cross coupling to achieve $M_{S2}=0.4889$ and keep J_{JG} unchanged.

The third CT filter has similar passband return loss but with two lowpass domain transmission zeros at $\Omega = -3$ and $\Omega = -2$. From the reversal property of the coupling matrix the absolute values of the matrix elements should equal to those of (4.2) and M_{11} , M_{22} , M_{33} , M_{44} , M_{S2} , M_{2S} , M_{3L} , and M_{L3} should change sign [98]. The coupling matrix is shown in (4.3).

$$M = \begin{bmatrix} 0 & 0.9167 & -0.4889 & 0 & 0 & 0 \\ 0.9167 & 0.7411 & 0.6714 & 0 & 0 & 0 \\ -0.4889 & 0.6714 & -0.4288 & 0.7357 & 0 & 0 \\ 0 & 0 & 0.7357 & -0.3471 & 0.8118 & -0.3179 \\ 0 & 0 & 0 & 0.8118 & 0.4744 & 0.9891 \\ 0 & 0 & 0 & -0.3179 & 0.9891 & 0 \end{bmatrix} \quad (4.3)$$

Thus, we may choose J_{AE} with capacitive cross coupling to achieve $M_{S2} = -0.4889$ and choose J_{JF} with capacitive cross coupling to achieve $M_{3L} = -0.3179$. Again, due to physical distances of node A to node E and node J to node F, two capacitive cross coupling in cooperation with two delay lines of electrical length 360° implement the desired J_{AE} and J_{JF} . The lowpass domain responses of the three CT filters are shown in Fig. 4.5.

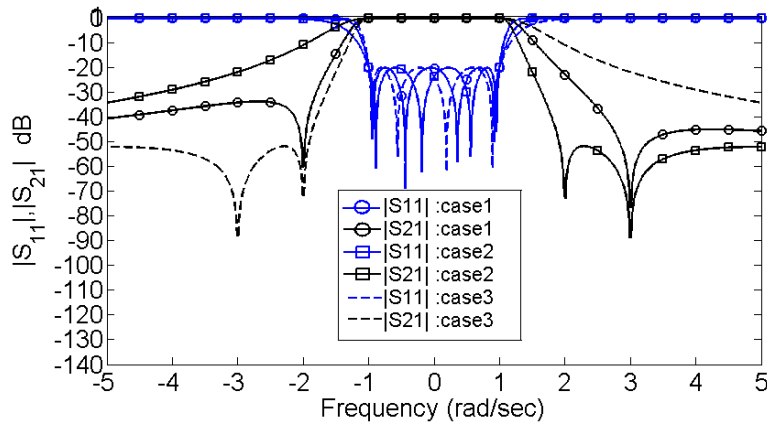


Fig. 4.5. The low-pass responses of the three CT filters with all in-band return loss 20dB. Case 1, normalized transmission zeros at $\Omega = 3$ and $\Omega = -2$. Case 2, normalized transmission zeros at $\Omega = 3$ and $\Omega = 2$. Case 3, normalized transmission zeros at $\Omega = -3$ and $\Omega = -2$.

Fig. 4.4(a) shows the coupling scheme of the fourth order mixed cascade quadruplet and trisection filter. This topology is particularly interesting because the quadruplet part can produce a pair of transmission zeros on both sides of the stopband, and the trisection part could generate another transmission zero on whatever location we want. Fig. 4.4(b) is the lumped-element equivalent circuit of a fourth-order

parallel-coupled filter with the mixed cascade quadruplet and trisection cross coupling where the nodes A-J in Fig. 4.4(b) correspond to the similar nodes in Fig. 4.1(a). Again, either the inverter J_{AF} or J_{AG} in Fig. 4.4(b) can implement the cross coupling M_{S3} in Fig. 4.4(a), and either the inverter J_{JF} or J_{JG} in Fig. 4.4(b) can realize the cross coupling M_{3L} in Fig. 4.4(a). Let us consider the quadruplet portion of the mixed cascade quadruplet and trisection filter first. Suppose that a capacitive coupling gap is applied at node F. From Table 4.1, a delay line with electrical length of 180° should be involved between source and capacitive coupling gap (node F) to create proper phases of the cross coupling ($-180^\circ - 90^\circ = -270^\circ = +90^\circ$ for $f < f_0$ and $f > f_0$) so that a pair of transmission zeros could create on both sides of the stopband. Oppositely, if the capacitive gap is applied at node G to realize the cross coupling, the inserted delay line between node A and G should be 360° . Considering the layout, a capacitive gap applied to the node F is preferable. The trisection portion of the mixed cascade quadruplet and trisection filter is similar to that of CT filter we discussed earlier. If a finite transmission zero on the upper stopband is wanted, one may choose the capacitive inverter J_{JG} in Fig. 4.4(b) to implement the cross coupling M_{3L} in Fig. 4.4(a). Contrarily, if a finite transmission zero on the lower stopband is wanted, the cross coupling M_{3L} in Fig. 4.4(a) could be realized by the capacitive inverter J_{JF} in Fig. 4.4(b). To reach nodes J-F a delay line with an electrical length of 360° should be involved.

The delay line and the coupling gap form an overall phase shift of -90° ($-360^\circ - 90^\circ = -90^\circ$ for $f < f_0$ and $f > f_0$). In brief, a mixed cascade quadruplet and trisection filter can have not only a pair of transmission zeros on both sides of the stopband but also another transmission zero on either upper or lower stopband.

4.4 Filter Design Examples

Since a mixed cascade quadruplet and trisection filter contains two types of cross couplings and is more general than a CT filter, two fourth-order parallel-coupled filters with the mixed cascade quadruplet and trisection cross coupling are chosen as examples in this section to demonstrate the feasibility of the proposed structures. A 0.508-mm-thick Rogers RO4003 substrate with a dielectric constant of 3.58 and loss tangent of 0.0021 is used to implement these mixed cascade quadruplet and trisection filters.

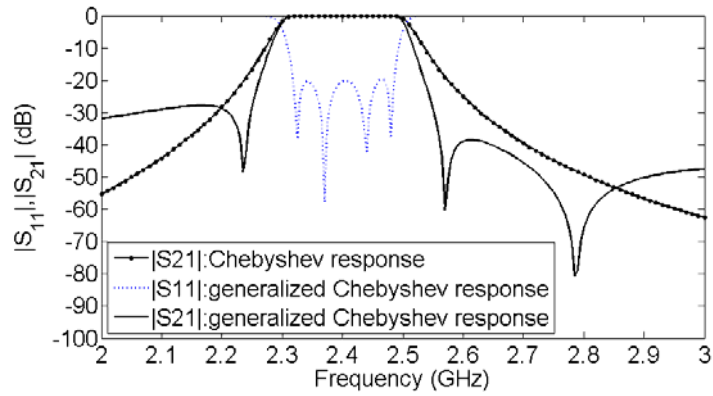
The first mixed cascade quadruplet and trisection filter is designed to have a pair of real frequency transmission zeros at normalized frequencies of $\Omega = \pm 2$, a real frequency transmission zero at a normalized frequency of $\Omega = 4$ in the lowpass domain, and a passband return loss of 20dB. Fig. 4.4(a) shows the coupling scheme of the mixed cascade quadruplet and trisection filter. Equation (4.4) is the synthesized coupling matrix.

$$M = \begin{bmatrix} 0 & 1.0039 & 0 & -0.1998 & 0 & 0 \\ 1.0039 & 0.0111 & 1.0020 & 0 & 0 & 0 \\ 0 & 1.0020 & 0.0317 & 0.5879 & 0 & 0 \\ -0.1998 & 0 & 0.5879 & 0.1788 & 0.8409 & 0.2136 \\ 0 & 0 & 0 & 0.8409 & -0.3487 & 1.0010 \\ 0 & 0 & 0 & 0.2136 & 1.0010 & 0 \end{bmatrix} \quad (4.4)$$

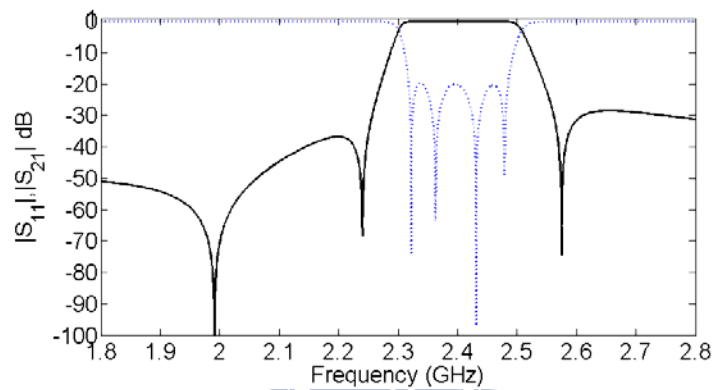
Then, the filter is transformed from the lowpass domain to the bandpass domain with the center frequency of $f_0 = 2.4$ GHz and the fractional bandwidth of 7%. The response after transformation is depicted in Fig. 4.6(a).

The design procedures are described briefly in the following.

First, calculate the initial design by applying Cohn's analytical synthesis method [99] to realize the in-line part of the coupling matrix. For our fourth-order filter, the in-line part coupling elements are M_{S1} , M_{12} , M_{23} , M_{34} and M_{4L} . That is to get the J -inverter values from these coupling elements, and using Cohn's formula to get the



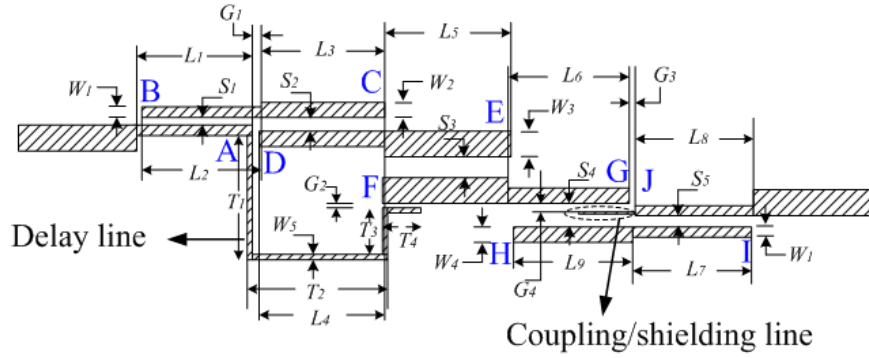
(a)



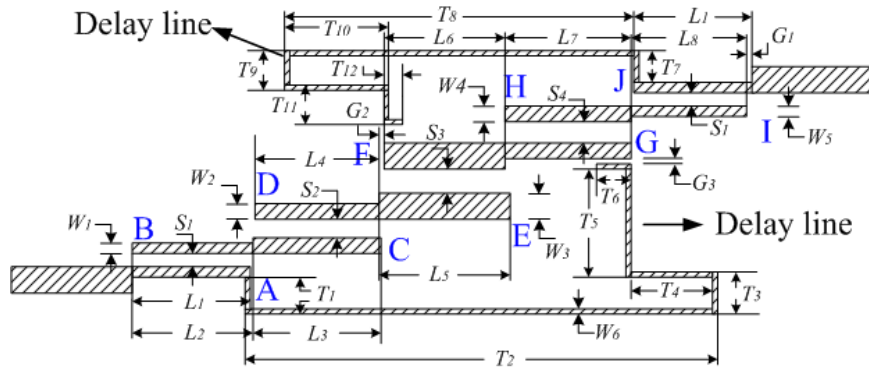
(b)

Fig. 4.6. The ideal responses of the two CQT filters. (a) The bandpass response corresponding to (4.4) with a typical Chebyshev response as a reference. (b) The bandpass response corresponding to (4.5).

even- and odd-mode impedances of each parallel-coupled section corresponding to the J -inverter values. Note that no cross couplings are introduced at this moment so that the electrical length of each parallel-coupled section is 90° . After this, the layout can be modified according to [69] that each resonator's vertical position can be vertically flipped to make cross couplings easy to apply. In this example, the source feeding line and the first resonator is vertically flipped so as the load feeding line and the last resonator such that the nodes to implement the cross coupling of M_{S3} and M_{3L} can be accessed. The parallel-coupled filter portion in Fig. 4.7(a) depicts the modification of the layout.



(a)



(b)

Fig. 4.7. The circuit layouts of the proposed filters. (a) The first designed mixed cascaded quadruplet and trisection filter. The length and line width of coupling/shielding line are 4.318 mm and 0.177 mm, respectively. (b) The second designed mixed cascaded quadruplet and trisection filter.

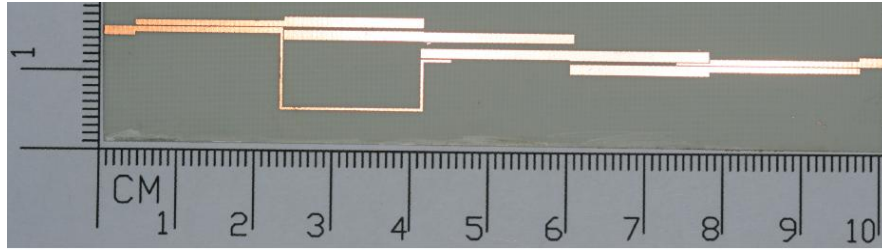
Second, if nodes A and F are chosen to implement the cross coupling of $M_{S3} = -0.1998$, a delay line with an electrical length of 180° in cooperation with a capacitive coupling should be used. The reason to use the 180° delay line is described in the previous section. The initial length of the capacitive coupling gap is obtained by the circuit simulator such as Agilent's Advanced Design System (ADS) [99]. For simplifying the layout, the width of the delay line is fixed to be 0.254 mm and the coupling gap between the delay line and the resonator 3 is also fixed to be 0.254 mm. Now, the resonator 3 is coupled to the source through the delay line. The electrical

length of the delay line is adjusted to be 180° at the center frequency. The coupling length can be easily adjusted by using the three-coupled-line model in ADS where the line widths and gap widths keep unchanged. Because tuning of the coupling length in the circuit simulator can be almost real time. The initial coupling length can be fast obtained as 3.937 mm. Therefore, the physical layout of the quadruplet portion of the first mixed cascade quadruplet and trisection filter is obtained.

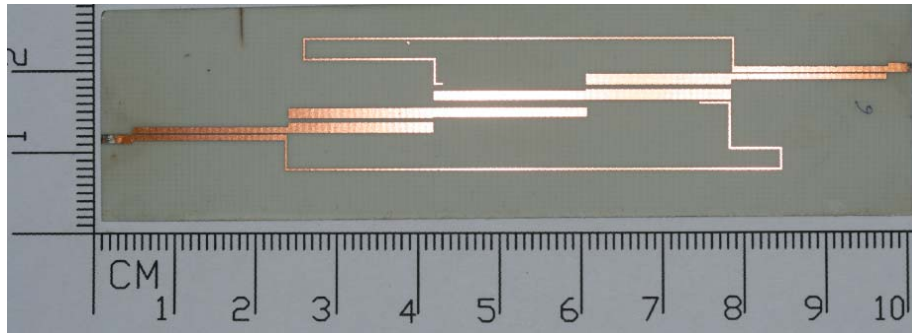
Finally, the trisection portion of this mixed cascade quadruplet and trisection filter is the same as that of CT filter described in [82] where an upper stopband transmission zero can be easily obtained. As the similar method proposed in [82], a coupling/shielding line is adopted here at the node J of the output feed line. This would be the simplest way to implement M_{3L} where a transmission zero at a normalized frequency of $\Omega=4$ could be created. Finally, fine tuning might be required using EM simulator. After fine tuning of the whole circuit with the commercial EM simulator Sonnet [100], all physical dimensions of the filter are obtained. The circuit layout and the detailed dimensions are shown in Fig. 4.7(a) and in Table 4.2, respectively, and the photo of the filter is depicted in Fig. 4.8(a).

The second mixed cascade quadruplet and trisection filter is designed to have a pair of real frequency transmission zeros at normalized frequencies of $\Omega=\pm 2$, a real frequency transmission zero at a normalized frequency of $\Omega=-5$ in the lowpass domain, and a passband return loss of 20dB. The synthesized coupling matrix is shown in (4.5).

$$M = \begin{bmatrix} 0 & 1.0041 & 0 & -0.1986 & 0 & 0 \\ 1.0041 & -0.0090 & 1.0019 & 0 & 0 & 0 \\ 0 & 1.0019 & -0.0250 & 0.5871 & 0 & 0 \\ -0.1986 & 0 & 0.5871 & -0.1435 & 0.8579 & -0.1700 \\ 0 & 0 & 0 & 0.8579 & 0.2785 & 1.0094 \\ 0 & 0 & 0 & -0.1700 & 1.0094 & 0 \end{bmatrix} \quad (4.5)$$

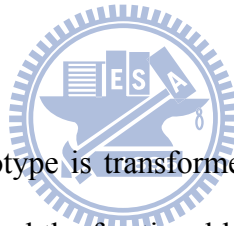


(a)



(b)

Fig. 4.8. The layouts of the implemented filters. (a) The first designed filter. (b) The second designed filter.



Similarly, the lowpass prototype is transformed into bandpass domain with the center frequency of $f_0=2.4$ GHz and the fractional bandwidth of 7%. The transformed bandpass response is depicted in Fig. 4.6(b). The initial dimensions of the parallel-coupled portion of the filter are calculated by the analytical method as described in the first filter. Again, let us look at the quadruplet portion of the filter first. This time, the nodes A and G in Fig. 4.4(b) are chosen to implement the cross coupling between source and resonator 3. From (4.5), the synthesized cross coupling value should be $M_{S3} = -0.1986$. Therefore, a delay line with an electrical length of 360° in cooperation with a capacitive coupling would be appropriate to implement the M_{S3} . Again, the width of the delay line is fixed to be 0.254 mm and the coupling gap is also fixed to be 0.254 mm. Then, the initial coupling length of 3.937 mm is obtained by the circuit simulator. Finally, let us look at the trisection portion of the filter. Now, the nodes J and F are chosen to implement the cross coupling between

The dimensions of the first designed mixed cascaded quadruplet and trisection filter corresponding to layout in Fig. 7(a) (in mm)						
L_1	L_2	L_3	L_4	L_5	L_6	L_7
18.999	19.181	17.779	17.830	19.253	17.729	19.253
L_8	L_9	S_1	S_2	S_3	S_4	S_5
19.075	17.729	0.177	0.508	0.965	0.558	0.177
W_1	W_2	W_3	W_4	W_5	G_1	G_2
0.660	1.143	1.092	1.193	0.254	0.254	0.254
G_3	G_4	T_1	T_2	T_3	T_4	
0.203	0.203	9.652	18.288	5.181	3.810	
The dimensions of the second designed mixed cascaded quadruplet and trisection filter corresponding to layout in Fig. 7(b) (in mm)						
L_1	L_2	L_3	L_4	L_5	L_6	L_7
19.100	19.253	19.805	17.754	18.872	18.669	17.754
L_8	S_1	S_2	S_3	S_4	W_1	W_2
19.050	0.177	0.508	0.939	0.558	0.736	1.270
W_3	W_4	W_5	W_6	G_1	G_2	G_3
1.143	1.320	0.711	0.254	0.203	0.076	0.254
T_1	T_2	T_3	T_4	T_5	T_6	T_7
3.733	60.960	2.794	6.045	5.588	3.810	3.632
T_8	T_9	T_{10}	T_{11}	T_{12}		
52.628	2.794	16.281	3.276	1.143		

Table 4.2. The physical dimensions of the two proposed filters.

resonator 3 and load. A delay line with an electrical length of 360° in cooperation with a capacitive cross coupling could realize the cross coupling with the correct phase and amplitude. The strip width of the delay line is still fixed to be 0.254 mm. Different from the former, the capacitive coupling gap is now fixed to be 0.762 mm in this case. Similarly, the initial coupling length of 1.143 mm is obtained by the circuit simulator. Same as the first filter, the initial physical dimensions of the second filter can be obtained from ADS, and then, the EM simulation to fine tune the physical dimensions

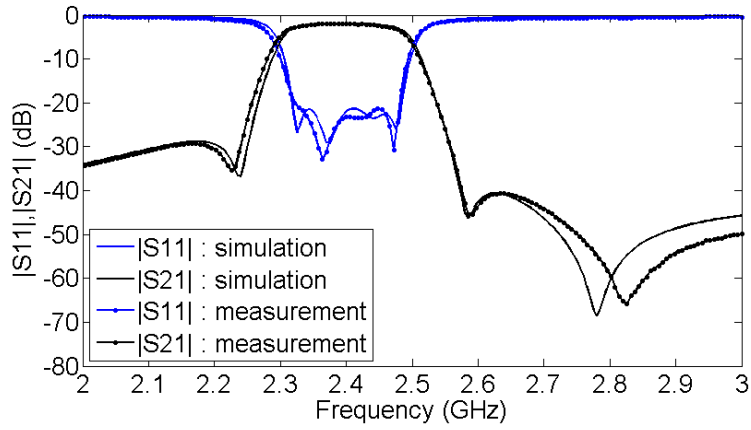
might be required. After fine tuning with the commercial EM simulator Sonnet, the circuit layout and the detailed dimensions are shown in Fig. 4.7(b) and in Table 4.2, respectively. The circuit photo is shown in Fig. 4.8(b).

4.5 Results and Discussion

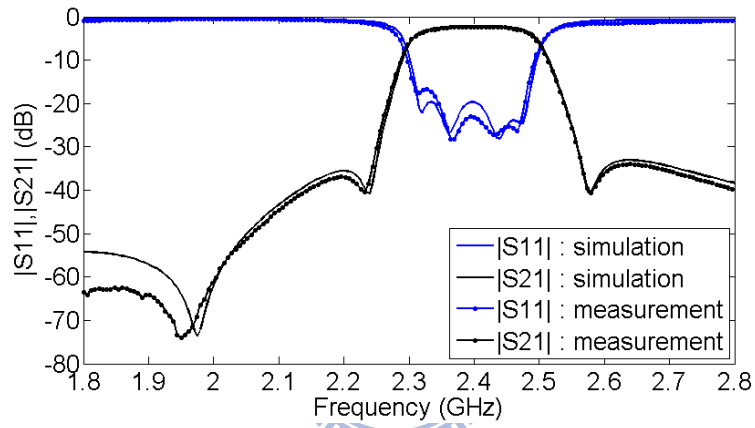
Shown in Fig. 4.9(a) are the measured and simulated performances of the first mixed cascade quadruplet and trisection filter. The measured center frequency, fractional bandwidth, and in-band insertion loss are 2.4GHz, 7%, and 1.8dB respectively which are in good agreement with the simulated results. The two transmission zeros contributed by the quadruplet part are at 2.23 GHz and 2.585 GHz, and also agree well with the simulation. The third transmission zero is at 2.82 GHz, and the little deviation might come from the much weaker and more sensitive coupling between the coupling/shielding line and resonator 3 than that of the quadruplet portion.

Fig. 4.9(b) shows the measured performance of the second mixed cascade quadruplet and trisection filter. Again, the measured center frequency, fractional bandwidth, in-band insertion loss, and two transmission zeros contributed by the quadruplet part of the filter are also in good agreement with the simulated results. The third transmission zero, similarly, shows a little frequency drift to lower frequency compared with the simulation.

The sensitivity analysis of the proposed filters to manufacturing tolerances can be performed in two conditions. One is over etching 0.0508 mm (2 mil), the other is under etching 0.0508 mm (2 mil). Take the first mixed cascade quadruplet and trisection filter as an example and simulate it in two conditions using EM simulator Sonnet. The simulated responses are shown in Fig. 4.10. It is found that the proposed cross-coupled filters are not very sensitive to the manufacturing tolerances.



(a)



(b)

Fig. 4.9. The measured and simulated performances of the two implemented filters. (a) The first designed filter. (b) The second designed filter.

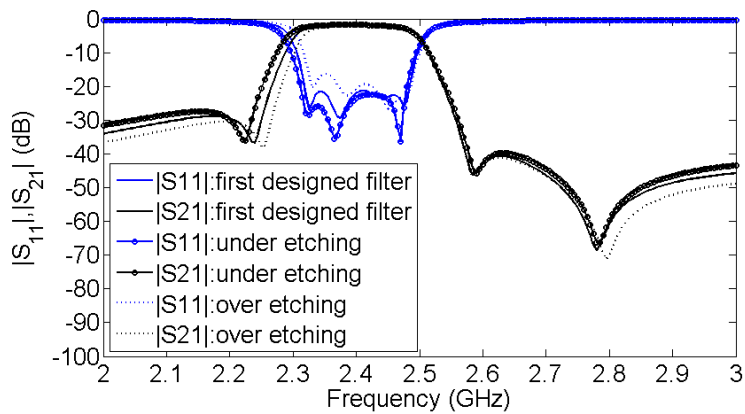


Fig. 4.10. The sensitivity analysis of the first mixed cascade quadruplet and trisection filter for under etching of 0.0508 mm (2mil) and over etching of 0.0508 mm respectively.

Another concern is that as the finite transmission zeros get closer to the passband, the values of the cross coupling should be higher and some dimensions of the circuit layouts must change. On the other hand, for a highly asymmetrical response with the transmission zeros very close to the pass-band, the lengths of the resonators should be modified because the trisection portion of the filter becomes highly asynchronously tuned. How close the transmission zeros to the passband can be before the layout becomes impractical for fabrication or the design becomes very difficult to get estimate.

The situation can be summarized in two cases. The first case is the pair of quadruplet transmission zeros very close to the passband, and the second case is the trisection transmission zero very close to the passband. Let us take the first mixed cascade quadruplet and trisection filter in Fig. 4.7(a) as an example to study these two cases.

In the first case, as the pair of quadruplet transmission zeros move from $\Omega = \pm 2$ to $\Omega = \pm 1.4$ in the lowpass domain, the corresponding coupling matrix M is obtained as

$$M = \begin{bmatrix} 0 & 0.8849 & 0 & -0.4935 & 0 & 0 \\ 0.8849 & -0.0108 & 1.0967 & 0 & 0 & 0 \\ 0 & 1.0967 & 0.0306 & 0.3780 & 0 & 0 \\ -0.4935 & 0 & 0.3780 & 0.1746 & 0.8488 & 0.2054 \\ 0 & 0 & 0 & 0.8488 & -0.3212 & 0.9940 \\ 0 & 0 & 0 & 0.2054 & 0.9940 & 0 \end{bmatrix} \quad (4.6)$$

Then, following the design procedures described above, the EM simulated response and the detailed dimensions are shown in Fig. 4.11 and Table 4.3, respectively. It is found that the coupled section length T_4 of the delay line is increased from 3.81 mm to 8.382 mm to achieve the proper value of M_{S2} . Also, it is reasonable that some dimensions such as S_1 , S_3 and G_2 in Fig. 4.7(a) are changed corresponding to the variation of matrix elements. It can be observed in Table 4.3 that

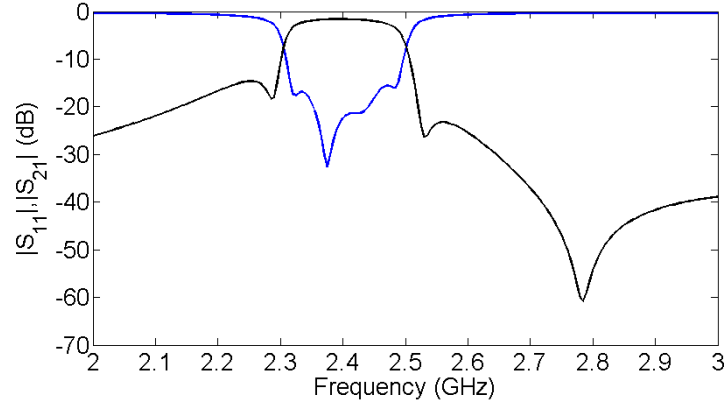


Fig. 4.11. The simulated performances of the first mixed cascaded quadruplet and trisection filter with finite transmission zeros at $\Omega = \pm 1.4, 4$.

the layout dimensions are still good for printed circuit board process. It seems that the cross coupling strength could be implemented much stronger. However, it must be noted that increasing the value of T_4 causes much higher unwanted coupling of M_{S2} . It may cause the transmission zeros to drift slightly. The drift of transmission zeros becomes worse as the cross coupling becomes stronger.

In the second case, as the trisection transmission zero moves from $\Omega = 4$ to $\Omega = 1.5$ and the pair of quadruplet transmission zeros move from $\Omega = \pm 2$ to $\Omega = \pm 3$ in the lowpass domain, the coupling matrix is obtained as

$$M = \begin{bmatrix} 0 & 1.0214 & 0 & -0.0955 & 0 & 0 \\ 1.0214 & 0.0453 & 0.9545 & 0 & 0 & 0 \\ 0 & 0.9545 & 0.1102 & 0.6936 & 0 & 0 \\ -0.0955 & 0 & 0.6936 & 0.4277 & 0.4560 & 0.6541 \\ 0 & 0 & 0 & 0.4560 & -0.9655 & 0.7903 \\ 0 & 0 & 0 & 0.2054 & 0.7903 & 0 \end{bmatrix} \quad (4.7)$$

As can be seen in the equation (4.7) that the highest absolute value of the diagonal elements is $M_{44} = -0.9655$. The high value of M_{44} means that the length of resonator 4 should be largely modified. If the length of coupled-line section changes too much, the main coupling strength may change such that the dimensions need to be adjusted. Also, for the highly asymmetric trisection transmission zero closer to the

The filter with finite transmission zeros at $\Omega=\pm 1.4$, 4. The length and line width of the coupling/shielding line are 4.318 mm and 0.177 mm, respectively						
L_1	L_2	L_3	L_4	L_5	L_6	L_7
18.923	19.227	17.907	17.78	19.431	17.627	19.177
L_8	L_9	S_1	S_2	S_3	S_4	S_5
19.075	17.627	0.228	0.482	1.194	0.584	0.203
W_1	W_2	W_3	W_4	W_5	G_1	G_2
0.660	1.066	1.092	1.193	0.254	0.330	0.178
G_3	G_4	T_1	T_2	T_3	T_4	
0.305	0.229	7.493	18.262	3.987	8.382	
The filter with finite transmission zeros at $\Omega=\pm 1.5$, ± 3 . The length and line width of the coupling/shielding line are 9.144 mm and 0.127 mm, respectively.						
L_1	L_2	L_3	L_4	L_5	L_6	L_7
18.186	18.135	19.304	19.304	17.830	19.075	18.110
L_8	L_9	S_1	S_2	S_3	S_4	S_5
18.542	18.618	0.152	0.584	0.711	1.066	0.228
W_1	W_2	W_3	W_4	W_5	G_1	G_2
0.711	1.168	1.194	0.889	0.254	0.330	0.508
G_3	G_4	T_1	T_2	T_3	T_4	
0.355	0.127	9.906	19.685	6.527	3.81	

Table 4.3. The dimensions of the first designed mixed cascaded quadruplet and trisection filter with finite transmission zeros closer to the passband.

passband, the width and length of the coupling/shielding line become narrower and longer, respectively. And the gap between the coupling/shielding line and the third resonator shown in Fig. 4.7(a) becomes too narrow to be realized. In this case the iteration process should be adopted. Nevertheless, this process can be done in the circuit simulator ADS so that it is not very time-consuming to get the initial layout. Then, in this condition of the highly asymmetric response, the EM simulation to fine tune the physical dimensions must be required. After fine tuning with the commercial

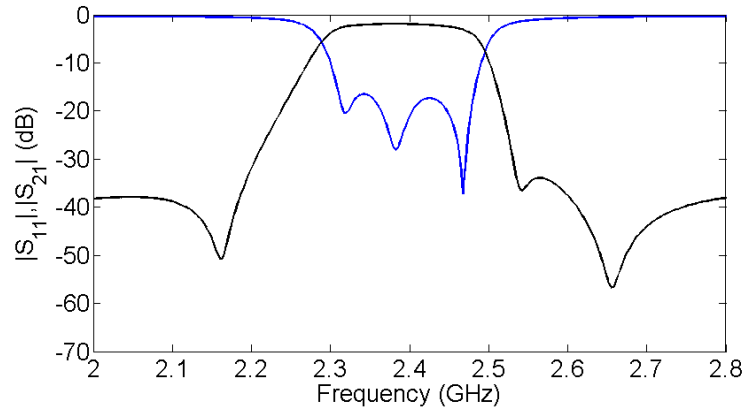


Fig. 4.12. The simulated performances of the first mixed cascaded quadruplet and trisection filter with finite transmission zeros at $\Omega=+1.5, \pm 3$

EM simulator Sonnet, the EM simulated response and the detailed dimensions are shown in Fig. 4.12 and in Table 4.3, respectively. It is found that the length and width of the coupling/shielding line are 9.144 mm and 0.127 mm, respectively. The gap G_4 is 0.127 mm. The manufacturing process can still support the narrow width and small gap.



Chapter 5 Bisymmetric Coupling Schemes for Implementation of Low-Order Generalized Chebyshev Planar Filters with Transmission Zeros Very Close to the Passband

This chapter proposes some new coupling schemes where the corresponding coupling matrices show the bisymmetric property. The proposed bisymmetric coupling schemes are suitable for low-order high selectivity planar filters. Using the bisymmetric coupling schemes, the strength of cross coupling can be much weaker than the conventional trisection or quadruplet filters with the same transmission zero positions. The source and load to nonadjacent resonators cross couplings are applied to implement the proposed bisymmetric coupling schemes. Most of the proposed coupling schemes have the properties of synchronous-tuned resonators, bisymmetric coupling matrices, and relatively weak cross-coupled strengths for finite transmission zeros close to the passband. The bisymmetric coupling matrix implies a symmetrical layout that fine tuning of the filter would be much easier. All of the proposed coupling schemes are compared with the conventional coupling schemes through the coupling matrices when synthesizing generalized Chebyshev filtering functions. Each proposed coupling scheme is realized by a microstrip parallel-coupled filter structure with cross couplings from source and load to nonadjacent resonators. Measured and simulated responses are presented.

5.1 Introduction

Filters are important components of microwave communication system. Among various filtering functions, the generalized Chebyshev filters are attractive because they offer excellent frequency responses with sharp cutoff skirts and low passband insertion loss. The sharp skirt is due to the presence of transmission zeros brought from infinite to finite frequencies. The transmission zeros at precise frequencies in a

microwave filter reject the specific unwanted signals. In the literatures, especially for cross-coupled filters, the cascade trisection (CT) and cascade quadruplet (CQ) are two of the most commonly used coupling schemes. They have been found many applications in many years [6], [7], [52], [61]. More progressively, source and load to nonadjacent resonator cross couplings [66], [67] can also achieve high selectivity responses such as trisection and quadruplet with low-order resonators but less passband loss. Other coupling scheme such as the doublet has the zero-shifting property that shifts a transmission zero from one side of passband to the other by just adjusting the resonant frequencies of two resonators [66], [89]. Among these coupling schemes, some of them are asynchronous-tuned, e.g. trisection, and doublet. In some particular situations, strong asynchronous-tuned resonators may cause problems during fine tuning of the filter especially for the planar filters.

For instance, the two-pole trisection coupling scheme in Fig. 5.1(a) [66] has the asynchronous-tuned resonators and the corresponding coupling matrix is not bisymmetric. As a result, when the transmission zero gets closer to the passband, the cross coupling M_{S2} may become too large to realize and the alignment of the resonant frequency could be a tough task. Another example as shown in Fig. 5.1(b) that the conventional third-order CT has two controllable transmission zeros. In this case, the corresponding coupling matrix is not bisymmetric no matter the response is symmetric or not. Again, when a finite transmission zero is very close to the band edge, the value of the cross coupling would be too large to implement and the resonators are highly asynchronous-tuned. In some cases, although the resonator is synchronous-tuned, the cross coupling may be too large to implement as the transmission zero gets close to the passband. For example, Fig. 5.1(c) depicts a third-order quadruplet [67], although the coupling scheme is synchronous-tuned, the coupling matrix would not be bisymmetric and the cross coupling M_{S3} would be large

as two transmission zeros are very close to the passband. It can be summarized that to implement a planar filter with transmission zeros very close to the passband usually encounters several difficulties. First, the layout is asymmetric unless the coupling matrix is bisymmetric. Second, the coupling strength might be too large to implement. Finally, for coupling schemes including a trisection, the alignment of asynchronous-tuned resonators might be a difficult task.

Parallel-coupled line filters as shown in [101] were proposed to achieve generalized Chebyshev responses. Due to the conventional parallel-coupled structure a good initial design can be obtained with the well-known analytical design method. The cross coupling of the filter from source or load to nonadjacent resonators can be easily introduced by adding delay lines with proper electrical lengths. Using this filter structure, however, to realize the conventional cascade quadruplets and cascade trisections with transmission zeros very close to the filter passband also encounters the problems of unrealizable cross coupling in planar form, highly asynchronously tuned resonators for a trisection and an asymmetric layout due to a symmetric coupling matrix.

Therefore, the objective of this chapter is to propose new coupling schemes as shown in Fig. 5.1(d)-(h) to solve or alleviate the problems described above. The proposed coupling schemes are suitable for implementations of low-order planar generalized Chebyshev filters with transmission zeros very close to the passband. The coupling scheme in Fig. 5.1(d) has two overlapped trisections that two trisections are with the identical coupling coefficients. The filter response of Fig. 5.1(d) is similar to that of single trisection when realizing a generalized Chebyshev response [35], [37]. It should be emphasized that the cross couplings, M_{S2} and M_{IL} , of two overlapped trisections in Fig. 5.1(d) share the energy of the cross coupling M_{S2} in Fig. 5.1(a). Similar overlapping configurations apply to Figs. 5.1(e) and (f) that two identical

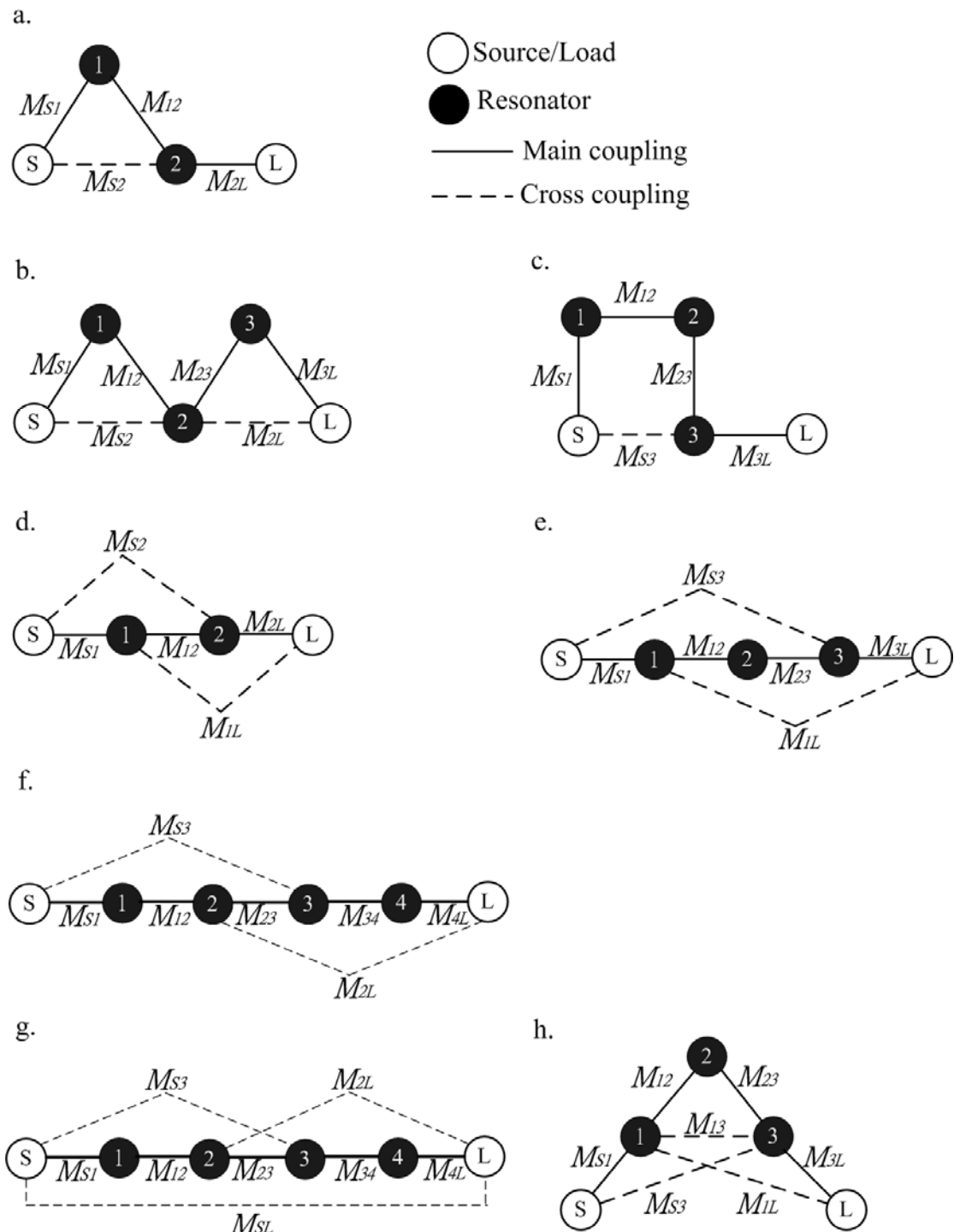
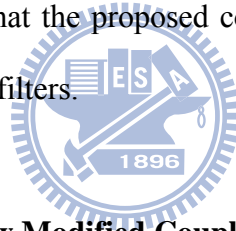


Fig. 5.1. Cross coupling schemes generating transmission zeros at precise frequencies. Conventional coupling schemes: (a) two-pole trisection. (b) three-pole cascade trisections (CQ). (c) three-pole quadruplet. Proposed coupling schemes: (d) two-pole interactive cross-coupling trisection scheme. (e) three-pole interactive cross-coupling quadruplet scheme. (f) four-pole interactive cross-coupling quadruplet scheme. (g) modified four-pole canonical form scheme with two pairs of transmission zeros. (h) modified three-pole cascade trisections (CT) scheme.

quadruplets in each figure are overlapped. Again, the generalized Chebyshev responses of Figs. 5.1(e) and (f) can be synthesized the same as single quadruplet. The coupling scheme in Fig. 5.1(g) is modified from Fig. 5.1(f) that an extra cross coupling from source to load is introduced. One additional pair of transmission zeros can be created by the source to load cross coupling. Consequently, two pairs of transmission zeros can be implemented with a fourth-order filter for maximum selectivity. Another proposed coupling scheme is shown in Fig. 5.1(h) that two identical overlapped trisections are applied to source and load to resonators 1 and 3 respectively and another trisection is implemented between resonators 1, 2, and 3. The generalized Chebyshev response of Fig. 5.1(h) is identical to that of two cascaded trisections in Fig. 5.1(b) that two transmission zeros can be located at any positions on the stopband. It will be shown that the proposed coupling schemes can facilitate the realizations of high performance filters.



5.2 The New Modified Coupling Schemes

In the following, all the coupling matrices are discussed corresponding to the generalized Chebyshev responses [35], [37].

A. Review of conventional coupling schemes

Figs. 5.1(a) and (c) show two coupling schemes, one is a two-pole trisection and the other is a three-pole quadruplet. Consider Fig. 5.1(a) first. By introducing the cross coupling M_{S2} a finite transmission zero occurs. The corresponding coupling matrix M of the trisection in Fig. 5.1(a) can be written as

$$M = \begin{bmatrix} 0 & M_{S1} & M_{S2} & 0 \\ M_{S1} & M_{11} & M_{12} & 0 \\ M_{S2} & M_{12} & M_{22} & M_{2L} \\ 0 & 0 & M_{2L} & 0 \end{bmatrix} \quad (5.1)$$

where $M_{S1} \neq M_{2L}$, $M_{11} \neq M_{22}$. The coupling matrix of the trisection is asynchronously tuned and symmetric. Although the matrix is symmetric, the physical structure of the filter is asymmetric. Another concerned coupling diagram is quadruplet shown in Fig. 5.1(c). The cross coupling M_{S3} generates two finite transmission zeros on both stopband. The corresponding coupling matrix M is

$$M = \begin{bmatrix} 0 & M_{S1} & 0 & M_{S3} & 0 \\ M_{S1} & 0 & M_{12} & 0 & 0 \\ 0 & M_{12} & 0 & M_{23} & 0 \\ M_{S3} & 0 & M_{23} & 0 & M_{3L} \\ 0 & 0 & 0 & M_{3L} & 0 \end{bmatrix} \quad (5.2)$$

where $M_{S1} \neq M_{3L}$, $M_{12} \neq M_{23}$. The coupling matrix is synchronously tuned and symmetric. Again, the physical layout is asymmetric.

A conventional three-pole CT is shown in Fig. 5.1(b). Two trisections can generate two transmission zeros due to the two corresponding cross couplings, M_{S2} and M_{2L} , respectively. The general form of the coupling matrix can be expressed as

$$M = \begin{bmatrix} 0 & M_{S1} & M_{S2} & 0 & 0 \\ M_{S1} & M_{11} & M_{12} & 0 & 0 \\ M_{S2} & M_{12} & M_{22} & M_{23} & M_{2L} \\ 0 & 0 & M_{23} & M_{33} & M_{3L} \\ 0 & 0 & M_{2L} & M_{3L} & 0 \end{bmatrix} \quad (5.3)$$

It can be observed from (3) that $M_{11} \neq M_{22} \neq M_{33}$, $M_{S1} \neq M_{3L}$, $M_{12} \neq M_{23}$, $M_{S2} \neq M_{2L}$. This means that the filter should be asynchronously tuned and should have an asymmetric layout.

In the following, the modified cross coupling schemes are proposed. They have a similar concept that is to guide a cross coupling path into two interacting cross coupling paths. Therefore, some interesting properties occur and may be useful for designing planar filters.

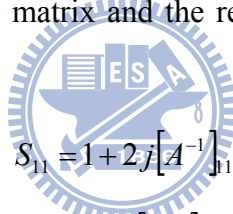
B. The proposed coupling schemes

The proposed coupling schemes are shown in Fig. 5.1(d)-(h) and will be discussed as follows.

As can be seen in the two-order trisection in Fig. 5.1(d), we introduce another identical cross coupling path M_{IL} to share energy of cross coupling M_{S2} . The coupling scheme becomes two identical overlapped trisections. Thus, the corresponding coupling matrix is synchronous tuned and bisymmetric as shown in (5.4).

$$M = \begin{bmatrix} 0 & M_{S1} & M_{S2} & 0 \\ M_{S1} & M_{11} & M_{12} & M_{S2} \\ M_{S2} & M_{12} & M_{11} & M_{S1} \\ 0 & M_{S2} & M_{S1} & 0 \end{bmatrix} \quad (5.4)$$

In (5.4), the matrix is bisymmetric because $M_{S1}=M_{2L}$, $M_{S2}=M_{1L}$, $M_{11}=M_{22}$. The relationships between a coupling matrix and the responses of $S_{11}(\Omega)$ and $S_{21}(\Omega)$ are shown as follows.



$$S_{11} = 1 + 2j[A^{-1}]_{11} \quad (5.5)$$

$$S_{21} = -2j[A^{-1}]_{N+2,1} \quad (5.6)$$

Here, $A = \Omega[U_0] + [M] - j[R]$ and the low-pass normalized domain to bandpass real frequency transformation is $\Omega = (f_0/\Delta f)(f/f_0 - f_0/f)$, $[U_0]$ is similar to the $(N+2) \times (N+2)$ identity matrix, except that $[U_0]_{11} = [U_0]_{N+2, N+2} = 0$, $[M]$ is the $(N+2) \times (N+2)$ coupling matrix, f_0 is the center frequency of the filter and Δf is its bandwidth, and $[R]$ is a $(N+2) \times (N+2)$ matrix whose only nonzero entries are $R_{11} = R_{N+2, N+2} = 1$. Also, the transfer polynomial for the generalized Chebyshev filtering function can be expressed as

$$S_{21}(\Omega) = \frac{P(\Omega)}{E(\Omega)} \quad (5.7)$$

Thus, one can obtain the position of finite transmission zero by solving the equation $P(\Omega) = 0$ using (5.6).

Applying $P(\Omega)=0$ to the coupling matrix (5.4) of the proposed two-order trisection filter, an explicit expression between the coupling elements and the transmission zero Ω is obtained as

$$\Omega = \frac{M_{12}(M_{S1}^2 + M_{S2}^2) + 2M_{11}M_{S1}M_{S2}}{2M_{S1}M_{S2}} \quad (5.8)$$

Based on (8), the following properties can be summarized.

- 1) $M_{S1}^2 + M_{S2}^2 > 2M_{S1}M_{S2}$, and in most cases $|M_{12}| > M_{11}$.
- 2) If $M_{S1} > 0$, $M_{S2} > 0$ and $M_{12} > 0$, Ω would be greater than zero. Thus, the finite transmission zero would be on the upper stopband.
- 3) If $M_{S1} > 0$, $M_{S2} < 0$ and $M_{12} > 0$, Ω would be smaller than zero. Thus, the finite transmission zero would be on the lower stopband.

Another coupling scheme in Fig. 5.1(e) is a third-order quadruplet filter. Similar to the proposed trisection filter, we introduce another cross coupling path M_{1L} to share energy of cross coupling M_{S3} . The coupling scheme becomes two identical overlapped quadruplets. Thus, the corresponding matrix M shown in (5.9) becomes a bisymmetric matrix.

$$M = \begin{bmatrix} 0 & M_{S1} & 0 & M_{S3} & 0 \\ M_{S1} & 0 & M_{12} & 0 & M_{S3} \\ 0 & M_{12} & 0 & M_{12} & 0 \\ M_{S3} & 0 & M_{12} & 0 & M_{S1} \\ 0 & M_{S3} & 0 & M_{S1} & 0 \end{bmatrix} \quad (5.9)$$

In (5.9), $M_{S1}=M_{3L}$, $M_{12}=M_{23}$, and $M_{S3}=M_{1L}$. From (5.9), the position of transmission zero Ω in the low-pass domain should satisfy (5.10).

$$\Omega^2 = \frac{-M_{12}^2(M_{S1} - M_{S3})^2}{2M_{S1}M_{S3}} \quad (5.10)$$

From (5.10), two possible conditions are described as following.

- 1) If $M_{S1}M_{S3} > 0$, it would result in $\Omega^2 < 0$. Thus, two imaginary frequency zeros can

be designed to have group-delay-flattening response.

2) If $M_{S1}M_{S3} < 0$, it would result in $\Omega^2 > 0$. Thus, it can be designed to generate a pair of attenuation poles.

Similarly, the coupling scheme in Fig. 5.1(f) also comprises two identical overlapped quadruplets, and the corresponding coupling matrix is bisymmetric and synchronously tuned. In addition, extra cross coupling from source to load can be applied as shown in Fig. 5.1(g) to generate two additional transmission zeros.

Finally, consider another modified third-order coupling diagram shown in Fig. 5.1(h). It also has a bisymmetric but asynchronously tuned coupling matrix as shown in (5.11)

$$M = \begin{bmatrix} 0 & M_{S1} & 0 & M_{S3} & 0 \\ M_{S1} & M_{11} & M_{12} & M_{13} & M_{S3} \\ 0 & M_{12} & M_{22} & M_{12} & 0 \\ M_{S3} & M_{13} & M_{12} & M_{11} & M_{S1} \\ 0 & M_{S3} & 0 & M_{S1} & 0 \end{bmatrix} \quad (5.11)$$

In the following section, we will take filter examples with defined specifications.

5.3 The Synthesized Coupling Matrices and the Parallel-Coupled Line Section

To compare the properties of the proposed coupling schemes with the conventional coupling schemes, all generalized Chebyshev filters described in this Section are normalized with the passband return loss of 20dB.

A. The element values of the synthesized coupling matrices

The first example corresponds to Figs. 5.1(a) and (d) where two-pole trisection filters with an upper stopband transmission zero at $\Omega=3$ are designed. Applying the synthesis technique in [37], [52], the coupling matrix (5.12) corresponds to Fig. 5.1(a) and the coupling matrix (5.13) corresponds to Fig. 5.1(d) are obtained.

$$M = \begin{bmatrix} 0 & 1.0788 & 0.6717 & 0 \\ 1.0788 & -0.8998 & 1.3075 & 0 \\ 0.6717 & 1.3075 & 0.7283 & 1.2708 \\ 0 & 0 & 1.2708 & 0 \end{bmatrix} \quad (5.12)$$

$$M = \begin{bmatrix} 0 & 1.2219 & 0.3493 & 0 \\ 1.2219 & -0.0858 & 1.5402 & 0.3493 \\ 0.3493 & 1.5402 & -0.0858 & 1.2219 \\ 0 & 0.3493 & 1.2219 & 0 \end{bmatrix} \quad (5.13)$$

From (5.12), large values of $M_{11}=-0.8998$ and $M_{22}=0.7283$ cause the length of the resonators to be largely adjusted that the main coupling would be affected accordingly. Moreover, the large value of $M_{S2}=0.6717$ implies a strong cross coupling from source to resonator 2.

In contrast, the newly proposed coupling matrix shown in (5.13) is synchronously tuned and has very small value of $M_{11}=-0.0858$ that the resonator length only needs a tiny adjustment. Furthermore, the value of cross coupling $M_{S2}=0.3493$ reduces to about half of the conventional one. Also, one can quickly tune a filter based on (5.4) due to its bisymmetric property.

Changing the position of the transmission zero from $\Omega=3$ to $\Omega=-5$ and applying the synthesis technique in [37], [52] the coupling matrices corresponding to Fig. 5.1(a) and Fig. 5.1(d) can be obtained as shown in (5.14) and (5.15), respectively.

$$M = \begin{bmatrix} 0 & 1.1725 & -0.4051 & 0 \\ 1.1725 & 0.5784 & 1.5278 & 0 \\ -0.4051 & 1.5278 & -0.4774 & 1.2405 \\ 0 & 0 & 1.2405 & 0 \end{bmatrix} \quad (5.14)$$

$$M = \begin{bmatrix} 0 & 1.2234 & -0.2054 & 0 \\ 1.2234 & 0.0505 & 1.6165 & -0.2054 \\ -0.2054 & 1.6165 & 0.0505 & 1.2234 \\ 0 & -0.2054 & 1.2234 & 0 \end{bmatrix} \quad (5.15)$$

The second example corresponds to Figs. 5.1(b) and (f) that both filters are designed with two transmission zeros at $\Omega=1.6$, and -2 . The synthesized coupling matrices corresponding to Fig. 5.1(b) and Fig. 5.1(h) are shown in (5.16) and (5.17), respectively.

$$M = \begin{bmatrix} 0 & 0.7516 & 0.7555 & 0 & 0 \\ 0.7516 & -1.0914 & 0.5112 & 0 & 0 \\ 0.7555 & 0.5112 & 0.0198 & 0.7223 & -0.6193 \\ 0 & 0 & 0.7223 & 0.9886 & 0.8673 \\ 0 & 0 & -0.6193 & 0.8673 & 0 \end{bmatrix} \quad (5.16)$$

$$M = \begin{bmatrix} 0 & 1.0418 & 0 & -0.2246 & 0 \\ 1.0418 & 0.0725 & 0.9444 & 0.2289 & -0.2246 \\ 0 & 0.9444 & -0.2281 & 0.9444 & 0 \\ -0.2246 & 0 & 0.9444 & 0.0725 & 1.0418 \\ 0 & -0.2246 & 0 & 1.0418 & 0 \end{bmatrix} \quad (5.17)$$

For the conventional CT filter in (5.16), the asynchronous tuning of the resonator length would be as high as -1.0914 and 0.9886 which correspond to 2.66% length decrease and 2.5% length increase of original length change respectively when fractional bandwidth of the filter is 5%. This would certainly causes the difficulties during fine tuning of the filter. Moreover, the strong cross coupling $M_{S2}=0.7555$ which is even stronger than the main coupling $M_{S1}=0.7516$. Again, implementation of such a strong cross coupling would be a problem.

The proposed filter in (5.17) has much smaller length adjustment of $M_{22}=-0.2281$ and $M_{11}=M_{33}=0.0725$ which correspond to 0.56% length decrease and 0.18% length increase of original length change respectively when fractional bandwidth of the filter is 5%. According to our experience, this will not be hard to fine tune. Furthermore, the cross couplings of $M_{13}=0.2289$ and $M_{S3}=M_{1L}=-0.2264$ are less than one third of the cross couplings in the conventional CT filter in (5.16).

The third example corresponds to Figs. 5.1(c) and (e) that both filters are

designed with two finite transmission zeros at $\Omega=\pm 1.6$. The synthesized coupling matrices corresponding to Fig. 5.1(c) and Fig. 5.1(e) are shown in (5.18) and (5.19), respectively.

$$M = \begin{bmatrix} 0 & 0.9128 & 0 & -0.5697 & 0 \\ 0.9128 & 0 & 1.1642 & 0 & 0 \\ 0 & 1.1642 & 0 & 0.6458 & 0 \\ -0.5697 & 0 & 0.6458 & 0 & 1.0760 \\ 0 & 0 & 0 & 1.0760 & 0 \end{bmatrix} \quad (5.18)$$

$$M = \begin{bmatrix} 0 & 1.0344 & 0 & -0.2963 & 0 \\ 1.0344 & 0 & 0.9414 & 0 & -0.2963 \\ 0 & 0.9414 & 0 & 0.9414 & 0 \\ -0.2963 & 0 & 0.9414 & 0 & 1.0344 \\ 0 & -0.2963 & 0 & 1.0344 & 0 \end{bmatrix} \quad (5.19)$$

Due to very close transmission zeros of $\Omega=\pm 1.6$, the cross coupling $M_{S3}=-0.5697$ in (5.18) is very strong. Moreover, the layout of the filter must be asymmetric. However, in (5.19), the coupling matrix is bisymmetric, and the cross couplings $M_{IL}=M_{S3}=-0.2963$ are only about half of the conventional quadruplet filter in (5.18). Again, the bisymmetric coupling matrix in (5.19) implies a symmetrical layout that fine tuning of the filter would be much easier.

Two overlapped quadruplet structure in Fig. 5.1(e) can be extended to the fourth-order filter as shown in Fig. 5.1(f). In this case, the transmission zeros can be even more close to the passband. For example, the coupling matrix of transmission zeros at $\Omega=\pm 1.3$ is obtained as (5.20).

$$M = \begin{bmatrix} 0 & 0.9654 & 0 & -0.2986 & 0 & 0 \\ 0.9654 & 0 & 1.0059 & 0 & 0 & 0 \\ 0 & 1.0059 & 0 & 0.3597 & 0 & -0.2986 \\ -0.2986 & 0 & 0.3597 & 0 & 1.0059 & 0 \\ 0 & 0 & 0 & 1.0059 & 0 & 0.9654 \\ 0 & 0 & -0.2986 & 0 & 0.9654 & 0 \end{bmatrix} \quad (5.20)$$

Again, the coupling matrix implies a symmetric layout and moderate cross couplings of $M_{2L}=M_{S3}=-0.2986$.

The coupling scheme in Fig. 5.1(f) can be further extended by applying the cross coupling from source to load (M_{SL}) as shown in Fig. 5.1(g). The coupling scheme in Fig. 5.1(g) has two additional transmission zeros on both side of passband. For instance, the coupling matrix of the filter with two pairs of transmission zeros located at $\Omega=\pm 1.3, \pm 3$ are obtained as (5.21).

$$M = \begin{bmatrix} 0 & 0.9584 & 0 & -0.2963 & 0 & 0.0655 \\ 0.9584 & 0 & 1.0190 & 0 & 0 & 0 \\ 0 & 1.0190 & 0 & 0.3259 & 0 & -0.2963 \\ -0.2963 & 0 & 0.3259 & 0 & 1.0190 & 0 \\ 0 & 0 & 0 & 1.0190 & 0 & 0.9584 \\ 0.0655 & 0 & -0.2963 & 0 & 0.9584 & 0 \end{bmatrix} \quad (5.21)$$

Because of the synthesized coupling matrices corresponding to the definite specifications, the properties of the three conventional coupling schemes and the proposed coupling schemes described above can be summarized as follows. For the trisection filters in Figs. 5.1(a) and (b), if the transmission zeros are very close to passband, the filters will be highly asynchronously tuned, and the cross couplings will be very large. The circumstances can be observed in (5.12) and (5.16). Thus, it results in manufacturing problems of planar forms such as microstrip. The planar filters of these kinds have two difficulties. First, the implementation of strong cross couplings always causes serious unwanted cross couplings and distorts the filter response. Second, the alignment of resonant frequencies of the seriously asynchronously tuned resonators always affects the desired coupling strength. For the filter in Fig. 5.1(c), although the quadruplet filter is synchronously tuned, the first difficulty still exists. It can be inspected in (5.18). The problems can be solved by the proposed modified

cross coupling schemes. By observing the coupling matrices in (5.13), (5.17) and (5.19), the proposed coupling schemes can implement filters with transmission zeros much closer to the passband than conventional CT and CQ filters. It should be noted that the coupling matrix in (5.17) corresponding to the coupling scheme in Fig. 5.1(h) has much smaller values of the cross couplings and much less asynchronous tuning frequencies than that of Fig. 5.1(b). In addition, the coupling matrices show the bisymmetric property. Bisymmetric matrices can have symmetric physical layouts. The symmetric layouts make the fine tuning of the filters much easier than the filters with asymmetric layouts because the number of tuning variables is halved in the symmetric case.

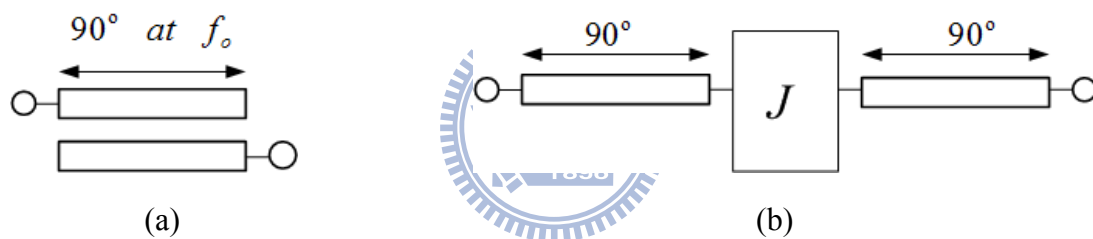


Fig. 5.2. (a) Parallel-coupled line section and (b) its equivalent circuit using a J -inverter.

B. The Parallel-Coupled Line Realizations

All of the proposed coupling schemes have the property that they all have the cross couplings between source and load and nonadjacent resonators. Therefore, the proposed coupling schemes are extremely suitable for parallel-coupled filter realizations [69], [93], [97], [101]. Fig. 5.2(a) shows the parallel-coupled line section and its equivalent circuit is illustrated in Fig. 5.2(b). Each coupled-line section has an electrical length of 90° at the frequencies according to the values of diagonal elements in the coupling matrix. Thus, the values of the admittance inverters corresponding to the main coupling element values of the coupling matrix can be obtained from (5.22).

$$\frac{J_{01}}{Y_o} = M_{S1} \sqrt{\frac{\pi \Delta f}{2 f_o}}, \quad \frac{J_{N,N+1}}{Y_o} = M_{NL} \sqrt{\frac{\pi \Delta f}{2 f_o}},$$

$$\frac{J_{i,i+1}}{Y_o} = \frac{\pi}{2} M_{i,i+1} \frac{\Delta f}{f_o} \quad (i = 1, 2, \dots, N-1) \quad (5.22)$$

After calculating each J -inverter, the even- and odd-mode characteristic impedances of each coupled-line section can be approximately obtained from (23).

$$Z_{oei} = Z_o \left[1 + \frac{J_{i-1,i}}{Y_o} + \left(\frac{J_{i-1,i}}{Y_o} \right)^2 \right]$$

$$Z_{ooi} = Z_o \left[1 - \frac{J_{i-1,i}}{Y_o} + \left(\frac{J_{i-1,i}}{Y_o} \right)^2 \right] \quad (i = 1, 2, \dots, N+1) \quad (5.23)$$

After achieving the core portion of the parallel-coupled filter, the cross couplings are then applied following the procedures described in [101].

5.4 Design Examples and Experiment Results

Several examples in this section will be implemented using microstrip line. The Rogers RO4003 substrate with a dielectric constant of 3.58 and thickness of 20 mils is chosen for implementations of the filters.

A. The trisection filters corresponding to Figs. 5.1(d) and (h)

The first two examples are two-order modified trisection filters and their coupling scheme is shown in Fig. 5.1(d). The transmission zero is located at $\Omega=3$ for one filter and $\Omega=-5$ for the other. The corresponding coupling matrices are shown in (5.13) and (5.15) respectively. The transformed matrices responses with a center frequency of 2.45 GHz and fractional bandwidth of 3% are shown in Fig. 5.3. From (5.22) and (5.23) the electrical parameters of the main coupling path can be obtained as $Z_{oe1} = Z_{oe3} = 66.78 \Omega$, $Z_{oo1} = Z_{oo3} = 40.25 \Omega$, $Z_{oe2} = 53.89 \Omega$, and $Z_{oo2} = 46.63 \Omega$

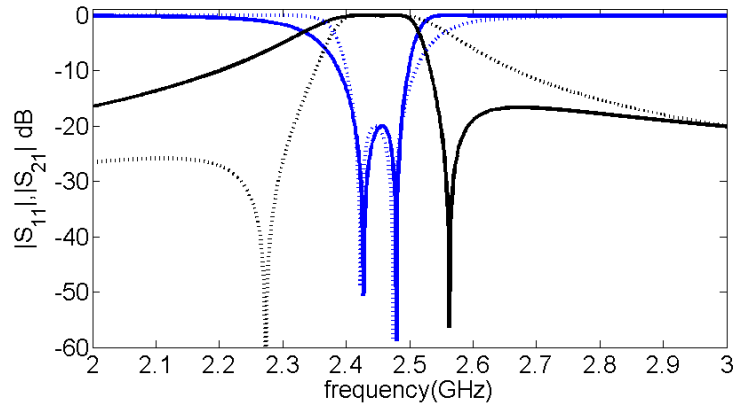
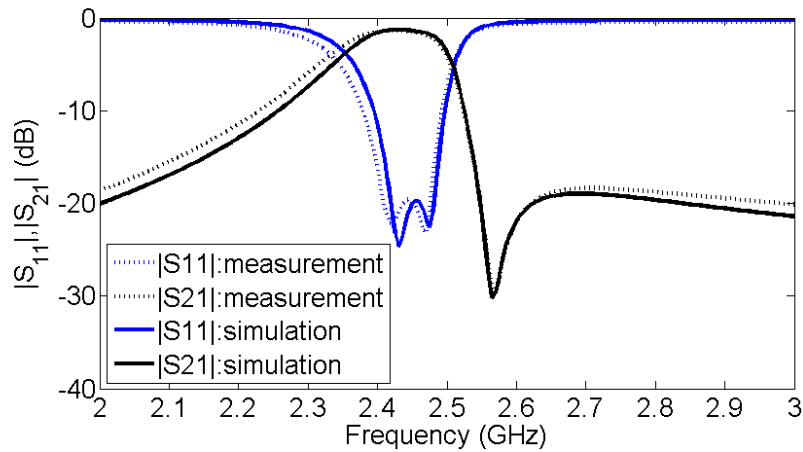
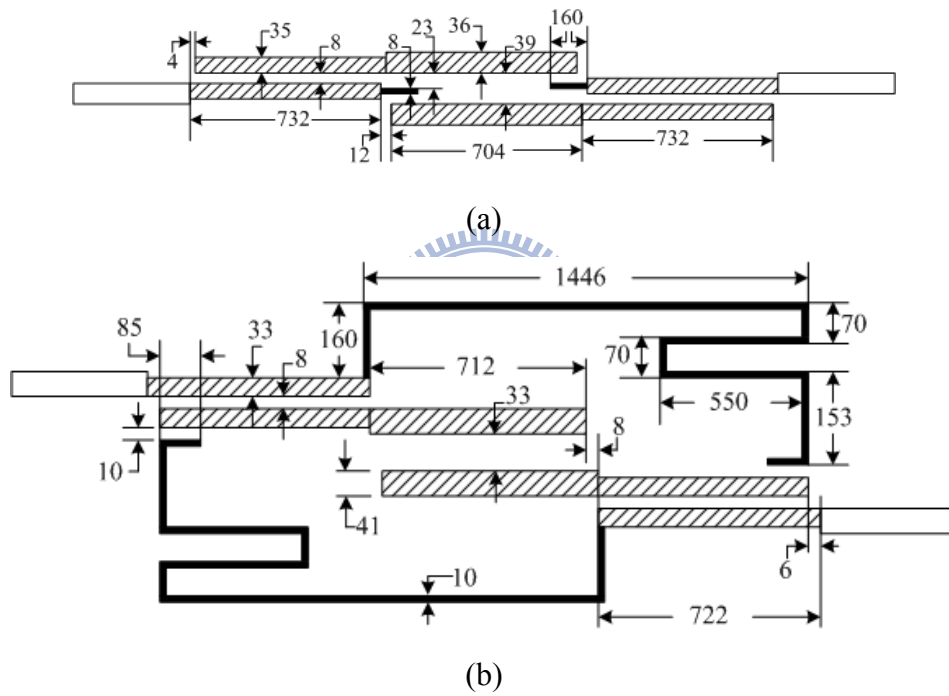
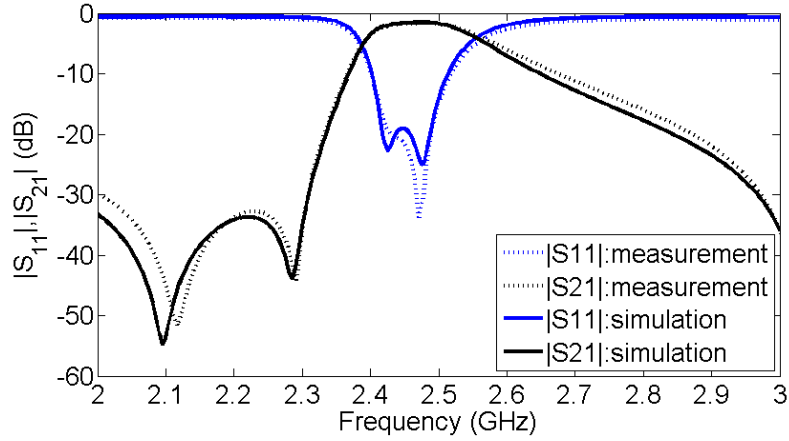


Fig. 5.3. Ideal performances calculated from the synthesized coupling matrices in (5.13) solid line, and (5.15) dotted line.

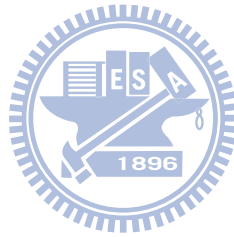


(c)

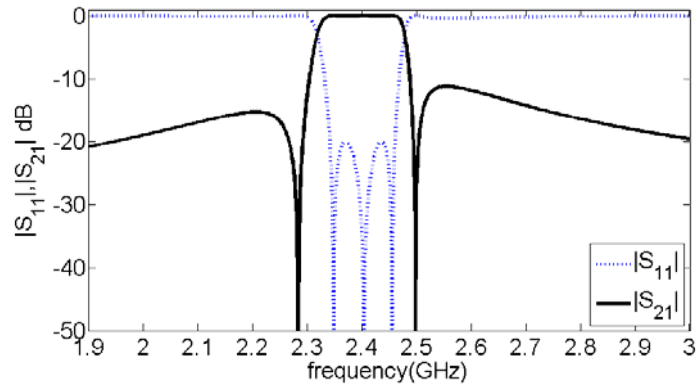


(d)

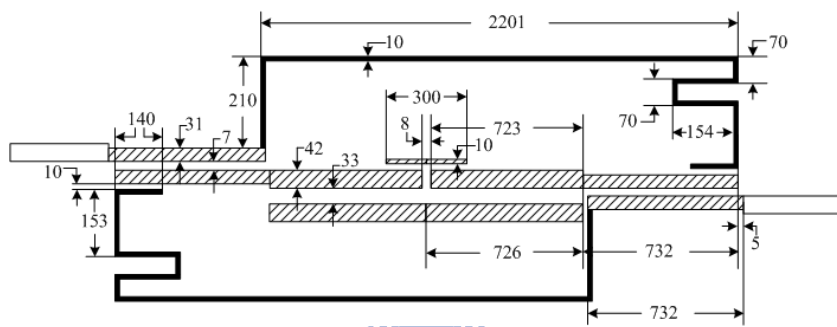
Fig. 5.4 The layouts and the simulated and measured performances of the filters in Fig. 5.1(d). (a) Layout for the design with a transmission zero at $\Omega=3$ (unit: mils). (b) Layout for the design with a transmission zero at $\Omega=-5$ (unit: mils). (c) Simulated and measured results corresponding to Fig. 5.4(a). (d) Simulated and measured results corresponding to Fig. 5.4(b).



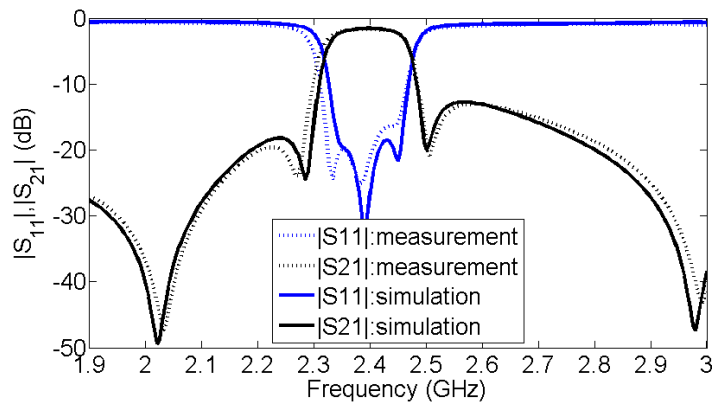
corresponding to (13), and $Z_{oe1} = Z_{oe3} = 66.81 \Omega$, $Z_{oo1} = Z_{oo3} = 40.25 \Omega$, $Z_{oe2} = 54.10 \Omega$, and $Z_{oo2} = 46.48 \Omega$ corresponding to (5.15). The electrical lengths of the coupled-line sections are all 90° at 2.45 GHz. Due to the very small frequency shifts caused by M_{11} and M_{22} , there is almost no need to modify the length of the resonator. Then, follow [103] to add cross coupling paths. Figs. 5.4(a) and (b) show the physical dimensions of the filters. In Fig. 5.4(b), the electrical length of two identical delay lines is 360° at center frequency for realizing the cross couplings M_{S2} and M_{IL} . The full EM simulated results of the filter structures were performed to take all the EM effects into consideration by using a commercial electromagnetic simulator Sonnet [100]. The EM simulated and measured results of the two filters are shown in Fig. 5.4(c) and Fig. 5.4(d). In Fig. 5.4(d), there is an additional transmission zero at about 2.1 GHz due to



(a)



(b)



(c)

Fig. 5.5. The proposed three-order CT filter. (a) Ideal real frequency responses. (b) Layout (unit: mils). (c) Simulated and measured results.

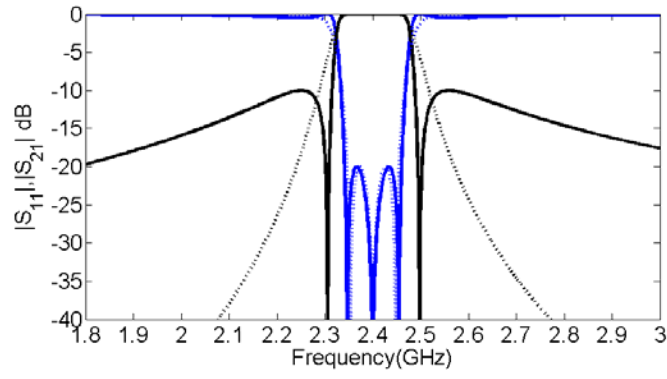
the unwanted cross coupling M_{SL} . For the CT filter corresponding to Fig. 5.1(h), the calculated ideal bandpass responses with $\Omega=1.6$ and -2 , center frequency of 2.4 GHz, and fractional bandwidth of 5% are shown in Fig. 5.5(a). Then, taking the similar procedures as described above, and performing a full EM simulation to fine tune the

responses, the final layout is obtained as shown in Fig. 5.5(b). It should be emphasized that the J -inverter equivalent in Fig. 5.2(b) is only valid at center frequency. The more the asynchronous tuning is, the more discrepancy of the equivalent circuit will be. Here, the equivalent circuit model is still valid because the asynchronous tuning is small. The electrical length of the two identical delay lines is 360° at the center frequency. Fig. 5.5(c) depicts the EM simulated and measured results. In Fig. 5.5(c), there are two additional transmission zeros at about 2.02 GHz and 2.98 GHz due to the unwanted cross coupling M_{SL} .

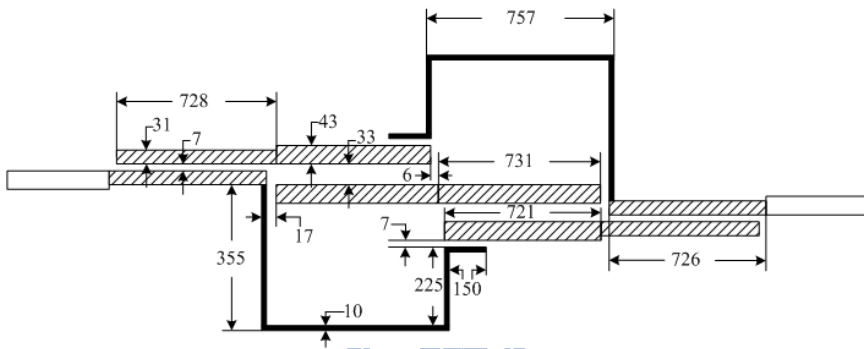
B. The quadruplet filters corresponding to Figs. 5.1(e) and (f) and the modified canonical-form filter corresponding to Fig. 5.1(g)

For the quadruplet filter in Fig. 5.1(e), the ideal bandpass responses calculated from (5.19) with transmission zeros at $\Omega = \pm 1.6$, center frequency of 2.4 GHz, and fractional bandwidth of 5% are depicted in Fig. 5.6(a). The ideal bandpass responses excluding all cross coupling elements in (5.19) are also shown in Fig. 5.6(a). It can be obviously seen that adding the cross couplings in the proposed coupling scheme influence the in-band responses very little even for transmission zeros very close to the passband. Figs. 5.6(b) and 5.6(c) show the physical dimensions and the simulated and measured performances. In order to reveal the merit of the proposed filter, a quadruplet filter with coupling scheme in Fig. 5.1(c) with the same specification is designed, and its synthesized coupling matrix is in (5.18). The detail dimensions to achieve the specification are shown in Fig. 5.6(d). As can be seen in the layout that the gap used to realize the cross coupling M_{S3} in Fig. 5.1(c) is only 1 mil (0.025mm) which is far beyond the limit of standard printed circuit board process.

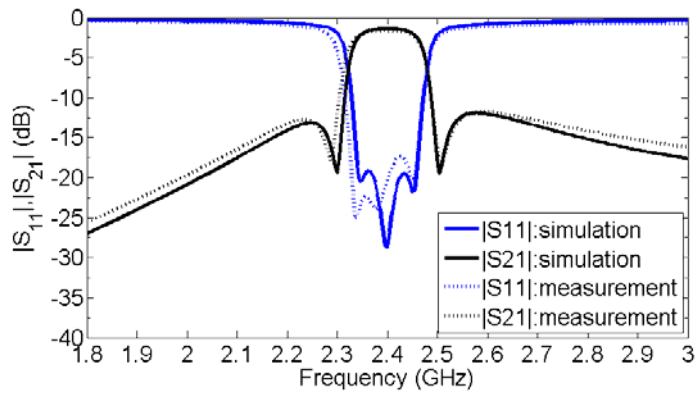
Similarly, the same concept of the filter in Fig. 5.1(e) can also be applied to the fourth-order quadruplet filter in Fig. 5.1(f). Again, two finite transmission zeros at



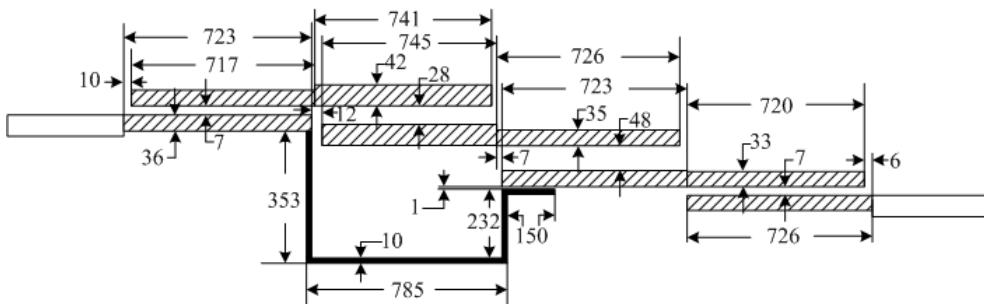
(a)



(b)



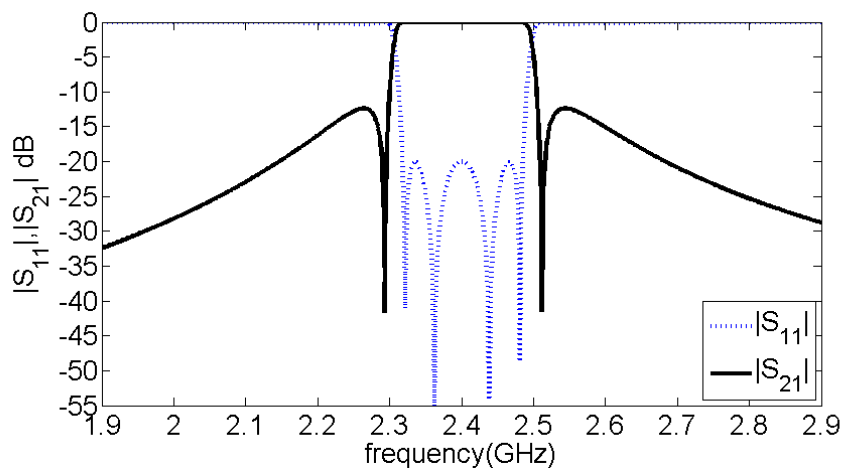
(c)



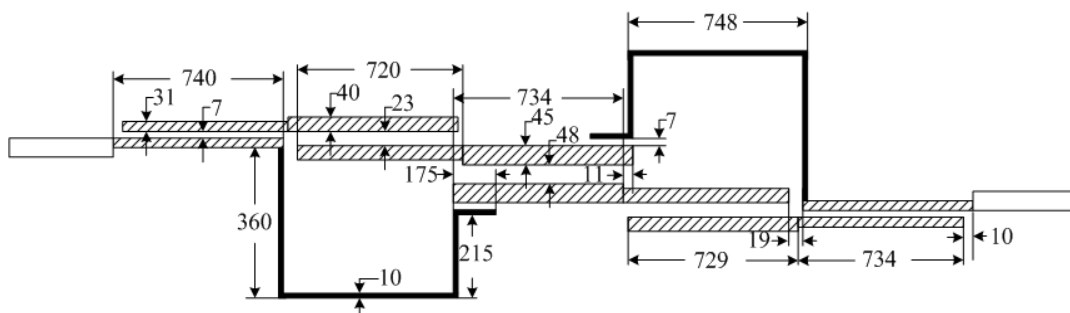
(d)

Fig. 5.6. The proposed third-order quadruplet filter. (a) Two ideal frequency responses: one is to consider the matrix in (5.19) solid line and the other is to exclude all the cross-coupling elements in (5.19) dotted line. (b) Layout (unit: mils). (c) Simulated and measured performances. (d) Layout for realizing the coupling scheme in Fig. 5.1(c).

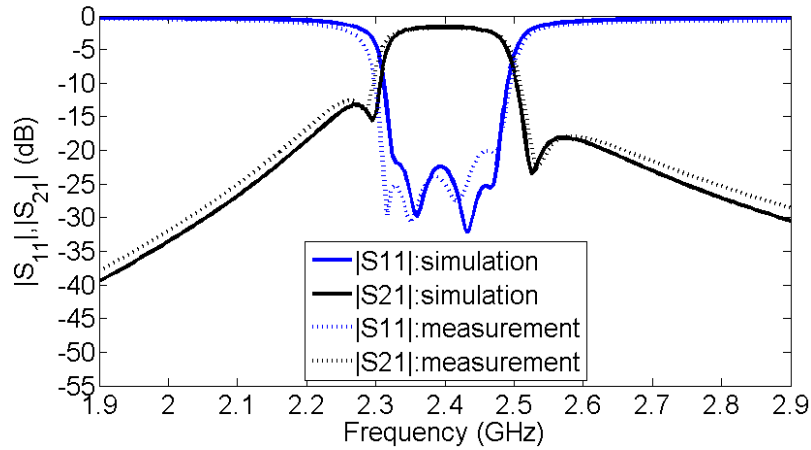
$\Omega = \pm 1.3$ are very close to the passband. The synthesized coupling matrix is shown in (5.20). The bandpass filter is designed with a center frequency of 2.4 GHz and fractional bandwidth of 7%. The ideal responses, physical dimensions, and the simulated and measured results are shown in Fig. 5.7.



(a)



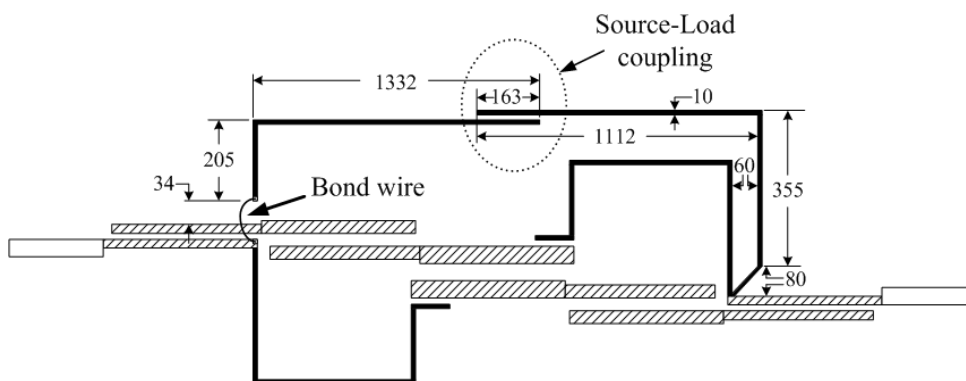
(b)



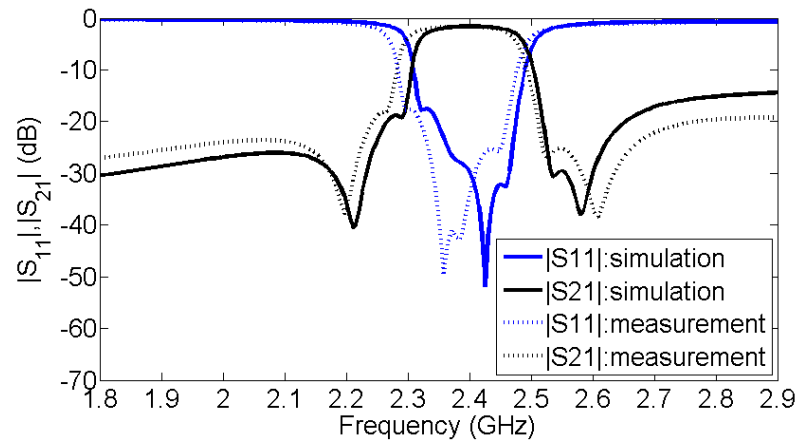
(c)

Fig. 5.7. The modified fourth-order quadruplet filter. (a) Ideal responses. (b) Layout (unit: mils). (c) Simulated and measured performances.

By introducing the source-load cross coupling as shown in Fig. 5.1(g), the canonical form response with two additional transmission zeros than the quadruplet on both sides of passband are created. In this example, two additional transmission zeros at $\Omega=\pm 3$ are chosen. The synthesized coupling matrix is shown in (5.21). The observation between the coupling matrices in (5.20) and (5.21) shows that it is no need to modify the main structure. The physical layout is shown in Fig. 5.7(b) that only modification is to add two extra delay lines to realize the coupling M_{SL} . The ideal responses, physical dimensions, and the simulated and measured results are shown in Fig. 5.8. Due to the physical layout of the filter, a bond wire is needed to realize M_{SL} .

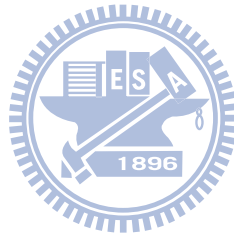


(a)



(b)

Fig. 5.8. The modified fourth-order quadruplet filter with source-load cross coupling. (a) Layout (unit: mils). (b) Simulated and measured performances.



Chapter 6 Exact Synthesis of New High-Order Wideband Marchand Balun

New high-order Marchand baluns with ultra wideband performances are proposed in this chapter. The Marchand baluns are synthesized based on an S -plane highpass prototype using the Richards' transformation. The responses of the synthesized high-order Marchand baluns are exactly predicted at all real frequencies. The electrical lengths of all the transmission line elements are a quarter-wavelength long at the center frequency. Two fifth-order Marchand baluns with synthesized reflection coefficients -20.53dB and -21.71dB which correspond to 131% and 152% bandwidth respectively are directly realized using the combinations of microstrip line, slotline and coplanar stripline sections. Simulated and measure results are showed. In addition, the sixth-order prototype of Marchand balun is presented to discuss.

6.1 Introduction

Baluns [119] are widely used in many radio frequency and microwave communication systems. The main function of baluns is to transform an unbalanced transmission signal to a balanced transmission signal, and vice versa. Thus, baluns can be used in antennas excitation or balanced circuit topologies such as balanced mixers, push-pull amplifiers, and phase shifters. There are many types of baluns as proposed in [111], [112], [123], [124]. Among the various kinds of balun, Marchand balun [102], [106], [107], [115], [120] is extremely popular because of its comparative good wideband amplitude and phase balance than that of the others. Several methods of fabrication have been proposed to realize Marchand balun [102], [106], [107], [115], [120], [121], [122], [125], [126], [141], [142].

In designing coupled-line Marchand balun, various analysis methods were presented. In [122], [141], using relationships of the power wave in a balun to derive the scattering parameters can analyze a symmetrical Marchand balun, but it is exact

only at the center frequency. In [125], inclusion of the parameter of the electrical length of the transmission line can predict broadband performances, but the approach lacks generality. Furthermore, to achieve wider bandwidth multi-conductor coupled lines to realize tight couplings were presented. Another method is the even- and odd-mode analysis method. However, it is limited to the case of a symmetrical coupled-line Marchand balun with maximum flat responses. Actually, exact synthesis of conventional Marchand baluns has been presented in [102], [106], [107], [115]. A Chebyshev response can be synthesized using the synthesis method. In focusing on planar coupled-line technology to realize Marchand baluns, useful design values of even- and odd-mode parameters in each coupled line are available in [115]. Nevertheless, when bandwidth of a balun is a major consideration, one should concern the limited range of practical even- and odd-mode impedance values of coupled lines.

The purpose of this chapter is to propose new higher-order wideband Marchand baluns. Emphasis is placed on new Marchand baluns with higher order more than a conventional fourth-order Marchand balun and realizable ultra-wideband baluns in planar technology. In synthesizing Marchand balun, exact synthesis of filters with circuit analysis to then obtain prescribed characteristic functions [134], [135] can be used to extract element values of Marchand balun. Thus, the design of the proposed baluns is based on S -plane high-pass prototype using Richards' transformation $S = j\tan(\pi/2(f/f_0))$, where f_0 is the center frequency of the passband, and f and S are the real frequency domain and Richards' frequency domain variables, respectively. By applying proper circuit transformations, the original distributed circuit of the proposed Marchand balun as shown in Fig. 6.1 can be converted into a fifth-order S -plane high-pass prototype balun. With the aid of synthesis method, all elements of the synthesized prototype can be obtained. Thus, the design parameters of the original

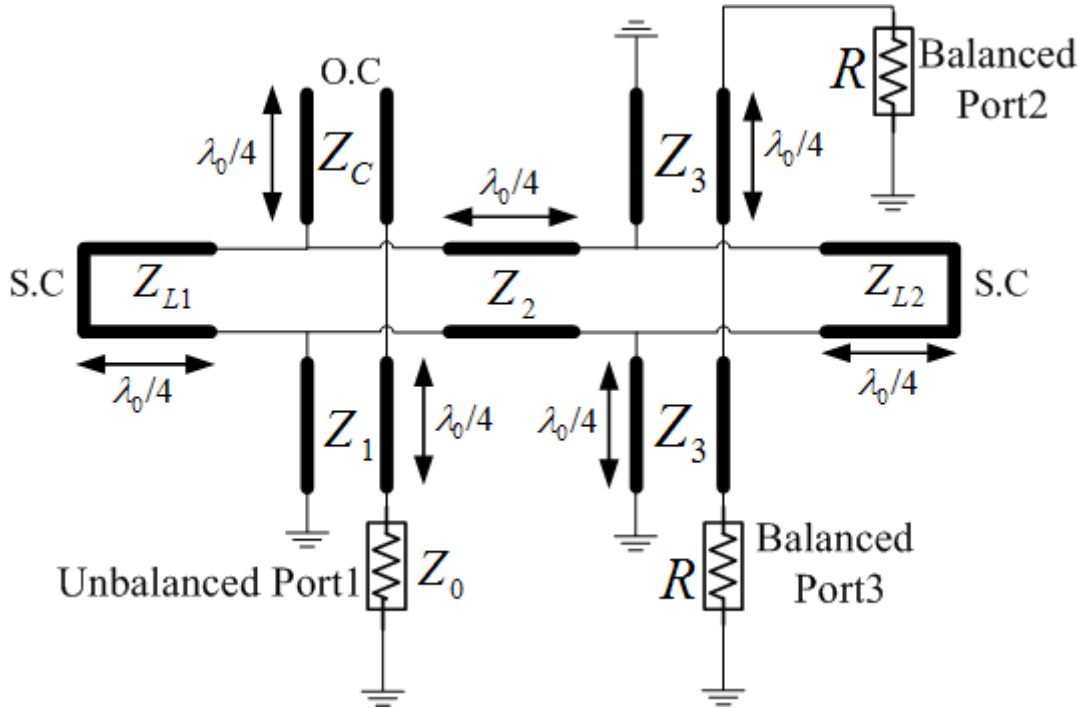


Fig. 6.1. The distributed circuit of the proposed fifth-order Marchand balun.

circuit in Fig. 6.1 can be controlled. Direct realization of the proposed original balun circuit with very wideband responses is presented in planar form. In addition, a six-order Marchand balun is presented to discuss.

6.2 Derivation of a Fifth-Order Marchand Balun

The proposed distributed circuit of Marchand balun shown in Fig. 6.1 is composed of one open-ended stub, two short-ended stubs, one uniform transmission line connected to input port (unbalanced port), one uniform transmission line connected to two short-ended stubs, and two identical uniform transmission lines individually connected to two output ports (balanced ports) with impedance values corresponding to Z_C , Z_{L1} and Z_{L2} , Z_1 , Z_2 , Z_3 , respectively. The electrical lengths of all the stubs and uniform transmission lines are 90° at center frequency. Due to differential outputs, the two output ports can be combined into one port. Thus, the two-port distributed circuit can be simplified that is shown in Fig. 6.2(a). Its equivalent S -plane high-pass prototype is shown in Fig. 6.2(b). S is the Richards

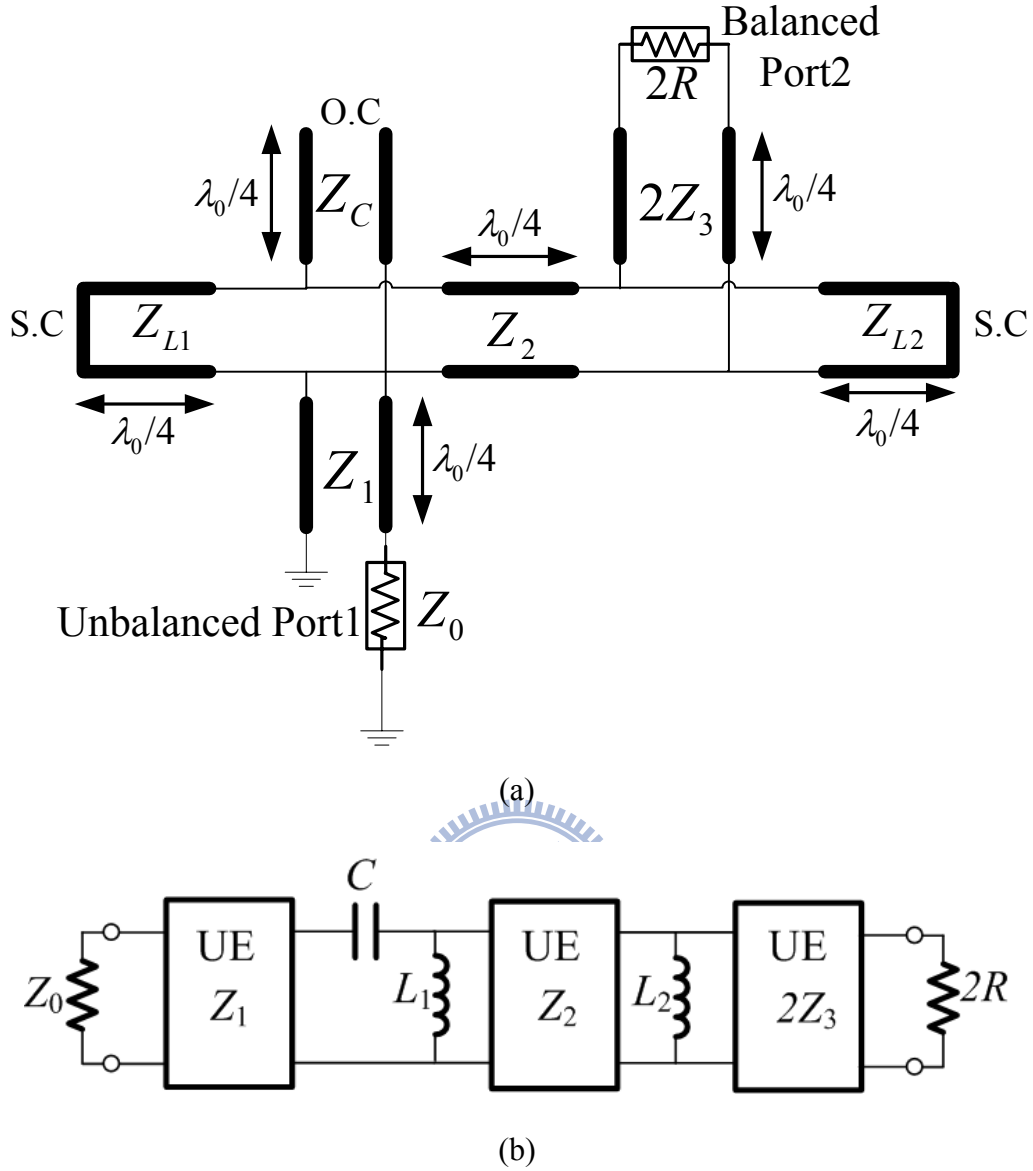


Fig. 6.2. The proposed fifth-order Marchand balun. (a) The two-port distributed circuit simplified in Fig. 6.1. (b) Its S -plane high-pass circuit.

variable defined as

$$S = j\Omega = j \tan \theta = j \tan \left(\frac{\pi f}{2f_0} \right) \quad (6.1)$$

where f_0 is the center frequency of the passband, and f and S are the real frequency domain and Richards' frequency domain variables, respectively. The open-ended and short-ended stubs in the f -plane become a capacitor and inductors, respectively, in the S -plane. The interconnecting uniform transmission lines in the f -plane are turned into

Circuits in the f -plane	Circuits in the S -plane	ABCD Parameters
		$\begin{bmatrix} 1 & \frac{1}{SC} \\ 0 & 1 \end{bmatrix}$
		$\begin{bmatrix} 1 & 0 \\ \frac{1}{SL} & 1 \end{bmatrix}$
		$\frac{1}{\sqrt{1-S^2}} \begin{bmatrix} 1 & ZS \\ S/Z & 1 \end{bmatrix}$

Table 6.1 The relationships between distributed circuits in the f -plane and high-pass circuits in the S -plane, and the corresponding $ABCD$ parameters.

the unit elements (UE) in the S -plane though the effect of the Richards transformation. The description of the parameters of the three important components in high-pass prototype is shown in Table 6.1.

To derive a final fifth-order Marchand balun, circuit transformations will be used. Firstly, the circuit transformation to be used is the Kuroda's identity as shown in Fig. 6.3(a) [131]. The Kuroda transformation is now applied to the shunt inductor L_1 in Fig. 6.2(b), thus changing the position of the shunt inductor from one side of the unit element Z_2 to another side. The transformed circuit is shown in Fig. 6.3(b) with the following transformation equation.

$$n^2 = 1 + \frac{Z_2}{L_1} \quad (6.2)$$

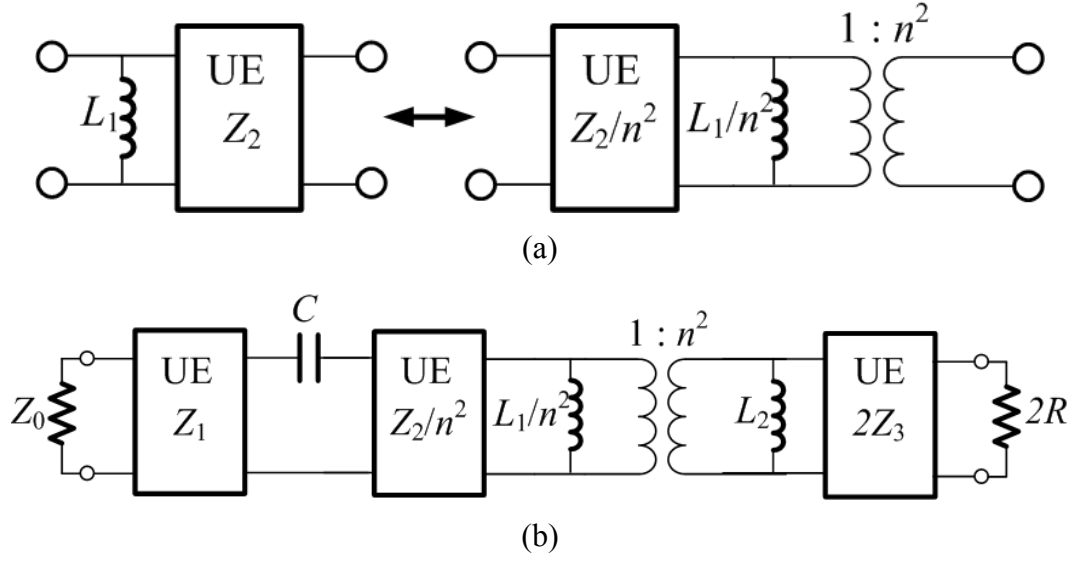


Fig. 6.3. The first transformation. (a)The kuroda identity transformation from [131]. (b) After kuroda identity transformation in Fig. 6.2(b).

Secondly, observation of the two shunt inductors connected by the $1 : n^2$ transformer shown in Fig. 6.3(b) shows that one redundant shunt inductor exists. Hence, to combine the redundant element, a new circuit transformation should be derived. Consider the new circuit transformation in Fig. 6.4(a). The $ABCD$ -parameters of the left circuit in Fig. 6.4(a) are

$$\begin{aligned}
 & \frac{1}{\sqrt{1-S^2}} \begin{bmatrix} \frac{1}{n^2} & 0 \\ 0 & n^2 \end{bmatrix} \begin{bmatrix} 1 & 0 \\ \frac{1}{SL_2} & 1 \end{bmatrix} \begin{bmatrix} 1 & Z_{UE1}S \\ \frac{S}{Z_{UE1}} & 1 \end{bmatrix} \\
 &= \frac{1}{\sqrt{1-S^2}} \begin{bmatrix} \frac{1}{n^2} & \frac{Z_{UE1}S}{n^2} \\ \frac{n^2}{SL_2} + \frac{n^2S}{Z_{UE1}} & \frac{n^2Z_{UE1}}{L_2} + n^2 \end{bmatrix} \quad (6.3)
 \end{aligned}$$

And the $ABCD$ -parameters of the right circuit in Fig. 6.4(a) are

$$\begin{aligned}
 & \frac{1}{\sqrt{1-S^2}} \begin{bmatrix} 1 & 0 \\ \frac{1}{SL_2'} & 1 \end{bmatrix} \begin{bmatrix} 1 & Z_{UE3}S \\ \frac{S}{Z_{UE3}} & 1 \end{bmatrix} \begin{bmatrix} \frac{1}{n^2} & 0 \\ 0 & n^2 \end{bmatrix} \\
 &= \frac{1}{\sqrt{1-S^2}} \begin{bmatrix} \frac{1}{n^2} & Z_{UE3}Sn^2 \\ \frac{1}{n^2SL_2'} + \frac{S}{n^2Z_{UE3}} & \frac{n^2Z_{UE3}}{L_2'} + n^2 \end{bmatrix} \quad (6.4)
 \end{aligned}$$

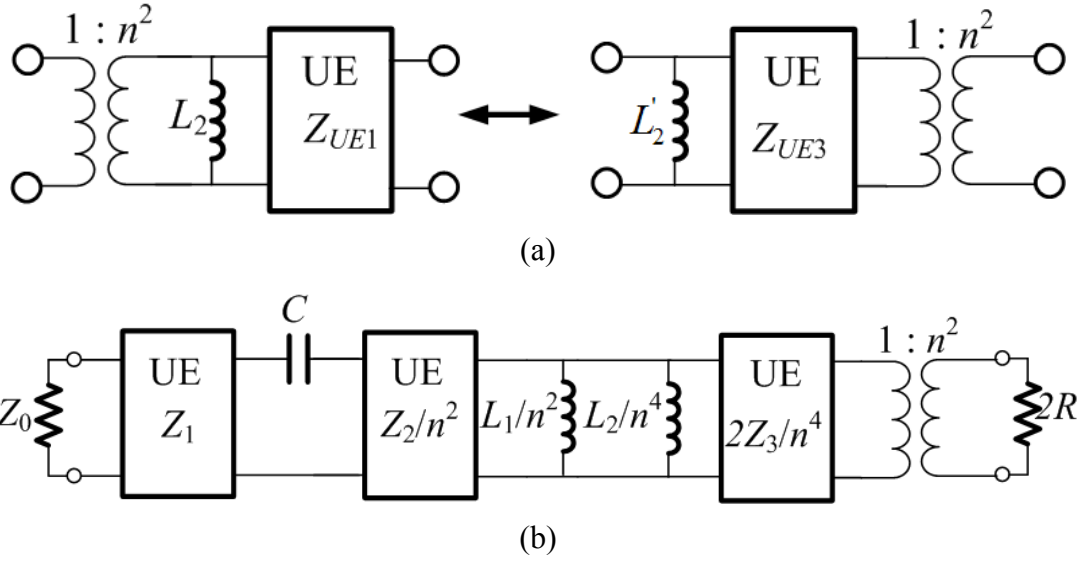


Fig. 6.4. The second transformation. (a) New exact circuit transformation. (b) Apply exact circuit transformation in Fig. 6.4(a) to Fig. 6.3(b).

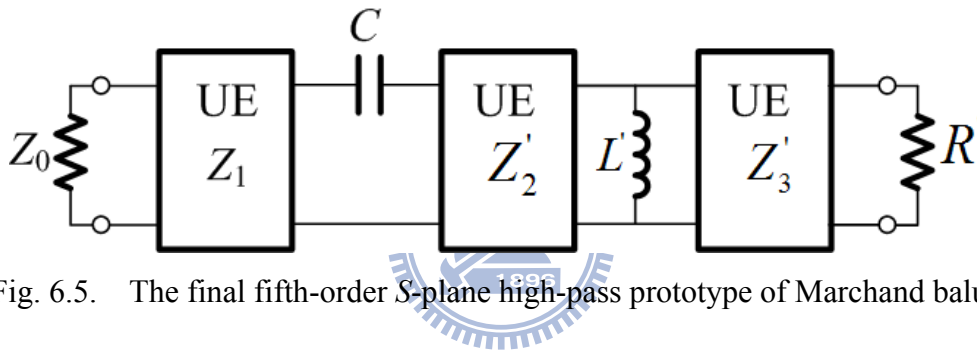


Fig. 6.5. The final fifth-order S -plane high-pass prototype of Marchand balun.

Assume that (6.3) equal to (6.4), the transformed parameters can be obtained as follows.

$$\begin{aligned} L'_2 &= \frac{L_2}{n^4} \\ Z_{UE3} &= \frac{Z_{UE1}}{n^4} \end{aligned} \quad (6.5)$$

Thirdly, by applying the new derived circuit transformation the further transformed circuit can be obtained, which is shown in Fig. 6.4(b). Finally, the two shunt inductors can be combined, and the $1:n^2$ transformer can be absorbed into the load termination. Consequently, the final fifth-order Marchand balun prototype is shown in Fig. 6.5 with the following relations:

$$Z'_2 = \frac{Z_2}{n^2} \quad (6.6)$$

$$L' = \frac{L_1 L_2}{n^2 (L_1 n^2 + L_2)} \quad (6.7)$$

$$Z'_3 = \frac{2Z_3}{n^4} \quad (6.8)$$

$$R' = \frac{2R}{n^4} \quad (6.9)$$

The design parameters in (6.2) and (6.6)-(6.9) complete the transformation of the balun prototype of Fig. 6.2(b) into that of Fig. 6.5.

6.3 Synthesis and Design of Two Balun Examples

A. Synthesis Procedures

Before designing the proposed balun, two important points should be addressed in the following. The first point is to determine a characteristic transfer function of the fifth-order Marchand balun. The second point is to apply exact synthesis to the proposed balun such that the wideband responses can be predicted.

By observing the prototype circuit in Fig. 6.5, the suitable characteristic function exhibiting the Chebyshev responses, which is comprehensively discussed in [135], is given by:

$$|K(S)|^2 = \varepsilon^2 \left[T_m \left(\frac{S_C}{S} \right) T_n \left(\frac{\sqrt{1-S_C^2}}{\sqrt{1-S^2}} \right) - U_m \left(\frac{S_C}{S} \right) U_n \left(\frac{\sqrt{1-S_C^2}}{\sqrt{1-S^2}} \right) \right]^2 \quad (6.10)$$

where $S_C = j \tan(\pi f_C / 2 f_0)$, f_C is the filter cutoff frequency that is used to determine the bandwidth of the balun, ε specifies equal-ripple value, and $T_m(x)$ and $U_m(x)$ are the unnormalized Chebyshev polynomials of the first and second kinds of degree m , respectively. In (10), the subscript m and n denote the number of high-pass ladder elements (series capacitors and shunt inductors) and unit elements, respectively.

Given $|K(S)|^2$, the square of the magnitude of the input reflection coefficient is

obtained using

$$|S_{11}(S)|^2 = \frac{|K(S)|^2}{1+|K(S)|^2} \quad (6.11)$$

Then, $S_{11}(S)$ can be found with the knowledge that

$$|S_{11}(S)|^2 = S_{11}(S)S_{11}(-S) \quad (6.12)$$

The relationship between input impedance $Z_{in}(S)$ and $S_{11}(S)$ with a normalized source resistance of $1-\Omega$ is

$$Z_{in}(S) = \frac{1+S_{11}(S)}{1-S_{11}(S)} \quad (6.13)$$

The circuit prototype to be synthesized is shown in Fig. 6.5. The first element type to be extracted is the unit element. By applying Richards' theorem a unit element can be obtained using

$$Z_{UE,i} = Z_{in,i}(1) \quad (6.14)$$

where $Z_{UE,i}$ denotes the impedance value of i^{th} unit elements and $Z_{in,i}(1)$ is the input impedance looking from i^{th} unit elements.

The input impedance of the remaining network after removal of the unit element is

$$Z'_{in,i}(S) = Z_{in,i}(1) \frac{SZ_{in,i}(1) - Z_{in}(S)}{SZ_{in}(S) - Z_{in,i}(1)} \quad (6.15)$$

where the common (S^2-1) factor can be cancelled.

The second and third element types to be extracted are the series capacitor and shunt inductor. The method that is used to synthesize lumped element ladder networks can be applied to this balun prototype and obtain the element values of the series capacitor and shunt inductor.

B. Two Example Designs

The two examples of fifth-order equal ripple wideband Marchand baluns corresponding to the S -plane high-pass prototype as shown in Fig. 6.5 are considered in this chapter.

The first designed balun is with a center frequency f_0 of 2 GHz, a normalized cutoff frequency of $S_C=j0.6$ corresponding to bandwidth of 131%, and ripple level $\varepsilon=0.0945$ corresponding to a return loss of 20.53 dB. By using (6.10), the characteristic polynomial $|K(S)|^2$ can be constructed as

$$|K(S)|^2 = \frac{0.1965S^8 + 0.9304S^6 + 1.4332S^4 + 0.7855S^2 + 0.1400}{-S^{10} + 3S^8 - 3S^6 + S^4} \quad (6.16)$$

Then, the square of the magnitude of the input reflection coefficient is established by (6.11), and with the knowledge of (6.12) it can lead to

$$S_{11}(S) = \frac{0.4433S^4 + 1.0496S^2 + 0.3743}{S^5 + 3.7102S^4 + 5.2847S^3 + 3.8768S^2 + 1.4545S + 0.3741} \quad (6.17)$$

Use of (6.13) can obtain the polynomial of the input impedance as

$$Z_{in}(S) = \frac{S^5 + 4.1535S^4 + 5.2847S^3 + 4.9264S^2 + 1.4545S + 0.7484}{S^5 + 3.2669S^4 + 5.2847S^3 + 2.8272S^2 + 1.4545S} \quad (6.18)$$

The following step is to synthesize the element values in Fig. 6.5. To extract a unit element and obtain the input impedance of the remaining network, (6.14) and (6.15) are used. And the standard synthesis procedure of lumped element ladder networks is to extract a series capacitor and a shunt inductor. Thus, the circuit parameters of the first designed balun in a normalized source resistance of 1- Ω are:

$$\begin{aligned}
Z_1 &= 1.27 \\
C &= 1.1561 \\
Z_2' &= 1 \\
L' &= 1.1563 \\
Z_3' &= 0.7871 \\
R' &= 1
\end{aligned} \tag{6.19}$$

And then substituting (6.19) into (6.2) and (6.6)-(6.9) and de-normalizing to 50- Ω system give the design parameters of Fig. 6.1 as follows.

$$\begin{aligned}
Z_1 &= 63.5 \Omega \\
Z_C &= 43.25 \Omega \\
Z_{L1} &= 170.71 \Omega \\
Z_2 &= 70.71 \Omega \\
Z_{L2} &= 221.93 \Omega \\
Z_3 &= 39.36 \Omega
\end{aligned} \tag{6.20}$$

The second designed balun is with a center frequency f_0 of 2 GHz, a normalized cutoff frequency of $S_C=j0.4$ corresponding to bandwidth of 152%, and ripple level $\epsilon=0.08243$ corresponding to a return loss of 21.71 dB. Similarly, follow the synthesized procedures as described in the first designed balun. The polynomial of the input impedance $Z_{in}(S)$, the circuit parameters corresponding to Fig. 6.5 in a normalized source resistance of 1- Ω , and the design parameters of Fig. 6.1 in 50- Ω system are shown in (6.21)-(6.23), respectively.

$$Z_{in}(S) = \frac{S^5 + 3.7080S^4 + 4.1420S^3 + 2.7908S^2 + 0.5574S + 0.1700}{S^5 + 3.0432S^4 + 4.1420S^3 + 1.8277S^2 + 0.5574S} \tag{6.21}$$

$$\begin{aligned}
Z_1 &= 1.1701 \\
C &= 2.4243 \\
Z_2' &= 1 \\
L' &= 2.4243 \\
Z_3' &= 0.8546 \\
R' &= 1
\end{aligned} \tag{6.22}$$

$$\begin{aligned}
Z_1 &= 58.51 \, \Omega \\
Z_C &= 20.62 \, \Omega \\
Z_{L1} &= 170.71 \, \Omega \\
Z_2 &= 70.71 \, \Omega \\
Z_{L2} &= \text{O.C } \Omega \\
Z_3 &= 42.73 \, \Omega
\end{aligned}
\tag{6.23}$$

The ideal responses of the two designed balun corresponding to the circuit of Fig. 6.5 are shown in Fig. 6.6.

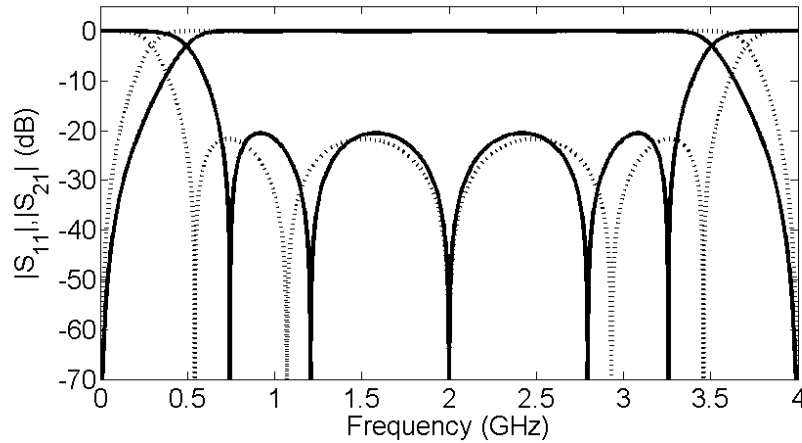


Fig. 6.6. The ideal responses of the first and second designed baluns with bandwidth of 131% and 152%, respectively.

6.4 Physical Implementation and Experimental Results

The implementations of the two designed wideband baluns in Section 6.3.B are constructed using hybrid microstrip line, slotline and coplanar stripline structures. A 0.635-mm-thick RT/Duroid 6010 substrate with a dielectric constant of 10.2 and a loss tangent of 0.0023 is used to implement these wideband balun circuits. The distributed circuits to be directly realized are the circuit shown in Fig. 6.1. Here, the two short-ended stubs Z_{L1} and Z_{L2} , the uniform transmission line Z_2 , the open-ended stub Z_C , and other uniform transmission lines Z_1 and Z_3 are implemented by coplanar striplines, a slotline, and microstrip lines, respectively [138]-[140]. All the stubs and uniform transmission lines are with electrical lengths of 90° at center frequency of $f_0=2$ GHz.

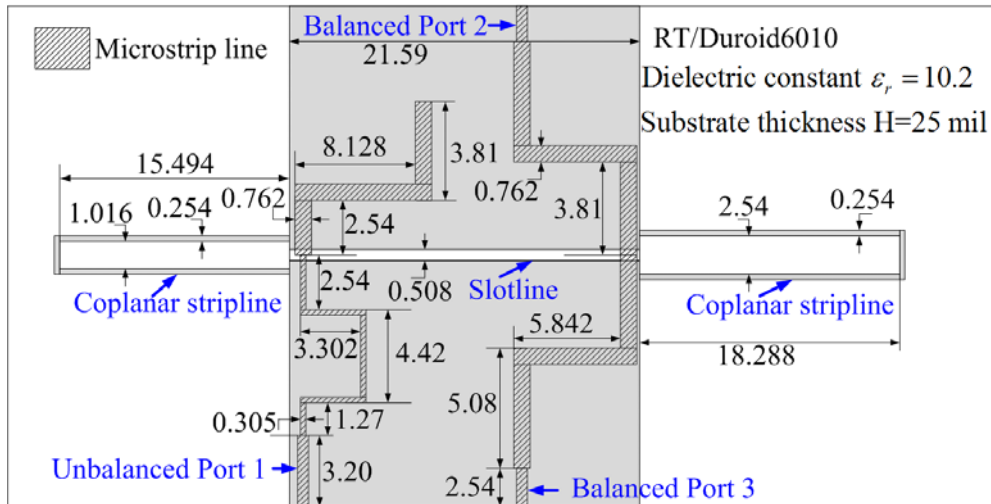
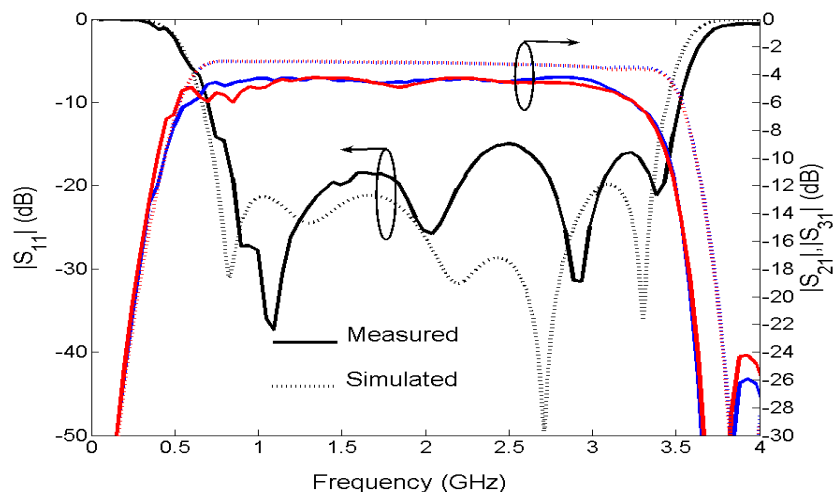


Fig. 6.7. Physical layout of the first designed fifth-order balun with $S_C=j0.6$ (unit: mm).

The first designed wideband balun with design parameters of (6.20) is implemented and its detailed physical dimensions are shown in Fig. 6.7. The design was accomplished with a commercial EM simulator Ansoft's High Frequency Structure Simulator (HFSS). Fine tuning in HFSS was performed to take all the EM effects into consideration. Fig. 6.8(a) shows the magnitudes of the ideal synthesized, simulated and measured performances. The measured return losses are better than 10 dB from 0.7 to 3.5 GHz. The measured amplitude balance and phase difference are shown in Fig. 6.8(b). The amplitude balance is within ± 1 dB from 0.72 to 3.62 GHz and the phase difference is within $180^\circ \pm 10^\circ$ from 0.7 to 3.53 GHz.



(a)

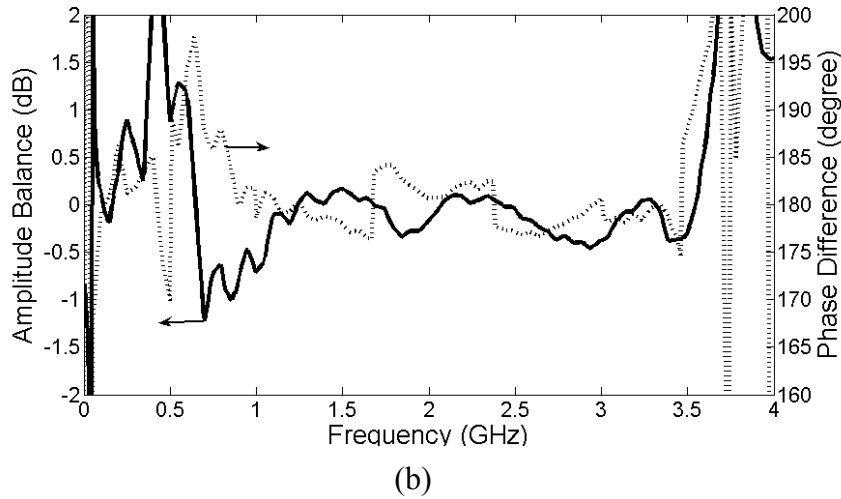


Fig. 6.8. Measured and simulated performances of the first designed fifth-order balun. (a) $|S_{11}|$, $|S_{21}|$ and $|S_{31}|$. (b) Amplitude balance and phase difference.

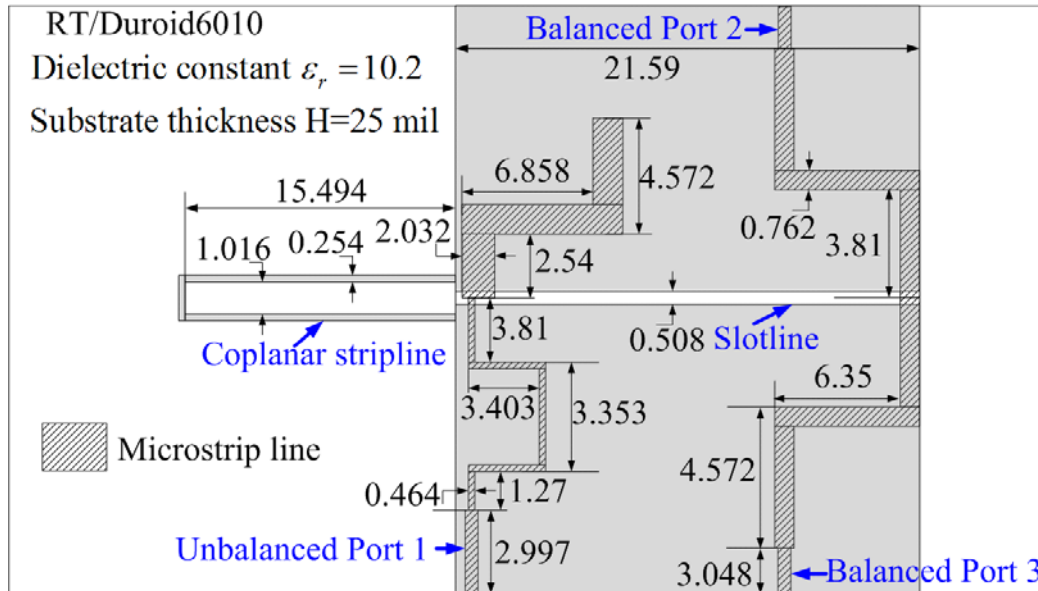
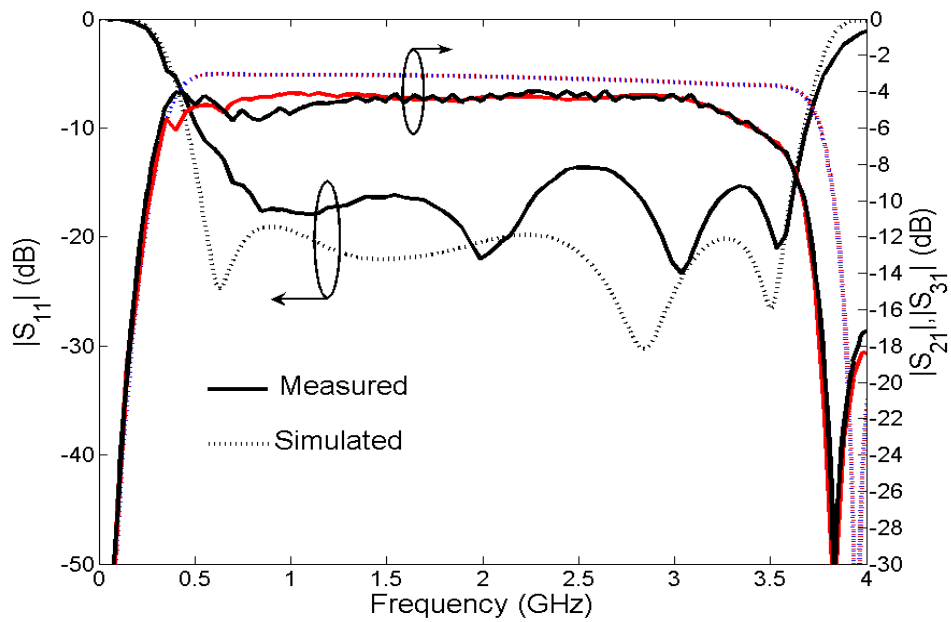


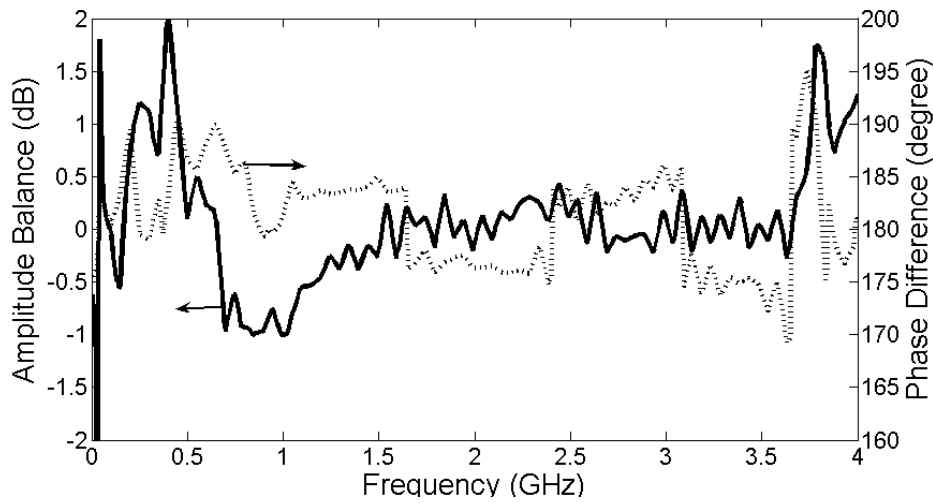
Fig. 6.9. Physical layout of the second designed fifth-order balun with $S_C=j0.4$ (unit: mm).

A second implementation is the second designed wideband balun with design parameters of (6.23). It should be pointed out that the impedance value of Z_{L2} is higher than 1000Ω , thus leading to the removal of the Z_{L2} section. The physical balun layout with detailed dimensions is shown in Fig. 6.9. The magnitudes of the ideal synthesized, simulated and measured performances are shown in Fig. 6.10(a). The measured return losses are better than 10 dB from 0.52 to 3.68 GHz. Fig. 6.10(b)

shows the measured amplitude balance and phase difference. The amplitude balance is within ± 1 dB from 0.46 to 3.75 GHz and the phase difference is within $180^\circ \pm 10^\circ$ from 0.46 to 3.62 GHz.



(a)



(b)

Fig. 6.10. Measured and simulated performances of the second designed fifth-order balun. (a) $|S_{11}|$, $|S_{21}|$ and $|S_{31}|$. (b) Amplitude balance and phase difference.

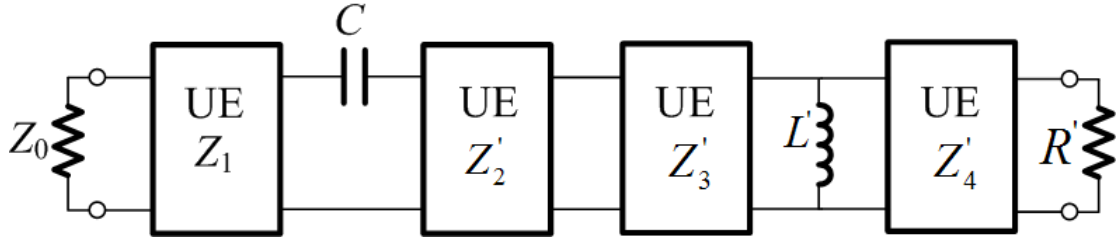


Fig. 6.11. The sixth-order S -plane high-pass prototype of Marchand balun.

6.5 A Sixth-Order S -plane Prototype Balun

An effective way to increase the order of Marchand balun is to add nonredundant unit elements. Fig. 6.11 shows the S -plane prototype circuit of a sixth-order Marchand balun. The best description of its rationality of the circuit is to present a synthesis example. Here, define a ripple level $\varepsilon=0.1807$ corresponding to a return loss of 14.9 dB and a normalized cutoff frequency of $S_c=j0.3$ corresponding to bandwidth of 162.88%. Following the procedures in (6.10)-(6.13), the polynomial of the input impedance can be obtained as

$$Z_{in}(S) = \frac{1.1779S^6 + 4.2950S^5 + 9.2555S^4 + 6.3402S^3 + 4.0811S^2 + 0.6273S + 0.2090}{0.8221S^6 + 4.2950S^5 + 5.9081S^4 + 6.3402S^3 + 1.8829S^2 + 0.6273S} \quad (6.24)$$

which is then synthesized using standard element extraction. The circuit parameters with a little optimization in a normalized source resistance of 1- Ω are

$$\begin{aligned} Z_1 &= 1.3074 \\ C &= 2.2339 \\ Z_2' &= 1.1595 \\ Z_3' &= 0.7626 \\ L' &= 1.9815 \\ Z_4' &= 0.676 \\ R' &= 1 \end{aligned} \quad (6.25)$$

Therefore, upon the values of the circuit parameters, such a sixth-order prototype circuit of Marchand balun is suited for designs of very wideband baluns.

Chapter 7 Conclusion and Future Work

7.1 Conclusion

This dissertation is devoted to the design of parallel-coupled filters with cross coupling, stepped impedance resonator filters with sharper selectivity and wide stopband rejection, development of new cross coupling schemes, and novel wideband Marchand balun.

A review of related filter synthesis methods, impedance and admittance inverters, coupled-line circuits, stepped impedance resonators, segmentation method using coupled-resonators theory, and distributed transmission line theory including Richards theory and element extraction are given in Chapter 2.

In chapter 3, the proposed cross-coupled filters are simple and easy to design. The cross-coupled filters have the advantages of small circuit size, high selectivity and wide rejection bandwidth. The circuit layout is easy to apply the source-load coupling and adjust the coupling strength.

The parallel-coupled filters with generalized Chebyshev responses are introduced in Chapter 4. The proposed filters can be quickly designed due to the well-known analytical design method based on a conventional parallel-coupled structure. The arbitrarily located transmission zeros have been fully discussed by observing the relative phase shifts of the lumped-element equivalent circuit of the parallel-coupled filter. With this approach, it is easy to design the parallel-coupled filter with a CT, a CQ, or a mixed cascaded quadruplet and trisection response. This newly proposed filter structure has shown properties of insensitive layout, flexible responses, good performance, and quick design procedures.

The success in the development of novel coupling schemes which are all with the properties of bisymmetric coupling matrix, weak cross couplings, and synchronous-tuned or very tiny asynchronous-tuned resonators has been demonstrated

in chapter 5. Due to the bisymmetric coupling matrices, the physical layouts of the filters to be realized may be symmetric. The proposed bisymmetric coupling schemes are suitable for designing microwave filters with transmission zeros very close to the passband.

In chapter 6, higher-order Marchand baluns have been proposed. The initial distributed circuit of fifth-order Marchand balun to be directly realized can be transformed into the final prototype circuit via a series of circuit transformations. Two examples of fifth-order Marchand baluns with ideal bandwidth of 131% and 152% are synthesized and implemented. In addition, the sixth-order Marchand balun has been introduced and discussed.

7.2 Future Work

The higher-order Marchand baluns have been synthesized based on S -plane high-pass prototype. The design of high-pass prototype is that the electrical length of all the transmission line sections is 90° at the center frequency of f_0 . To reduce the circuit size, an S -plane bandpass prototype of Marchand balun may be proposed so that the electrical length of each transmission line section is less than 90° at the center frequency of f_0 . A description of the synthesis technique based on S -plane bandpass prototype is given in [143]. With the synthesis technique, higher-order Marchand baluns with compact sizes and wideband performances will be studied in the future.

References

- [1] S. B. Cohn, "Microwave filters, and advancing art", *IEEE Trans. Microwave Theory Tech.*, vol. MTT-13, pp. 487-488, Sep. 1965.
- [2] S. J. Campanella et al., "Satellite Communications Systems and Technology, Circa 2000," *Proc. IEEE* Vol. 78, pp. 1039-1056, July 1990.
- [3] Ralph Levy and S. B. Cohn, "A history of microwave filter research, design, and development", *IEEE Trans. Microwave Theory Tech.*, vol. MTT-32, pp. 1055-1067, Sep. 1984.
- [4] Ralph Levy, Richard V. Snyder, and George Matthaei, " Design of microwave filters", *IEEE Trans. Microwave Theory Tech.*, vol. 50, pp. 783-793, March 2002.
- [5] Ian C. Hunter, Laurent Billonet, Bernard Jarry, and Pierre Guillon, "Microwave filters--- applications and technology" , *IEEE Trans. Microwave Theory Tech.*, vol. 50, pp. 794-805, March 2002.
- [6] J. S. Hong and M. J. Lancaster, *Microstrip Filters for RF/Microwave Applications*. New York: Wiley, 2001.
- [7] R. J. Cameron, C. Kudsia, and R. Mansour, *Microwave Filters for Communication Systems*. Hoboken, NJ: Wiley, 2007.
- [8] S. Darlington, "Synthesis of reactance 4-poles," *J. Math Phys.*, vol. 18, pp. 257-353, Sep. 1939.
- [9] S. B. Cohn, "Direct-coupled-resonator filters", *Proc. IRE*, vol. 45, pp. 187-196, Feb. 1957.
- [10] L. Young, "Direct-coupled cavity filters for wide and narrow bandwidths," *IEEE Trans. Microwave Theory Tech.*, vol. MTT-11, pp. 162-178, May 1963.
- [11] R. Levy, "Theory of direct coupled-cavity filters," *IEEE Trans. Microwave Theory Tech.*, vol. MTT-15, pp. 340-348, June 1967.
- [12] J. R. Pierce, "Guide-wave frequency range transducer," U.S. Patent 2626990, filed May 4, 1948, issued Jan. 27, 1953.



- [13] R. M Kurzrok, "General three-resonator filters in waveguide," *IEEE Trans. Microwave Theory Tech.*, vol. MTT-14, pp. 46-47, Jan 1966.
- [14] R. M Kurzrok, "General four-resonator filters at microwave frequencies," *IEEE Trans. Microwave Theory Tech.*, vol. MTT-14, pp. 295-296, June 1966.
- [15] J. D. Rhodes, "The theory of generalized interdigital networks," *IEEE Trans. Circuit Theory*, vol. CT-16, pp. 280-288, Aug. 1969.
- [16] J. D. Rhodes, "The design and synthesis of a class of microwave band pass linear phase filters," *IEEE Trans. Microwave Theory Tech.*, vol. MTT-17, pp. 189-204, Apr 1969.
- [18] C. L. Ren, "On the analysis of general parallel coupled TEM structures including non-adjacent couplings," *IEEE Trans. Microwave Theory Tech.*, vol. MTT-17, pp. 242-249, May 1969.
- [19] A. E. Williams, "A four-cavity elliptic waveguide filter", *IEEE Trans. Microwave Theory Tech.*, vol. MTT-18, pp. 1109-1114, Dec. 1970.
- [20] A. E. Atia and A. E. Williams, "Newtypes of bandpass filters for satellite transponders," *COMSAT Tech. Rev.*, vol. 1, pp. 21-43, Fall 1971.
- [21] A. E. Atia and A. E. Williams, "Narrow-bandpass waveguide filters," *IEEE Trans. Microwave Theory Tech.*, vol. MTT-20, pp. 258-265, Apr. 1972.
- [22] J. D. Rhodes, "Filters approximating ideal amplitude and arbitrary phase characteristics," *IEEE Trans. Circuit Theory*, vol. CT-20, pp. 120-124, Mar. 1973.
- [23] A. E. Atia, A. E. Williams, and R. W. Newcomb, "Narrow-band multiple-coupled cavity synthesis," *IEEE Trans. Circuits Syst.*, vol. CAS-21, pp. 649-655, Sept. 1974.
- [24] R. Levy, "Filters with signal transmission zeros at real or imaginary frequencies," *IEEE Trans. Microwave Theory Tech.*, vol. MTT-24, pp. 172-181, Apr 1976.
- [25] R. J. Wenzel, "Exact design of wideband equal-ripple bandpass filters with non-adjacent resonator couplings," in 1976 *IEEE MTT-S Int. Microwave Sump. Dig.*,

pp. 125-127, June 1976.

[26] I. C. Hunter, *Theory and Design of Microwave Filters*, ser. Electromagnetic Wave 48. London, U.K., : IEE Press, 2001.

[27] G. L. Mattheai, L. Young, and E. M. T. Jones, *Microwave Filters, Impedance Matching Networks and Coupling Structures*. Norwood, MA: Artech House, 1980.

[28] J. O. Scanlan, "Theory of microwave coupled-line networks," *Proc IEEE*, vol. 68, pp. 209-231, Feb. 1980.

[29] C. M. Kudsia and M. N. S. Swamy, "Computer-aided optimization of microwave filter networks for space applications," in *IEEE MTT-S Int. Microwave Symp. Dig.*, Washington, DC, May 1980. pp. 410-412.

[30] J. D. Rhodes and I. H. Zabalawi, "Synthesis of symmetric dual-mode in-line prototype networks," *Int. J. Circuit Theory Application.*, vol. 8, no. 2, pp. 145-160, 1980.

[31] R. J. Cameron, "Fast generation of Chebyshev filter prototypes with asymmetrically prescribed transmission zeros," *ESA J.*, vol. 6, pp. 83-95, 1982.

[32] R. J. Cameron and J. D. Rhodes, "Asymmetric realizations for dual-mode bandpass filters," *IEEE Trans. Microwave Theory Tech.*, vol. MTT-29, pp. 51-58, Jan 1981.

[33] C. Kudsia, R. Cameron, and W. Tang, "Innovations in microwave filters and multiplexing networks for communication satellite systems," *IEEE Trans. Microwave Theory Tech.*, vol. MTT-40, pp. 1133-1149, June 1992.

[34] S. Amari, "Synthesis of cross-coupled resonator filters using an analytical gradient-based optimization technique," *IEEE Trans. Microwave Theory Tech.*, vol. 48, no. 9, pp. 1559–1564, Sep. 2000.

[35] S. Amari, U. Rosenberg, and J. Bornemann, "Adaptive synthesis and design of resonator filters with source/load-multi-resonator coupling," *IEEE Trans. Microwave Theory Tech.*, vol. 50, no. 8, pp. 1969–1978, Aug. 2002.

- [36] R. J. Cameron, "General coupling matrix synthesis methods for Chebyshev filtering functions," *IEEE Trans. Microwave Theory Tech.*, vol. 47, pp. 433–442, Apr. 1999.
- [37] R. J. Cameron, "Advanced coupling matrix synthesis techniques for microwave filters," *IEEE Trans. Microwave Theory Tech.*, vol. 51, pp. 1–10, Jan. 2003.
- [38] M. Dishal, "Alignment and adjustment of synchronously tuned multiple-resonator-circuit filters," *Proc. IRE*, vol. 39, no. 11, pp. 1448-1455, Nov. 1951.
- [39] A. E. Atia and A. E. Williams, "Measurements of intercavity couplings," *IEEE Trans. Microwave Theory Tech.*, vol. MTT-23, pp. 519–522, June. 1975.
- [40] H. L. Thal, "Computer-aided filter alignment and diagnosis," *IEEE Trans. Microwave Theory Tech.*, vol. MTT-26, pp. 958–963, Dec. 1978.
- [41] M. H. Chen, "Short-circuit tuning method for singly terminated filters," *IEEE Trans. Microwave Theory Tech.*, vol. MTT-25, pp. 1032–1036, Dec. 1977.
- [42] P. Harscher, R. Vahldieck, and S. Amari, "Automated filter tuning using generalized low-pass prototype networks and gradient-based parameter extraction," *IEEE Trans. Microw. Theory Tech.*, vol. 49, no. 12, pp. 2532–2538, Dec. 2001.
- [43] M. Yu and W.-C. Tang, "A fully automated filter tuning robots for wireless basestation diplexers," presented at the *IEEE MTT-S Int. Microwave Symp. Workshop*, 2003, presentation.
- [44] G. Pepe, F.-J. Gortz, and H. Chaloupka, "Computer-aided tuning and diagnosis of microwave filters using sequential parameter extraction," in *IEEE MTT-S Int. Microw. Symp. Dig.*, 2004, pp. 1373–1376.
- [45] H. T. Hsu, H. W. Yao, K. A. Zaki and A. E. Atia, "Design of coupled resonators group delay equalizers," *IEEE MTT-S International Microwave Symposium Digest*, May 2001.
- [46] H.-T. Hsu, H.-W. Yao, K. A. Zaki, and A. E. Atia, "Computer-aided diagnosis and

tuning of cascaded coupled resonators filters,” *IEEE Trans. Microw. Theory Tech.*, vol. 50, no. 4, pp. 1137–1145, Apr. 2002.

[47] H.-T. Hsu, Z. Zhang, K. A. Zaki, and A. E. Atia, “Parameter extraction for symmetric coupled-resonator filters,” *IEEE Trans. Microw. Theory Tech.*, vol. 50, no. 12, pp. 2971–2978, Dec. 2002.

[48] A. García-Lampérez, S. Llorente-Romano, M. Salazar-Palma, and T. K. Sarkar, “Efficient electromagnetic optimization of microwave filters and multiplexers using rational models,” *IEEE Trans. Microw. Theory Tech.*, vol. 52, pp. 508–521, Feb. 2004.

[49] A. García-Lampérez, T. K. Sarkar, and M. Salazar-Palma, “Generation of accurate rational models of lossy systems using the cauchy method,” *IEEE Microw. Wireless Compon. Lett.*, vol. 14, no. 10, pp. 490–492, Oct. 2004.

[50] Giuseppe Macchiarella, and Daniele Trina, “A formulation of the Cauchy method suitable for the synthesis of lossless circuit models of microwave filters from lossy measurements”, *IEEE Microw. Wireless Compon. Lett.*, vol. 16, no. 5, pp. 243–245, May 2006.

[51] Piotr Kozakowski , Adam Lamecki, Piotr Sypek, and Michal Mrozowski, “Eigenvalue approach to synthesis of prototype filters with source/load coupling”, *IEEE Microwave and Wireless Component Lett.*, vol. 15, pp.98–100, Feb. 2005.

[52] C. K. Liao and C. Y. Chang, “Design of microstrip quadruplet filters with source/load couplings,” *IEEE Trans. Microw. Theory Tech.*, vol. 53, no. 7, pp. 2302-2308, Jul. 2005.

[53] S. Amari, and U. Rosenberg, “On the sensitivity of coupled resonator Filters without some direct couplings,” *IEEE Trans. Microwave Theory Tech.*, vol. 51, pp. 1767–1773, June 2003.

[54] N. Yildirim, M. Karaaslan, Y. Sen, and O. A. Sen, “Cascaded triplet filter design using cascade synthesis approach,” in *IEEE MTT-S Int. Microw. Symp. Dig.*, 1999, pp. 903–906.

[55] H. C. Bell, “Canonical asymmetric coupled-resonator filters,” *IEEE Trans. Microwave Theory Tech.*, vol. MTT-30, no. 9, pp. 1335–1340, Sep 1982.

- [56] R. Levy, "Direct synthesis of cascaded quadruplet (CQ) filters," *IEEE Trans. Microwave Theory Tech.*, vol. 43, no 12, pp. 2940–2945, Dec 1995.
- [57] R. Levy and P. Peter, "Design of CT and CQ filters using approximation and optimization," *IEEE Trans. Microwave Theory Tech.*, vol. 49, no 12, pp. 2350–2356, Dec 2001.
- [58] O. A. Sen, Y. Sen, and N. Yildirim, "Synthesis of cascaded quadruplet filters involving complex transmission zeros," in *IEEE MTT-S Int. Microw. Symp. Dig.*, 2000, pp. 1177–1180.
- [59] R. N. Gajaweera and L. F. Lind, "Coupling matrix extraction for cascaded triplet (CT) topology," in *IEEE MTT-S Int. Microw. Symp. Dig.*, 2003, pp. 1463–1465.
- [60] J. R. Montejo-Garai, "Synthesis of physically asymmetrical N -trisection filters with transmission zeros at N different real frequencies," *Electron. Lett.*, vol. 35, no. 3, pp. 226-227. Feb. 1999.
- [61] J. B. Thomas, "Cross-coupling in coaxial cavity filters—a tutorial overview," *IEEE Trans. Microwave Theory Tech.*, vol. 51, no. 4, pp. 1368–1376, Apr. 2003.
- [62] H. C. Bell, "The coupling matrix in low-pass prototype filters," *IEEE Microwave Mag.*, vol. 8, no. 2. pp. 70-76, Apr. 2007.
- [63] J. R. Montejo-Garai, "Synthesis of N -even order symmetric filters with N transmission zeros by means of source-load cross coupling," *Electron. Lett.*, vol. 26, no. 3, pp. 232-233. Feb. 2000.
- [64] S. Amari, "Direct synthesis of folded symmetric resonator filters with source-load coupling," *IEEE Microw. Wireless Compon. Lett.*, vol. 11, no. 6, pp. 264-266, Jun. 2001.
- [65] J. S. Hong, "Computer-aided synthesis of mixed cascaded quadruplet and trisection (CQT) filters," in *Proc. 31st Eur. Microw. Conf.*, London, U.K., Sep. 2001, vol. 3, pp. 5-8.
- [66] U. Rosenberg and S. Amari, "Novel coupling schemes for microwave resonator

filters,” *IEEE Trans. Microw. Theory Tech.*, vol. 50, no. 12, pp. 2896-2902, Dec. 2002.

[67] S. Amari and U. Rosenberg, “New building blocks for modular design of elliptic and self-equalized filters,” *IEEE Trans. Microw. Theory Tech.*, vol. 52, no. 2, pp. 721-736, Feb. 2004.

[68] K. T. Jokela, “Narrow-band stripline or microstrip filters with transmission zeros at real and imaginary frequencies,” *IEEE Trans. Microw. Theory Tech.*, vol. MTT-28, no. 6, pp. 542-547, Jun. 1980.

[69] C. Y. Chang and T. Itoh, “A modified parallel-coupled filter structure that improves the upper stopband rejection and response symmetry,” *IEEE Trans. Microw. Theory Tech.*, vol. 39, no. 2, pp. 310-314, Feb. 1991.

[70] J. S. Hong and M. J. Lancaster, “Canonical microstrip filter using square open-loop resonators,” *Elec. Lett.*, vol. 31, pp. 2020-2022, 1995.

[71] J. S. Hong and M. J. Lancaster, “Couplings of microstrip square open-loop resonators for cross-coupled planar microwave filters,” *IEEE Trans. Microw. Theory Tech.*, vol. 44, no. 12, pp. 2099-2108, Dec. 1996.

[72] J. S. Hong and M. J. Lancaster, “Cross-coupled microstrip hairpin-resonator filters,” *IEEE Trans. Microw. Theory Tech.*, vol. 46, no. 1, pp. 118-122, Jan. 1998.

[73] C. C. Yang and C. Y. Chang, “Microstrip cascade trisection filter,” *IEEE Microw. Guided Wave Lett.*, vol. 9, pp. 271-273, July 1999.

[74] K. S. K. Yeo and M. J. Lancaster, “The design of microstrip six-pole quasi-elliptic filter with linear phase response using extracted-pole technique,” *IEEE Trans. Microw. Theory Tech.*, vol. 49, no. 2, pp. 321-327, Feb. 2001.

[75] C. C. Chen, Y. R. Chen, and C. Y. Chang, “Miniaturized microstrip cross-coupled filters using quarter-wave or quasi-quarter-wave resonators,” *IEEE Trans. Microw. Theory Tech.*, vol. 51, no. 1, pp. 120-131, Jan. 2003.

[76] Y. S. Lin, C. H. Wang, C. H. Wu, and C. H. Chen, “Novel compact parallel-coupled microstrip bandpass filters with lumped-element K-inverters,” *IEEE Trans. Microw. Theory Tech.*, vol. 53, no. 7, pp. 2324-2328, July. 2005.

- [77] C. H. Wu, Y. S. Lin, C. H. Wang, and C. H. Chen, "Compact microstrip coupled-line bandpass filter with four transmission zeros," *IEEE Microw. Wireless Compon. Lett.*, vol. 15, no. 9, pp. 579-581, Sep. 2005.
- [78] S. C. Lin, Y. S. Lin, and C. H. Chen, "Extended-stopband bandpass filter using both half- and quarter-wavelength resonators," *IEEE Microw. Wireless Compon. Lett.*, vol. 16, no. 1, pp. 43-45, Jan. 2006.
- [79] P. H. Deng, Y. S. Lin, C. H. Wang, and C. H. Chen, "Compact microstrip bandpass filters with good selectivity and stopband rejection," *IEEE Trans. Microw. Theory Tech.*, vol. 54, no. 2, pp. 533-539, Feb. 2006.
- [80] C. L. Hsu and J. T. Kuo, "Design of cross-coupled quarter-wave SIR filters with plural transmission zeros," in *IEEE MTT-S Int. Microwave Symp. Dig.*, San Francisco, 2006, pp. 1205-1208.
- [81] C. K. Liao and C. Y. Chang, "A novel five-pole microstrip cascade quadruplet filter," in *Proc. Asia-Pacific Microwave Conf.*, Suzhou, China, 2005, pp. 433-436.
- [82] C. K. Liao and C. Y. Chang, "Modified parallel-coupled filter with two independently controllable upper stopband transmission zeros," *IEEE Microw. Wireless Compon. Lett.*, vol. 15, no. 12, pp. 841-843, Dec. 2005.
- [83] C. H. Chen, C. K. Liao, and C. Y. Chang, "Novel multifold finite-ground-width CPW quarter-wavelength filters with attenuation poles," *IEEE Trans. Microw. Theory Tech.*, vol. 55, no. 1, pp. 128-136, Jan. 2007.
- [84] C. H. Wu, C. H. Wang, Y. S. Lin, and C. H. Chen, "Parallel-coupled coplanar-waveguide bandpass filter with multiple transmission zeros," *IEEE Microw. Wireless Compon. Lett.*, vol. 17, no. 2, pp. 118-120, Feb. 2007.
- [85] N. Yang, C. Caloz, K. Wu, and Z. N. Chen, "Broadband and compact coupled coplanar stripline filters with impedance steps," *IEEE Trans. Microw. Theory Tech.*, vol. 55, no. 12, pp. 2874-2886, Dec. 2007.
- [86] R. J. Cameron, A. R. Harish, and C. J. Radcliffe, "Synthesis of advanced microwave filters without diagonal cross-couplings," *IEEE Trans. Microw. Theory*

Tech., vol. 50, no. 12, pp. 2862-2872, Dec. 2002.

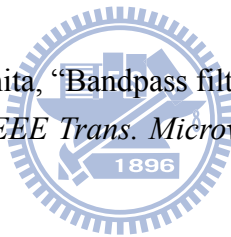
[87] A. E. Williams, J. I. Upshur, and M. M. Rahman, "Asymmetric response bandpass filters having resonators with minimum coupling," U.S. Patent 6 337 610, Jan. 8, 2002.

[88] S. Amari, G. Tadeson, J. Cihlar, R. Wu, and U. Rosenberg, "Pseudo-elliptic microstrip line filters with zero-shifting properties," *IEEE Microw. Wireless Compon. Lett.*, vol. 14, no. 7, pp. 346-348, Jul. 2004.

[89] C. K. Liao, P. L. Chi, and C. Y. Chang, "Microstrip realization of generalized Chebyshev filters with box-like coupling schemes," *IEEE Trans. Microw. Theory Tech.*, vol. 53, no. 1, pp. 147-153, Jan. 2007.

[90] C. K. Liao, "Tuning and diagnosis of cross-coupled microstrip filters," Ph. D. Dissertation, 2007, Department of Communication Engineering, University of Chiao-Tung in Hsinchu, Taiwan.

[91] M. Makimoto and S. Yamashita, "Bandpass filters using parallel coupled stripline stepped impedance resonators" *IEEE Trans. Microw. Theory Tech.*, vol. MTT-28, no. 12, pp. 1413-1417, Dec. 1980.



[92] M. Makimoto and S. Yamashita, *Microwave Resonators and Filters for Wireless Communication*. New York: Springer, 2001.

[93] H. M. Lee and C. M. Tsai, "Improved coupled-microstrip filter design using effective even-mode and odd-mode characteristic impedances," *IEEE Trans. Microw. Theory Tech.*, vol. 53, no. 9, pp. 2812-2818, Sep. 2005.

[94] C. Y. Chang, *Microwave passive and active circuit design theory & lab*, Microwave Engineering Course Textbook, Department of Communication Engineering, University of Chiao-Tung in Hsinchu, Taiwan.

[95] C. Y. Chang and C. C. Chen, "A novel coupling structure suitable for cross-coupled filters with folded quarter-wave resonator," *IEEE Microw. Wireless Compon. Lett.*, vol. 13, no. 12, pp. 517-519, Dec. 2003.

[96] J. S. Hong and M. J. Lancaster, "Transmission line filters with advanced filtering

characteristics,” in *IEEE MTT-S Int. Microw. Symp. Dig.*, 2000, pp. 319-322.

[97] S. B. Cohn, “Parallel-coupled transmission-line-resonator filters,” *IRE Trans. Microw. Theory Tech.*, vol. MTT-6, no. 4, pp. 223-231, Apr. 1958.

[98] R. J. Cameron, J. C. Faugere, and F. Seyfert, “Coupling matrix synthesis for a new class of microwave filter configuration,” in *IEEE MTT-S Int. Microw. Symp. Dig.*, 2005, pp. 119-122.

[99] Advanced Design System (ADS), ver. 2003C, Agilent Technol., Santa Rosa, CA, 2003.

[100] “*EM User’s Manual*,” Sonnet Softw. Inc., Liverpool, NY, 2004.

[101] J. C. Lu, C. K. Liao, and C. Y. Chang, “Microstrip parallel-coupled filters with cascade trisection and quadruplet responses,” *IEEE Trans. Microw. Theory Tech.*, vol. 56, no. 9, pp. 2101-2110, Sep. 2008.

[102] N. Marchand, “Transmission line conversion transformers,” *Electronics*, vol. 17, no. 12, pp. 142-145, Dec. 1944.



[103] W. K. Roberts, “A new wide-band balun,” *Proc. IRE*, vol. 45, pp. 1628-1631, Dec. 1957.

[104] H. G. Oltman, “The compensated balun,” *IEEE Trans. Microw. Theory Tech.*, vol. MTT-14, no. 3, pp. 2812-2818, Mar. 1966.

[105] H. R. Phelan, “A wide-band parallel-connected balun,” *IEEE Trans. Microw. Theory Tech.*, vol. MTT-18, no. 5, pp. 259-263, May. 1970.

[106] J. H. Cloete, “Exact design of the Marchand balun,” *Microwave J.*, vol. 23, pp. 99-110, May. 1980

[107] J. Cloete, “Graphs of circuit elements for the Marchand balun,” *Microwave J.*, vol. 24, no. 5, pp. 125-128, May 1981.

[108] J. M. Seligman, E. S. Gillespie, and M. Ryken, “A quasi-lumped planar balun for printed circuit antennas,” *IEEE AP-S International Symp. Dig.*, pp. 15-19, 1987.

- [109] H. Shuhao, "The balun family," *Microwave J.*, vol. 30, pp. 227-229, Sep. 1987.
- [110] B. Climer, "Analysis of suspended microstrip taper baluns," *Proc IEE*, vol. 135, pp. 65-69, Apr. 1988.
- [111] A. M. Pavio and A. Kikel, "A monolithic or hybrid broadband compensated balun," in *IEEE MTT-S Int. Microw. Symp. Dig.*, 1990, vol. 1, pp. 483-486.
- [112] B. J. Minnis and M. Healy, "New broadband balun structures for monolithic microwave integrated circuits," in *IEEE MTT-S Int. Microw. Symp. Dig.*, 1991, pp. 425-428.
- [113] J. Rogers and R. Bhatia, "A 6 to 20 GHz planar balun using a Wilkinson divider and Lange couplers," in *IEEE MTT-S Int. Microw. Symp. Dig.*, 1991, pp. 865-868.
- [114] T. H. Chen, K. W. Chang, S. B. Bui, H. Wang, G. S. Dow, L. T. Liu, T. S. Lin, and W. S. Titus, "Broadband monolithic passive baluns and monolithic double-balanced mixer," *IEEE Trans. Microw. Theory Tech.*, vol. 39, no. 12, pp. 1980-1986, Dec. 1991.
- [115] C. L. Goldsmith, A. Kikel, and N. L. Wilkens, "Synthesis of Marchand baluns using multilayer microstrip structures," *Int. J. of Microwave and Millimeter-Wave Computer-Aided Engineering*, vol. 2, pp. 179-188, Jul. 1992.
- [116] C. M. Tsai and K. C. Gupta, "A generalized model for coupled lines and its applications to two-layer planar circuits," *IEEE Trans. Microw. Theory Tech.*, vol. 40, no. 12, pp. 2190-2199, Dec. 1992.
- [117] S. A. Mass and K. W. Chang, "A broadband, planar, doubly balanced monolithic ka-band diode mixer," *IEEE Microwave and Millimeter-Wave Monolithic Circuits Symp. Dig.*, 1993, pp. 53-56.
- [118] R. Schwindt and C. Nguyen, "Computer-aided analysis and design of a planar multilayer Marchand balun," *IEEE Trans. Microw. Theory Tech.*, vol. 42, no. 6, pp. 1429-1434, Jul. 1994.
- [119] R. Mongia, I. Bahl, and P. Bhartia, *RF and Microwave Coupled-Line Circuits*.

Norwood, MA: Artech House, 1999, pp. 391-442.

[120] K. S. Ang and I. D. Robertson, "Analysis and design of impedance-transforming planar Marchand baluns," *IEEE Trans. Microw. Theory Tech.*, vol. 49, no. 2, pp. 402-406, Feb. 2001.

[121] Y. S. Lin and C. H. Chen, "Lumped-element Marchand-balun type coplanar waveguide-to-coplanar stripline transitions," in *Proc. Asia-Pacific Microw. Conf.*, Dec. 2001, pp. 539-542.

[122] C. W. Tang and C. Y. Chang, "A semi-lumped balun fabricated by low temperature co-fired ceramic," in *IEEE MTT-S Int. Microwave Symp. Dig.*, Jun. 2002, pp. 2201-2204.

[123] K. S. Ang, Y. C. Leong, and C. H. Lee, "Multisection impedance-transforming coupled-line baluns," *IEEE Trans. Microw. Theory Tech.*, vol. 51, no. 2, pp. 536-541, Feb. 2003.

[124] D. Kuylenstierna and P. Linner, "Design of broad-band lumped-element baluns with inherent impedance transformation," *IEEE Trans. Microw. Theory Tech.*, vol. 52, no. 12, pp. 2739-2745, Dec. 2004.



[125] C. S. Lin, P. S. Wu, M. C. Yeh, J. S. Fu, H. Y. Chang, K. Y. Lin, and H. Wang, "Analysis of multiconductor coupled-line Marchand baluns for miniature MMIC design," *IEEE Trans. Microw. Theory Tech.*, vol. 55, no. 6, pp. 1190-1199, Jun. 2007.

[126] M. J. Chiang, H. S. Wu, and C. K. Tzuang, "A compact CMOS Marchand balun incorporating meandered multilayer edge-coupled transmission lines," in *IEEE MTT-S Int. Microwave Symp. Dig.*, Jun. 2009, pp. 125-128.

[127] D. H. Lee, J. Han, C. Park, and S. Hong, "A CMOS active balun using bond wire inductors and a gain boosting technique," *IEEE Microw. Wireless Compon. Lett.*, vol. 17, no. 9, pp. 676-678, Sep. 2007.

[128] B. J. Huang, B. J. Huang, K. Y. Lin, and H. Wang, "A 2-40 GHz active balun using 0.13 μm CMOS process," *IEEE Microw. Wireless Compon. Lett.*, vol. 19, no. 3, pp. 164-166, Mar. 2009.

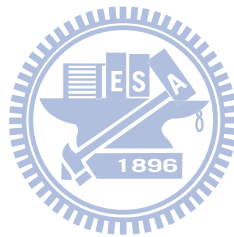
- [129] B. Godara and A. Fabre, "A highly compact active wideband balun with impedance transformation in SiGe Bicmos," *IEEE Trans. Microw. Theory Tech.*, vol. 56, no. 1, pp. 22-30, Jan. 2008.
- [130] P. I. Richards, "Resistor-transmission-line circuits," *Proc. IRE*, vol. 34, pp. 217-220, Feb. 1948.
- [131] D. M. Pozer, *Microwave Engineering*, 2nd. New York: Wiley, 1998. pp. 464.
- [132] H. J. Riblet, "The application of a new class of equal-ripple functions to some familiar transmission-line problems," *IEEE Trans. Microw. Theory Tech.*, vol. MTT-12, no. 7, pp. 415-421, Jul. 1964.
- [133] H. J. Carlin and W. Kohler, "Direct synthesis of band-pass transmission line structures," *IEEE Trans. Microw. Theory Tech.*, vol. MTT-13, no. 5, pp. 283-297, May. 1965.
- [134] H. J. Orchard and G. C. Temes, "Filter design using transformed variable," *IEEE Trans. Circuit Theory*, vol. CT-15, no. 12, pp. 385-408, Dec. 1968.
- [135] M. Horton and R. Wenzel, "General theory and design of optimum quarter-wave TEM filters," *IEEE Trans. Microw. Theory Tech.*, vol. MTT-13, no. 5, pp. 316-327, May. 1965.
- [136] H. J. Carlin, "Distributed circuit design with transmission line elements," *Proc. IEEE*, vol. 59, no. 7, pp. 1059-1081, Jul. 1971.
- [137] R. J. Wenzel, "Exact design of TEM microwave networks using quarter-wave lines," *IEEE Trans. Microw. Theory Tech.*, vol. MTT-12, pp. 94-111, Jan. 1964.
- [138] K. C. Gupta, R. Garg, and I. Bahl, *Microstrip Lines and Slotlines*. Dedham, MA: Artech House, 1979.
- [139] B. Schuppert, "Microstrip/Slotline transitions : modeling and experimental investigation," *IEEE Trans. Microw. Theory Tech.*, vol. 36, no. 8, pp. 1272-1282, Aug. 1988.
- [140] R. N. Simons, *Coplanar Waveguide Circuits Components & Systems*. New York:

Wiley, 2001.

[141] S. C. Tseng, C. C. Meng, C. H. Chang, C. K. Wu, and G. W. Huang, "Monolithic broadband Gilbert micromixer with an integrated Marchand balun using standard silicon IC process," *IEEE Trans. Microw. Theory Tech.*, vol. 54, no. 12, pp. 4362-4371, Dec. 2006.

[142] S. A. Mass, *The RF and Microwave Circuit Design Cookbook*. Norwood, MA: Artech House, 1998. pp. 109-114.

[143] R. J. Wenzel, "Synthesis of combline and capacitively loaded interdigital bandpass filters of arbitrary bandwidth," *IEEE Trans. Microw. Theory Tech.*, vol. MTT-19, no. 8, pp. 678-686, Aug. 1971.



簡歷

姓 名：呂哲慶

性 別：男

出生年月日：民國 71 年 5 月 18 日

籍 貫：台灣台南市

學 歷：交通大學電信所碩士班畢業



經 歷：高中畢業於台南一中，大學畢業於中山大學電機系。申請進入交通大學電信研究所電波組研讀，個人在碩博班期間之研究主題為微波被動元件之設計製作與最佳化。

論文題目：

Development and Design of Novel Cross-Coupled Filters and
Exact Synthesis of New High-Order Wideband Marchand Balun

Publication List

I. Journals

[1] **J. C. Lu**, C. K. Liao, and C. Y. Chang, "Microstrip parallel-coupled filters with cascade trisection and quadruplet responses," *IEEE Trans. Microwave Tech.*, vol-56, no. 9, pp. 2101-2110, Sep. 2008.

II. Conferences:

[1] **J. C. Lu** and C. Y. Chang, "Quarter-wave stepped-impedance resonator filters with quadruplet and canonical form responses," in *Proc. 38th Eur. Microwave Conf.*, 2008, pp. 504-507.

[2] **J. C. Lu** and C. Y. Chang, "Generalized Chebyshev response parallel-coupled filter with suppression of $2f_0$ spurious passband," in *Asia-Pacific Microwave Conf.*, Hong Kong, China, pp. 16-20, Dec. 2008.

[3] **J. C. Lu**, Y. W. Lin, C. K. Liao, and C. Y. Chang, "Five-pole parallel-coupled microstrip cascade quadruplet filters for high selectivity and flat group delay," accepted to be presented at the *Asia-Pacific Microwave Conf.*, Singapore, Dec. 2009.

[4] Y. W. Lin, **J. C. Lu**, C. Y. Chang, and C. K. Liao, "Six-pole parallel-coupled microstrip CQ filter with source-load and source/load to resonator cross coupling," accepted to be presented at the *Asia-Pacific Microwave Conf.*, Singapore, Dec. 2009.

Under Review

Journals

[1] **J. C. Lu**, C. K. Liao, and C. Y. Chang, "Bisymmetric coupling schemes for implementation of low-order generalized Chebyshev planar filters with transmission zeros very closed to the passband," Submitted to *IEEE Trans. Microwave Tech.*

[2] **J. C. Lu**, C. C. Lin, and C. Y. Chang, "Synthesis and implementation of high-order Wideband Marchand Balun," will submit to *IEEE Trans. Microwave Tech.*

[3] **J. C. Lu**, C. K. Liao, and C. Y. Chang, "Novel wheel-quadruplet-like cross coupling schemes with generalized Chebyshev responses," will submit to *Electronics Letters*.

[4] Y. T. Kuo, **J. C. Lu**, C. K. Liao, and C. Y. Chang, "Advanced coupling matrix synthesis techniques for multi-band microstrip parallel-coupled filters," will submit to *IEEE Trans. Microwave Tech.*